LUTMDN(TMMV-5246)1-136-2012

Jakob Dieterle

Influence of the Pulse Shape on Spot Welds in Laser Beam Micro Joining of Metallic Materials

Table Of Contents

Table Of Contents

Table of Abbreviations and Symbols

Abbreviation / Symbol	**Unit**	**Meaning**
b		Polynomial Coefficients
BPP	mm•mrad	Beam Parametric Product
C	F	Capacitor
CoV		Coefficient of Variation
cw		Continuous Laser Waves
d	mm	Beam Diameter
d_f	mm	Focus Diameter
DoE		Design of Experiment
DOF		Degress of Freedom
d_{of}	mm	Depth of Focus
D_{sch}		Schottky-Diode
E	J	Energy
e		Polynomial Errors
F		Test Quantity for Fischer-Snedecor Distribution
f	mm	Focal Length of Objective
f_c	mm	Focal Length of Collimator
FET		Field Effect Transistor
f_i		Outcome Predicted by System Equation
HAZ		Heat Affected Zone
HCW		Heat Conduction Mode Welding
i		Index of Observations
i_L		Current through Inductance
j		Index of Groups
k		Number of Groups
KW		Keyhole Welding

l		Number of Levels
L	H	Inductance
lcc		Light Conducting Cable
MS		Mean Squares
n		Number of Experimental Runs / Observations
NaN		Not a Number (equal to 0 in respective diagrams)
Nd:YAG		Neodym Yttrium-Aluminum-Granat
P	W	(Peak) Power
P_a / W_a / R_a / S_a	µm	Average height difference along Primary / Waviness / Roughness / Surface Profile
PEM		Power and Energy Measurement Unit
P_{ku} / R_{ku}		Kurtosis of Primary / Roughness Profile
P_q		Root Mean Square of Heights along the Primary Profile
P_{sk}		Skewness of Primary Profile
P_t / W_t / R_z / S_z	µm	Maximum height difference along Primary / Waviness / Roughness / Surface Profile
pw		Pulsed laser waves
R	Ω	Electrical Resistor
r		Residual
R^2		Coefficient of Determination
s		Standard deviation
SMPS		Switch Mode Power Supply
SSB		Sum of Squares Between Groups
SS_{err}		Sum of Squares of Errors
SST		Total Sum of Squares
SS_{tot}		Total Sum of Squares
SSW		Sum of Squares Within Groups
t_1	%	Relative set-point along time axis

t_2	%	Relative set-point along time axis
t_d	ms	Pulse Duration
U	V	Voltage
W_D	mm	Welding Depth
y_i		Single Experimental Observation
$\bar{y}$		Mean of Experimental Observation
$\bar{\bar{x}}$		Grand Mean
z		Number of Factors
Q	rad	Angle of Beam Spread

1 Introduction

A common understanding of the thesis' background and goal as well as the applied methodology is derived in the following.

1.1 Context and Goal of the Thesis

In many micro joining tasks for technical applications metallic materials have to be joined in an electrically conducting and mechanically secure way. Figure 1.1 shows a common combination of a winded wire and tube section joined by spot welding. The diameter of a wire lies between 0.1 - 0.2 mm.

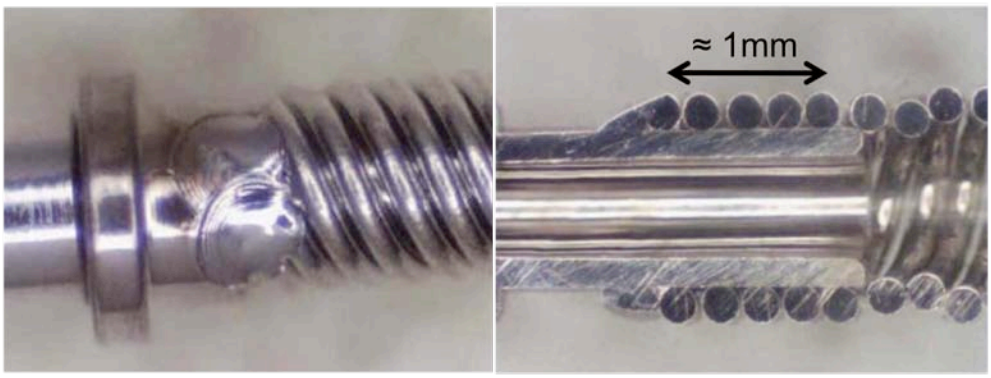

Figure 1.1: Typical join of wire and tube in laser micro welding (according to [SAARECHIEV & JIE 2004A]).

In order to achieve such joins laser beam welding and – due to the size of the joins in the range of micro- to few millimetres – especially spot welding is a common choice. This method is advantageous due to characteristics such as: limited heat deposition, absence of contact as well as no necessity of filler material or preparatory actions for the contact zones. Furthermore, can some of the most relevant parameters be directly controlled to design a dedicated welding process.

The latter aspect has especially gained significance in the field of pulsed laser beam welding. The development of marketable laser systems with an almost arbitrary modulation of the generated pulse shape is a major recent innovation [WILDEN 2009]. Thus the process has gained a controllable parameter which creates opportunities for optimization.

The goal of this thesis is hence to contribute to the understanding of the influence of the pulse shape as a control parameter for pulsed laser beam spot welding with regard to materials of current interest.

The state of the art as discussed in section 2 show that a basic understanding of the pulse shape's influence exist. Yet, these observations need to be confirmed for the given dimensions and materials.

A main priority is to examine the influence of the pulse shape on achievable mechanical strength of welded joins and on the risk of spatter during the process. These are two central quality characteristics, which often represent conflicting goals. A model relating these parameters is given below. Further quality demands are little permanent deformation and an overall smooth surface. These are however very case-specific and hard to quantify. Compared to the K.O-criteria mentioned before these demands are often rather soft. Moreover is deformation critical for e.g. copper-nickel alloys but less problematic for the materials examined in this work.

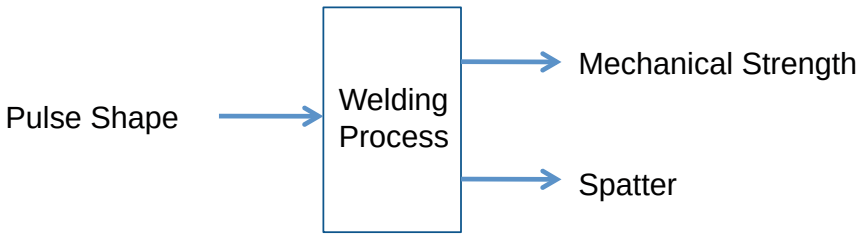

Figure 1.2: Basic parameter relations for the examined process.

1.2 Methodology

The system of interaction in the examined process consists of a laser system, material probes of different nature and a given set-up. By choosing selected controllable input factors (e.g. pulse shape) an interaction with the remaining inherent parameters (e.g. optical unit, material probe) takes place and results in a weld characterized by measurable quality characteristics (e.g join strength).

It is desirable to know the relation of input and quality quantities from the start as commonly expressed through physical equations. Yet, modelling the process through systems of differential equations is generally difficult in welding [DEY ET. AL 2009]. This is due to the amount of physical mechanisms involved as well as e.g. the inability to determine relevant material constants at all stages of the welding process (see 3.3.1 for physical processes and constants involved).

Hence, a global system equation is not available and has to be generated from experimental data. This is achieved through methods of design of experiments (DoE).

The conducted experiments start with a basic test of performance capability of the given laser system in terms of pulse shaping. This is done to determine the boundaries of operation regarding the control inputs. Following that, a reference experiment is conducted to prepare experimental designs for a further analysis by means of DoE.

Based on these results an experiment to produce partial penetration welds is designed. A concluding experiment provides an outlook on the pulse shape's influence on joining dissimilar metals.

The welding experiments focus on the influence of input factors (esp. pulse shape) on desired quality characteristics to define suitable process windows for production. For doing so the system equation derived through methods of DoE is analysed in various forms (parameter influences, contour plots etc.).

The experimental strategy is summarised in Figure 1.3 and elaborated upon in the following.

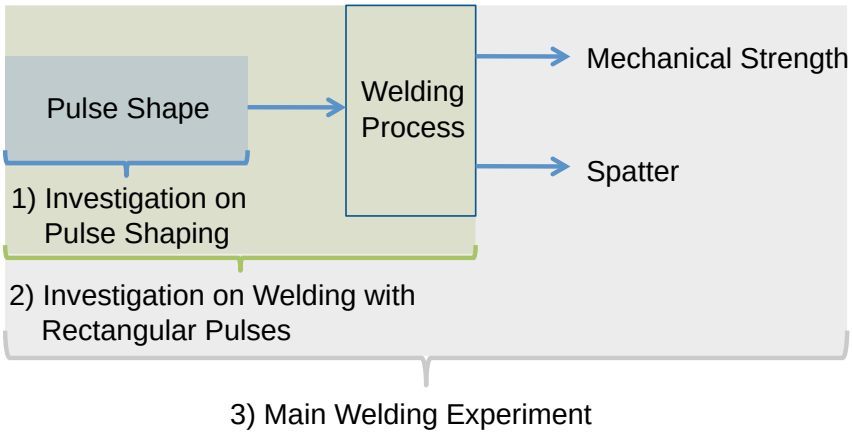

Figure 1.3: Experimental approach.

1.2.1 Experimental Approach

The applied pulses have durations of a few milliseconds and power levels up to 1500 W. It is known that the laser system is not fully capable of achieving all pulse shapes as set by the user. The resulting pulse shape will always deviate from the intended one.

For guaranteeing a high informational value and transferability of the results, these deviations need to be known. The parameter range for programming set-point sequences have to be constricted accordingly. This way an

acceptable level of congruency between set and action shape is achieved for the welding experiments. Such limits are derived from systematically comparing ideal and produced shape in the first investigation on pulse shaping capabilities.

The subsequent investigation serves to prepare the application of methods of DoE. By carrying out reference welds with a rectangular pulse over a large matrix of power levels and durations the experimental space is examined. Goals are to identify the degree of nonlinearity of the process (e.g. by a transition of HCW to KW) as well as deriving a basic process window to avoid spatter. Alongside are measurands to quantify the surface smoothness of the weld examined. This is necessary quantify whether a certain pulse shape causes high melt pool turbulences. The latter is thought to correlate with spatter formation and is partially reflected by irregularities of the weld surface.

In the main welding experiment partial penetration welds are carried out to examine the pulse shape's influence. In this case no join is produced and the achievable strength has to be evaluated with help of other measurands. These act as indicators in this case due to a presumed correlation. The same is applied for judging the risk of spatter.

The selected intermediate quantities are the weld volume and weld quality. Quality embraces all possible defects as well as the surface roughness. The latter indicates risk of spatter by reflecting possible melt pool turbulences. Further quality entities such as cracks, pores and notches may limit the achievable strength. The weld volume defines the possible amount of force transmitting material. Consequently can the parameter model be extended by considering these intermediate quality characteristics (see below).

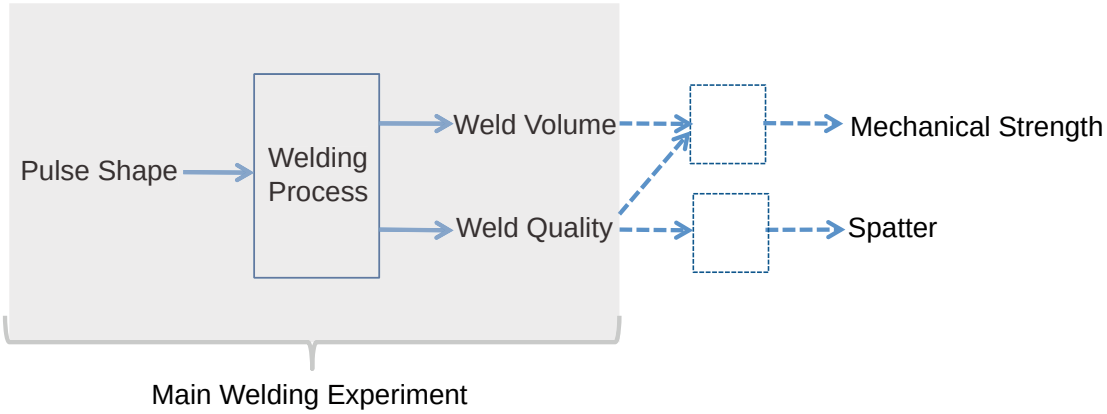

Figure 1.4: Consideration of intermediate quality characteristics for the experiments on partial penetration welding.

This estimation of possible strength via melt pool volume and quality is supported by calculation models in literature. Figure 1.5 shows the modelling of a spot weld through a shaft connection. Such a model is not confirmed to be applicable in the given case but can contribute a basic understanding. Note that the depicted case shows a weld produced by resistance welding. In laser welding the fusion zone typically strechtes from the surface of one partner into the material of the other.

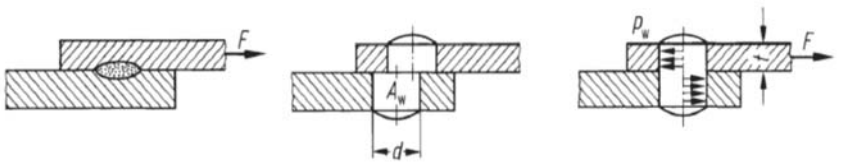

F = tensile force [N]
t = material thickness [mm]
d = spot weld diameter [mm]
p_w = surface pressure [N/mm]
A_w = weld cross-section [mm^2]

Figure 1.5: Modelling of spot weld through a pin connection (according to [NIEMANN ET AL. 2005])

Two failure modes are illustrated for tensile stresses: The middle case shows shearing due to stresses in the plane of the cross section at the join – the rightmost case shows stresses resulting from surface pressures along the spot weld boundaries. In any case do the dimensions of the weld define the amount of volume to withstand the stresses. To resist shearing large cross sections of the join are advantageous. A large volume e.g. through high penetration may increase resistance to surface pressure. The exact nature of the failure modes is further examined in section 6.

For the detailed calculation principles please consider [NIEMANN ET AL. 2005]. There residual stresses, supporting and notch effects are mentioned as a further potential influence on the strength. The latter case may be a consequence of surface roughness, cracks or pores as summarized by the term weld quality.

As a last experiment overlap joins are welded between dissimilar materials. This provides an outlook on possible pulse shape influences on these kind of tasks. The joins are examined in tensile tests.

The context and goal of the thesis were presented. The methodology and experimental strategy were introduced. After a summary of the state of the art, a theoretical part prepares the discussion of experimental investigations and results.

2 State of the Art

As discussed in section 1.1 it is hard to formulate universal statements on parameter influences in welding. There exist some basic of rules of thumb on the influence of pulse shaping [NAEEM 2004] but these need to be verified and adapted in each specific case.

In pulsed laser welding thermal as well as metallurgic pulse-shaping is applied. The latter attempts to influence the microstructure of the solidified weld by defined undercooling of the melt pool [WILDEN 2009]. In thermal pulse shaping the pulse shape is adapted to the process phases of coupling, melting, welding and solidification (see 3.3.1). This strategy is studied in this work.

The most basic pulse shape is a rectangular pulse. To overcome reflectivity or poor coupling (e.g. due to oxide surface layers) one can employ initial sparks or steep ramp-ups for initiating a quick melt pool formation. If a high thermal diffusivity is the case higher peak levels over longer periods are needed. Ramping down influences the solidification rate and should be chosen smoothly for materials with a high risk of solidification related defects (pores, cracks etc.). Smooth ramp-ups are sufficient when efficient coupling is guaranteed. This way overheating the melt pool which can result in spatter is limited. Such slow heating gradients can also deliver good results for coated materials as the heat energy is raised only after the coat has been removed [NAEEM 2004]. Experimental proof of these basic rules is partially given through [BERTRAND & POULON-QUINTIN 2011] and [KLAGES ET AL. 2004].

The influence of ramp-downs on quality aspects is confirmed for aluminium in [VDI-TPT 1995]. At the same time is the influence of ramp-downs on the penetration in copper and steel found to be insignificant in comparison to the average power level of the pulse.

The discussed pulse variants are illustrated below.

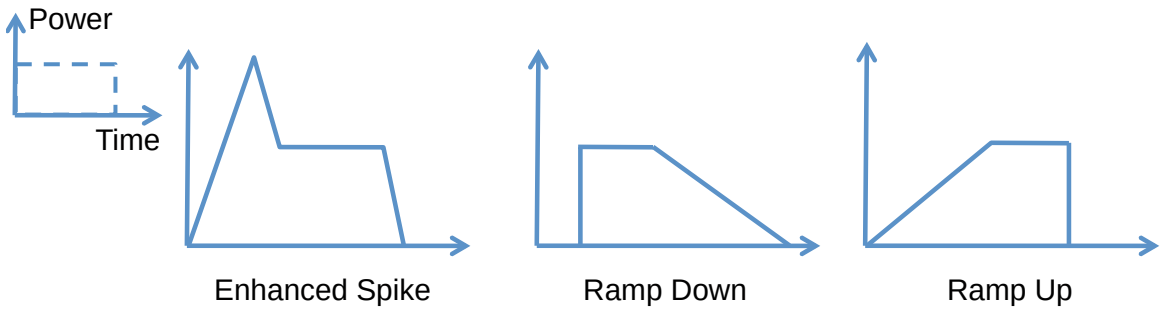

Figure 2.1: Typical pulse shape modulations based on a rectangular pulse (according to [NAEEM 2004]).

In practice a rectangular pulse shape is commonly modified to optimize the weld results for a specific task. However, there exists a basic trade-off between penetration depth and weld quality. The prior increases with energy and steep ramp-ups, which at the same time cause a turbulent melt pool and hence complicate the solidification [KAMENZ 2010]. [KAISER & SCHÄFER 2005] show a pulse (initial spark) which improves quality while maintaining the level of penetration when compared to a rectangular pulse.

A discussion on the informative value of the mentioned studies is included in section 6.5. In this section the work's results and the findings of the mentioned sources are systematically compared.

With regard to the given materials and especially their combinations, few studies exist that examine their welding capabilities [SAVARECHIEV & JIE 2004B].

In spot weld micro joining of dissimilar materials the blending of molten components due to melt pool dynamics has been found to outweigh diffusion-driven phase precipitation with regard to the influence on the solidified microstructure. In the latter case the duration is usually too short for this process to occur to an important degree [KLAGES ET AL. 2003]. Therefore pulse shaping can also be a significant parameter for these kinds of joining tasks.

3 Basics of Applied Technologies, Processes and Methods

The fundamentals and theoretical backgrounds of the aspects covered by this thesis are discussed. This includes laser systems and generation of laser pulses as well as laser welding, examined materials and applied methods of DoE.

3.1 Physical Principle of Solid State Lasers

The term “laser” refers to the physical effect of amplifying light from stimulated emission as well as the source of such emissions [HÜGEL & GRAF 2009]. Laser systems convert externally supplied energy into monochromatic light of high intensity.

The process of stimulated emission is one of three basic forms of material-light interaction, the other two being spontaneous emission and absorption. Figure 2.1 illustrates these processes on the atomic scale.

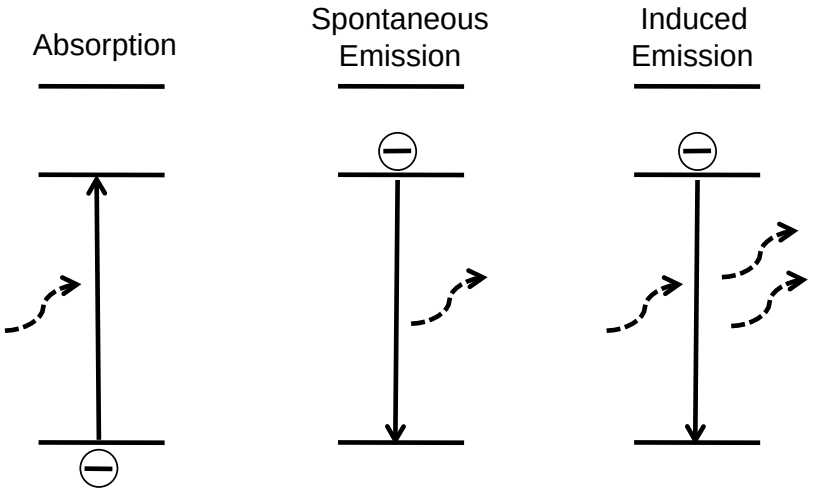

Figure 3.1: Material-light interaction on the atomic scale (according to [EICHLER & EICHLER 2006]).

During absorption, the energy of an incoming photon is consumed by an electron which is elevated to a higher energy level. Spontaneous emission describes the opposite case, in which an electron falls to a lower energetic state under release of a photon. In the case of induced emission the falling to a lower level is initiated by an incoming photon. In contrast to absorption does the electron release a photon itself and the incoming one persists. The two photons are monochromatic and coherent.

In a laser system all processes take place simultaneously. Yet, in order to generate an amplified light beam the process of induced emission has to outweigh the others. Simplified one can imagine the process of amplification to start with a spontaneous internal emission of a photon which sets of several induced emission.

A prerequisite for this concept to work is a higher density of electrons on the high energetic level. Such a state is referred to as population inversion and has to be artificially created by applying external energy. The latter process is named pumping which takes on different forms depending on the gain medium in use.

Instead of the above described two energy levels often three or four levels are applied in practice. Central design parameters are in this case the gaps between the levels as well as the electron probability densities along them. Overall, these should lead to probabilities of movement which favour inversion. Levels with high electron probability densities are referred to as stable in the following. A basic explanation of a four level design can be given with help of Figure 3.2.

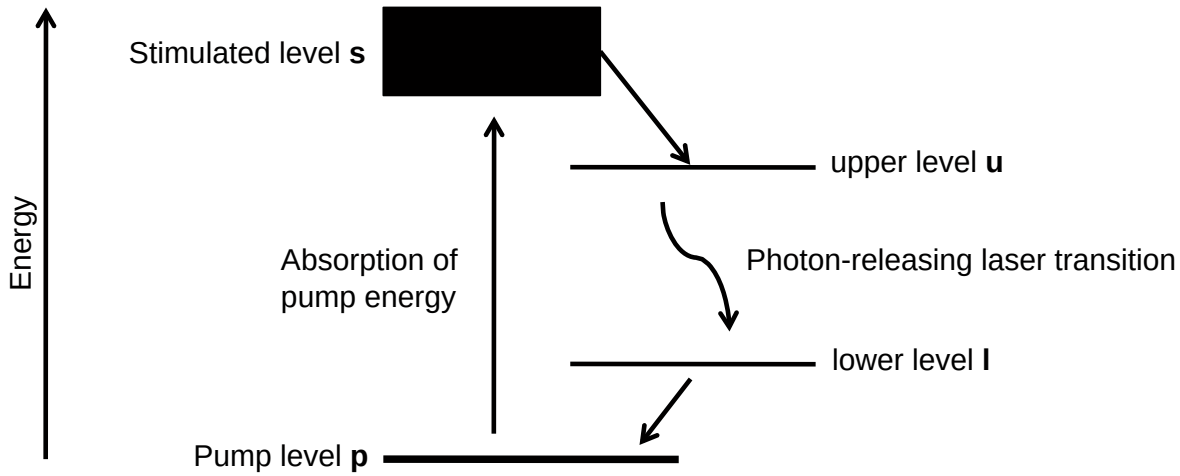

Figure 3.2: Basic concept of a four level laser design (adopted from [Hügel & Graf 2009]).

The figure shows four levels: stimulated (s), upper (u), lower (l) and pump level (p). The upper level is much more stable than its embracing ones. The stimulated level is comparatively wide to technically simplify the pumping (lower precision requirements). From level s to u the transfer takes place without any radiation involved (e.g. phonon-interaction in solid gain media). The stimulated emission process takes place between u and l. From level l the

electrons change again radiationless to a level from which the pumping enables them to return to level s. Since level u is the most stable one transfers from s to u and from l to the pump level are much more likely. Thus, when constantly applying external energy more electrons accumulate the upper level compared to the lower one (automatic fall to pump level) and inversion is achieved. The low electron probability density of the lower level also limits the counteraction of inversion by absorption-driven movements from level l to the upper one.

Given the specific demands on possible energy levels only certain materials are suited for laser systems. These are referred to as gain media. Solid state lasers are characterised by a high stability of the upper levels which increases the inversion and thus the potential to generate optical energy. This is favourable to extract intense pulses with short durations [EICHLER & EICHLER 2006].

3.2 System Design of Nd:YAG Lasers

As the applied laser for the experiments is of the type Nd:YAG in pulsed mode the, discussion focuses on this case. The gain medium is a YAG-crystal (Yttrium-Aluminum-Granat) doped with Neodym-Ions. The electrons within the ions interact with the incoming light as described in Figure 3.2. An advantage of Nd:YAG lasers for metal processing is the higher absorption coefficient for the emitted wavelengths when compared to e.g. CO_2-gas lasers (see [TRUMPF 1994]). In the applied system flash lamps are used for optical pumping. There also exists the possibility of pumping with another laser beam.

To increase the likelihood of induced emissions and overall photon density within the system resonator structures are applied, in which the photons oscillate. A resonator typically consists of two mirrors at the opposing ends of the gain medium. One mirror reflects the light by close to 100%, whereas the other allows for the defined release of laser light (e.g. window or partial permeance). Flash lamps and gain medium are often aligned in a mirrored cavity which directs the flashes to all areas of the gain medium. Furthermore is a cooling system necessary to counteract heat deposition through unabsorbed light as well as phonon related heat spreading within the gain medium. A typical design of a Nd:YAG resonator is given in Figure 3.3. Variants occur e.g. in form of flash lamps surrounding the gain medium as well as the addition of various cooling systems.

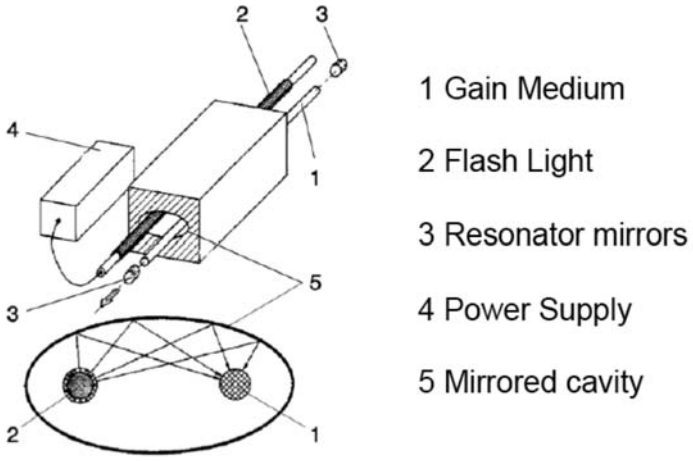

Figure 3.3: Typical design of a Nd:YAG Laser [adapted from TRUMPF 1994].

The components illustrated above are embedded in a central control loop. A possible design is given through Figure 3.4. Starting from a user-defined set value (power, pulse duration…) a reference voltage is calculated with help of of a system model. The latter should include considerations on inertias and dead times which will be addressed in chapter 4. The voltage is produced by a power supply, which activates flash lamp pumping. The produced laser beam is partially deflected towards a photo-diode based PEM-unit (Power and Energy Measurement). This way an action value and hence the measured error can be forwarded to the power supply's controller. The main control factor is in this case the switching frequency of the power supply which is introduced in section 3.2.2.

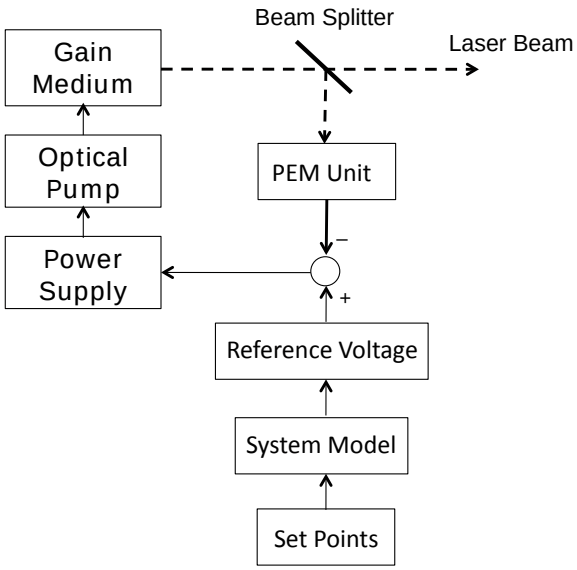

Figure 3.4: Possible system structure of a laser system and its a basic control loop.

3.2.1 Relevant Parameters of Beam Guidance

After leaving the resonator the laser beam propagates through an optical unit. In the applied set-up these structures are connected with a light conducting cabel (lcc). The optical unit typically consists of a collimator behind of which an objective (also referred to as focusing lens) is placed. The collimator serves to parallelise the beam, which widens after leaving the lcc. Eventually does the objective focus the beam to the spot of maximum intensity called ‘focus’. The applied laser beam has a top-hat profile (equal distribution of power over the beam cross section – see chapter 3) which is why the intensity can be defined as applied power divided by beam cross section.

As generally the case when propagating the beam widens again behind the focus. This results in a waisted shape after passing the objective. The intensity of the beam hence decreases before and after the focus. Determining the correct focus position is thus crucial for guaranteeing the maximum efficiency of material processing. If the positioning of the work piece is unstable the laser-matter-interaction may take place “out of focus”. This can result in less penetration. The distance from focus to the points of half intensity is called depth of focus. It is desired to be as large as possible in order to enlarge the positioning tolerance of the work piece [WEBERPALS 2010]. An exemplary optical unit is illustrated in Figure 3.5 below.

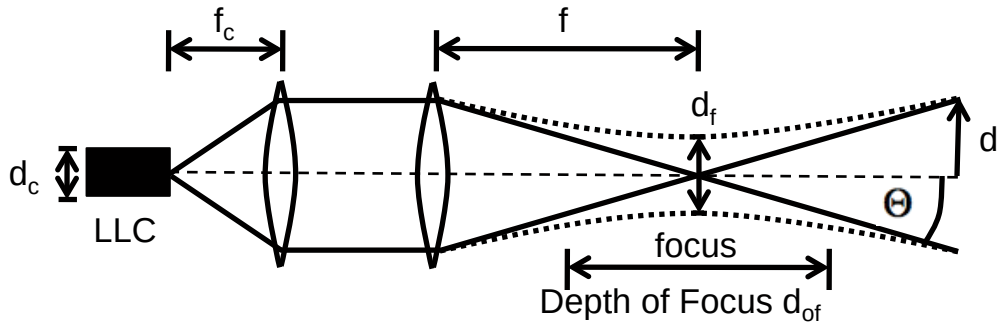

Figure 3.5: Optical unit of a laser system and relevant parameters (according to [PROPAWE 2005]).

The position of the focus and its reachable width (d_f) depend on the focal length of the collimator (f_c) and of the objective (f) as well as the core diameter of the llc (d_c). This is expressed through the following equation:

$$d_f = \frac{f}{f_c} \bullet d_c \quad (1)$$

This approached is based on modelling the beam according to geometric optics. In the following wave-models are commonly applied e.g. in form of so called Gaussian beams. This differentiation is supported by [WEBERPALS 2010] as well as [EICHLER & EICHLER 2006].

According to these models the depth of focus is a function of the focal width as well as the focusability as expressed through the beam parametric product (BPP):

$$d_{of} = 2 \bullet \frac{d_f^{\,2}}{4 \bullet BPP} \qquad (2)$$

The BPP describes a linear relationship of local waist diameter (d) to angle of beam spread (Q). The BPP remains constant throughout any widening or focussing. The equation below shows the respective relation.

$$BPP = \frac{1}{4} \bullet d \bullet \Theta \qquad (3)$$

The choice of the system design thus has a major influence on the reachable process efficiency and robustness. In the experiments equipment with the settings as listed in Table A1.1 was used. According to the equations above, a focus diameter of 300 µm and depth of focus of 2.82 mm is reached by applying a d_c of 400 µm (f=150 mm, f_c=100 mm).

3.2.2 Generation of Laser Pulses

The term “pulse shaping” or “pulse forming” can have different meanings depending on the context in which it is applied.

In the range of nanosecond-pulses and below “shaping” refers to varying pulse durations or peak powers of a constant of basic shape (e.g. Gaussian power density distribution). Such pulses are generated within the resonator itself but are not suited for the given task due to their low energy contents. Instead, pulses of a few milliseconds are applied. These are generated by pulsing the optical pump. When simultaneously modulating the pump’s activity the pulse shape can be altered. The resulting alteration of the relative power distribution over time is the appropriate definition of “pulse shaping” for the scenario at hand.

A simple pulse forming network (PFN) for sparking laser pulses via an optical pump is shown in Figure 3.6. A capacitor is charged by applying the voltage U. The flash lamp is non-conducting during this stage. After charging is completed the voltage is removed and the flash lamp is ionised through an electric trigger pulse (possibly generated by a similar capacitor network). By

doing so, the flash lamp becomes conducting and the energy stored in the capacitor is transformed into a short and intense optical pulse within circuit 2.

The produced pulse will however follow the discharge curve of the capacitor. To generate a more stable pulse several capacitors can be arranged in sequence. The individual discharging is spaced in time with help of parallel impedances. If spaced correctly an almost constant mean voltage can be achieved (see [GENERAL ATOMICS 2012] for details).

Note that in the applied system a simmer trigger is used. A constant current is applied to cause a stable operation of the flashlamp on a low level (102 W in the given system). Following that larger pulses are superimposed to reach the desired power [KOECHNER 1992]

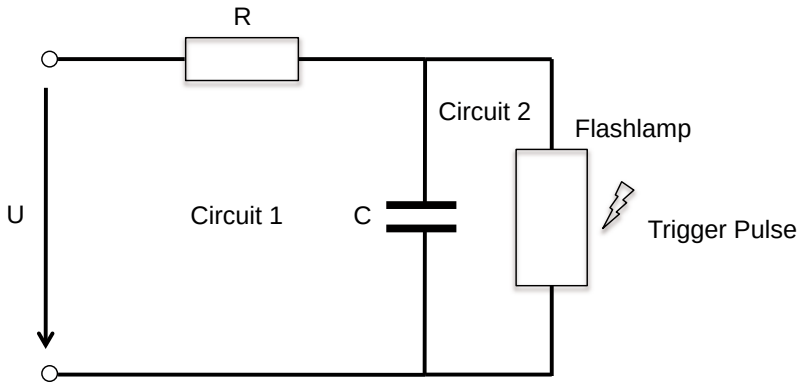

Figure 3.6: Simple pulse forming network for a flash-like discharge.

For modulating the shape of the flash lamp's pulse a continuous adaption of the provided electrical energy is required. This can be achieved by software controlled switched mode power supplies (SMPS) [NAEEM 2004].

As a basic explanation model the energy contents of the sub-circuits of a SMPS are studied. As shown in Figure 3.7 a circuit with an inductance is connected to a circuit with a load (e.g. flash lamp). A switch (field-effect transistor FET) in combination with a Schottky diode (D_{sch}) lets the current flow along different paths. At first the inductance is charged with energy by closing the switch and applying the voltage U_1. Following that the switch opens and inductance is discharged over the load.

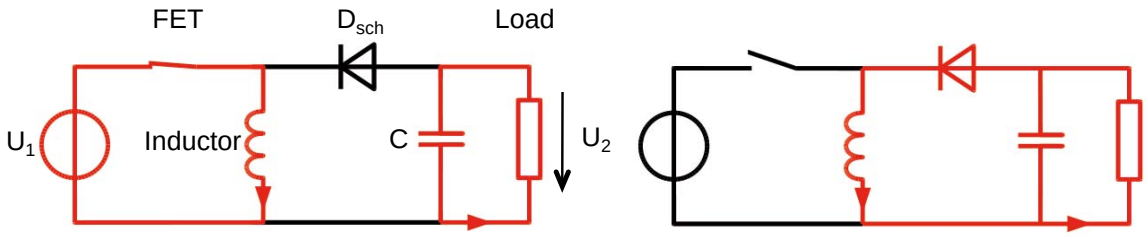

Figure 3.7: SMPS circuit in on- and off-configurations according to [Wikipedia 2011]. The capacitor is used for smoothing the voltage drop over the load when the switch is closed.

[GOßNER 2011] shows that the amount of current through the inductor is equal at both stages. This amount is defined by the times of operation in each configuration. Transposing the inductance equation (eq. 4 and 5 below) and equating these expressions shows that the voltage over the load is equally a function of the switching frequency.

$$\Delta i_{L,on} = \frac{U_1}{L} \bullet t_{on} \qquad (4)$$

$$\Delta i_{L,off} = \frac{U_2}{L} \bullet t_{off} \qquad (5)$$

$$U_2 = U_1 \bullet \frac{t_{on}}{t_{off}} \qquad (6)$$

The time-spans for both operating modes therefore define the generated level of optical and eventually laser power. Switching frequencies in the given application reach up to 20 kHz [WILDEN 2009]. This allows for the discreet approximation of basically any power trace.

Pulse shapes can be programmed in two standard ways for the applied system. In both cases are set-point sequences used as a basis for linear interpolation. On the one hand absolute levels of power and points of time can be set. Alternatively relative levels of power over time can be defined (e.g. 100% of maximum power at 60% of the time as illustrated in the Figure 3.8). This way the relative energy contents of single pulse sectors can be maintained, while scaling the pulse with user-defined input levels of e.g.: peak power and duration.

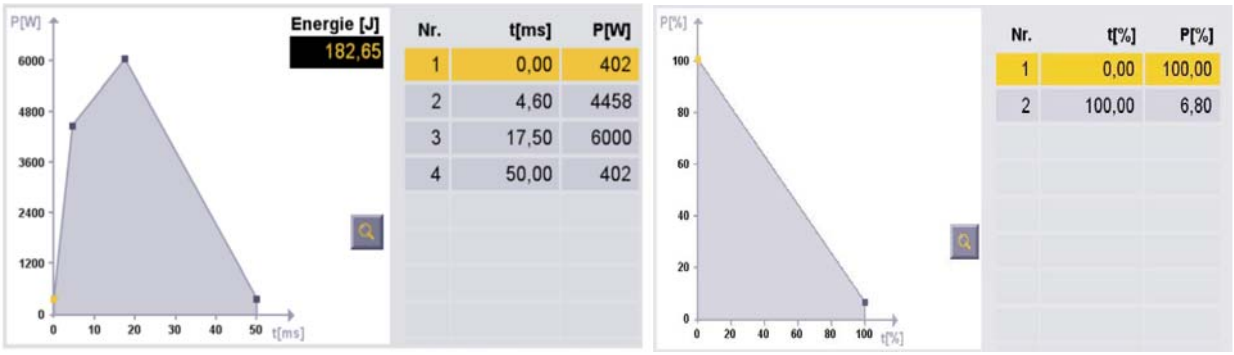

Figure 3.8: Absolute (left) compared to relative (right) programming of the pulse shape (according to: [TRUMPF 2009], [KAMENZ 2010])

3.3 Basics of Laser Beam Welding

In the following the basics of laser beam welding are discussed with respect to laser-matter-interaction, types of welding processes, typical defects and joining of dissimilar metals.

3.3.1 Laser-Matter-Interaction

A lot of different physical phenomena come into play during the interaction of a laser beam and matter. As in any case of interaction between electro-magnetic waves and solid materials the laser waves are either absorbed (as desired), reflected or transmitted. Once absorbed, losses may occur in form of heat conduction away from the emerging melt pool as well as radiation and convection. The latter two are estimated to accumulate to only a few deciwatts and are thus comparatively low with regard to the usually applied centi- or kilowatt-beams [HÜGEL & GRAF 2009]. The full amount of absorbed radiation is however very material-specific. For metals the degree of efficiency regarding absorption for Nd:YAG radiation is rarely above 50 % [HÜGEL & GRAF 2009]. Reflective materials such as copper, brass do not even reach 10 %, aluminium at most 12 % [VDI-TPT 1995].

The absorbed laser waves suffer an attenuation in amplitude which results in an exponential decrease of intensity with increasing penetration depth. In metals the penetration of laser waves amounts to few nanometres. This allows for the modelling of the laser beam as a surface-bound heat source as long as no vapourisation occurs [HÜGEL & GRAF 2009].

The mechanisms and influences of the interactions vary during the different phases of the welding process. These phases are illustrated in Figure 3.9. The discussion refers to the scenario of pulsed spot-welding. Furthermore do the degrees of reflection and absorption depend on the polarisation of the

incoming waves as well as on the angle of incidence [HÜGEL & GRAF 2009]. Both of these factors are however kept constant throughout this work and not further elaborated upon (perpendicular angle of incidence, unpolarised radiation).

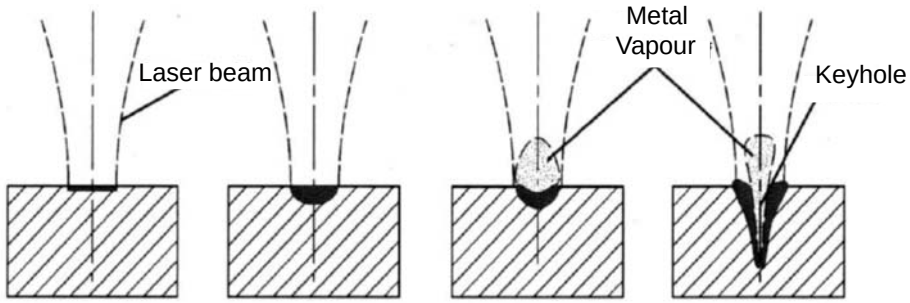

Figure 3.9: Phase sequence of laser beam welding. Note that the process time increases from left to right in low regions of micro- or nanoseconds (according to [BRASSEL 2002]).

Regarding the material the indices of refraction and absorption are highly significant during the interaction. The processes of conduction, melting, vapourizing etc. all involve further matter constants. Last but not least can the geometry of the work piece or joins be of decisive influence as well as pre-existing temperature distributions.

With reference to Figure 3.9 the single phases are examined in detail:

Absorption & Heating Up:

During absorption the incoming wave excites the electrons of the material. The electrons oscillate which is converted into heat. The heat energy then spreads by means of conduction. The efficiency of this phase is counteracted by reflection and transmittance. Due to the short process time of pulsed spot welding the surface roughness (generally increasing the absorption due to multiple reflection) and the formation of oxide layers (limits reflection) are negligible according to [VDI-TPT 1995] (see also section 5.7). Similarly is the temperature influence on the absorption insignificant in the wavelength range of Nd:YAG lasers [VDI-TPT 1995].

Heat conduction welding (HCW):

When reaching the melting temperature, a melting pool is established whose geometry is mainly influenced by heat conduction [VDI-TPT 1995]. As soon as the melting starts the so-called coupling ends. The melt pool grows homogenously and takes on a semicircular shape. With the occurrence of a melt pool, thermal and Marangoni convection come into play as further

mechanisms of energy transport. As the surface activity of the weld pool can generally be influenced by the applied shielding gas, the weld form can be modulated by this parameter as well [VDI-TPT 1995].

Keyhole welding (KW):

If the irradiation continues to the point of vapourisation a transition to keyhole welding takes place. Starting by a deformation of the weld pool through the backstroke pressure of the vapourised material a capillary forms, which further advances into the material. The displacement of material results in a concavity in the melt pool. Multiple reflections enhance the absorption and lead to a sudden increase in penetration. Thus the transition from HCW to KW is erratic and characterized by a threshold value. A stable process occurs when the capillary vapour pressure withstands the pressures of atmosphere and melt pool. Limits in the maximum achievable weld depth are set by e.g. the fraction of already absorbed laser power, which increases with penetration. The formation of a vapour plume may at high intensity also be accompanied by quality-limiting ejection of melt-particles. Note that plasma absorption is not to be expected in the wave length range of a Nd:YAG lasers [IWB 2011]. Overall does the weld take on a wedged shape.

Due to the less dynamic melt pool HCW is usually less prone to defects. Furthermore, the weld surface is rather smooth and the reproducibility higher. It is therefore preferred in the given applications. However, the reachable penetration may not suffice to achieve the desired strengths. The exact nature of the weld regime within the currently applied processes is unknown. It is assumed to lie in the region of HCW to KW transition for the most cases.

3.3.2 Types of Welding Processes

In laser welding the processes are usually differentiated according to the application of pulsed (pw) or continuous waves (cw). Furthermore, it is differentiated according to the production of seam or spot welds.

Spot welds are always the result of pulsed applications whereas seam welds can be achieved both ways. In case of pulsed applications the seam welds consist of a chain of overlapping spot welds. In any case HCW or KW can be applied depending on desired speed and quality. When generating seam welds the parameters speed parallel to longitudinal weld axis for continuous and additionally the pulse frequency for pulsed welding are highly significant.

In single spot welding there exist several parameters that determine the resulting weld. The most important ones are the shape, peak power and duration which define the total energy content. These quantities are defined with help of Figure 3.10.

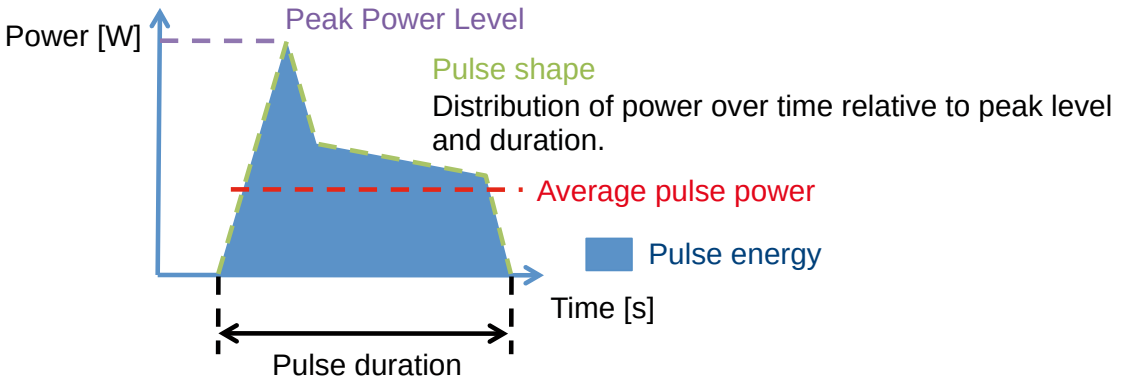

Figure 3.10: Definition of pulse parameters (according to [VDI-TPT 1995]).

As indicated the pulse shape is defined as the distribution of power relative to a set peak power and duration. It is thus comparable to the relative pulse programming technique illustrated in Figure 3.8. The energy is calculated as the absolute power integrated over the duration. The average pulse power is the pulse energy divided by the pulse duration.

Note that the pulse duration is defined as the maximum time interval during which the pulse exceeds half its peak power according to [VDI-TPT 1995]. The latter represents the ratio of pulse energy to duration. Throughout this thesis the pulse duration will however be regarded as the complete time span during which the laser beam is applied. This corresponds to the definition of the control settings of the laser system in use.

3.3.3 Defects

When designing a welding process it is crucial to understand the origins of typical defects. These are discussed in the following without claim to completeness and refer largely to [IWB 2011] and [KELKAR 2011]. Section 2 lists some common strategies in pulse shaping to limit the discussed phenomena.

Pore Formation:

If the gases from the vapourised material or a collapsing vapour capillary cannot reach the surface before the melt pool solidifies pores may occur. This can be caused by a sudden decrease of the energy supply into the melt pool or the diffusion of undesired gases into the weld zone (e.g. by vapourising

deposits on the surface). Apart from these process-related origins pores may also be caused by a high solubility of gases in a specific material (e.g. hydrogen in aluminium [GREF 2005]).

Spatter:

If large intensities are applied the vapourisation may take place explosively and cause the ejection of melt particles. This is e.g. the case if the gradient of absorbed energy exceeds the thermal diffusivity potential of the material. The heat energy is then contained locally in a very small region a may lead to a sudden vapourisation. The expulsion of material from the weld zone can lead to craters, which worsen the surface quality.

Shrink Holes:

Shrink holes are cavities that occur during the solidification process. Causes may be an inhomogeneous cooling rate along the weld, which leads to different densities and thus stresses within the material.

Surface Roughness:

Depending on the course of the solidification process the surface can be smooth, crenated or convex (see section 5.7). The latter can be an indication of pore formation. Furthermore can the surface be waved e.g. from a turbulent melt pool. Crenation can be accompanied with bulging edges. In other cases crenations at the edge itself are possible. Such deficiencies can have a detrimental effect on the mechanical properties of the weld.

3.3.4 Joining of Dissimilar Materials

When joining dissimilar materials the different material characteristics complicate the welding process. This refers first of all to different heat diffusivity and melting points as well as absorption capacities and reflectivity. Overall does this result in a dissimilar coupling efficiency. Combined with the geometry of the join partners, the type of the join itself and potential gap sizes these characteristics mainly define the distribution of the heat energy between the partners. A partner with low thermal diffusivity e.g. tends to accumulate the introduced heat, whereas the partner with high diffusivity may not be able to retain the heat by the same degree. Consequently does this material act as a relative heat source. For overlap joins it is a preferable scenario if the material on top has a high coupling efficiency, high diffusivity and high melting point to conduct as much energy to the second material before melting itself.

When the melt pool has formed the mutual solubility of the components is of high significance. In the optimal case a homogeneous phase forms during solidification. Negative effects can occur in form of brittle intermetallic phases or complete insolubility. The latter scenario requires a bonding of the phases through a third material or the existence of an eutetic which solidifies as a third phase [FRITZ & SCHULZE 2008]. Furthermore can different coefficients of thermal expansion lead to stresses and cracks within the melting zone during soldification.

For these reasons the design of join processes for dissimilar materials goes along with multifarious challenges in each specific case.

3.4 Examined Materials

The material characteristics with special regard to relevance for laser welding are discussed in the following and summarized in Table 3.1 below.

Material A:

Material A is highly resistant to corrosion, which makes it suitable for applications in hostile environments (chemical plants, human body, sea water). The material has been reported to show a susceptibility to cracking during the currently applied laser welding processes.

Material B:

In the molten state, Material B has a high solubility to atmospheric gases. Hence the application of shielding gas is mandatory for high precision welds to avoid discoloration and brittleness. Laser welding is an advantageous method since the material has a high absorption for the Nd:YAG wavenlength and low thermal diffusivity. This favours large penetration depths as large amounts of energy are coupled and contained locally to form a melt pool.

Material C:

Material C is an alloy of biocompatible metals. No studies regarding the material characteristics for laser welding are known.

3.5 Applied Methods of Design of Experiments

The general purpose of conducting experiments with help of DoE is to derive system equations, which quantify parameter influences on quality characteristics. This quantification is hampered by the influence of noise or uncontrollable inputs as shown in Figure 3.11. Uncontrollable inputs are mostly system-inherent (optical unit, material), whereas noise summarizes unknown or random influences on the process (fluctuations in gas supply, measurement

distortions). In order to limit their influence the uncontrollable inputs are to be kept constant. The biasing effect of noise can be limited with help of repetitions (application of means) and randomization of the experimental sequence. The latter also serves to randomly spread trends within the set-up over the experimental population.

In DoE the inputs are referred to as “factors”, which have “effects” on the quality characteristics of interest. The ranges of the factors span the experimental space.

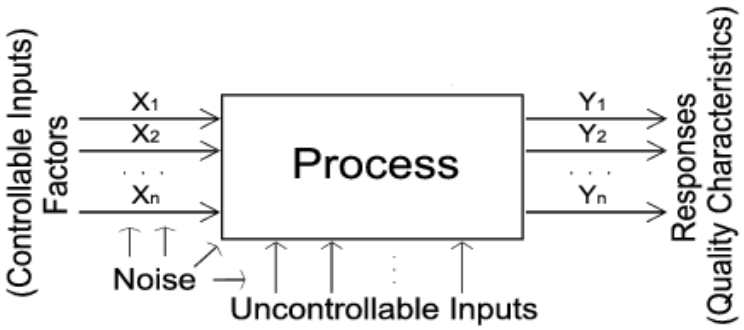

Figure 3.11: Process model as examined during a DoE [ROTH 2011].

A typical sequence of a DoE-based process examination consists of a factorial design through which experimental data is accumulated. Based on that regression modelling is conducted to relate factors and quality characteristics in form of a system equation. This model is statistically verified through an analysis of variances (ANOVA). In the following the single steps are discussed in detail.

Factorial Designs

Figure 3.12 compares typical experimental designs. Two input parameters (x_1 and x_2) and one quality characteristic (y) are considered. The unit E quantifies the closeness to optimum yield in percent. Graph a) shows the actual relation of x_i and y in form of a contour plot. The remaining graphs illustrate various experimental approaches to examine this relation.

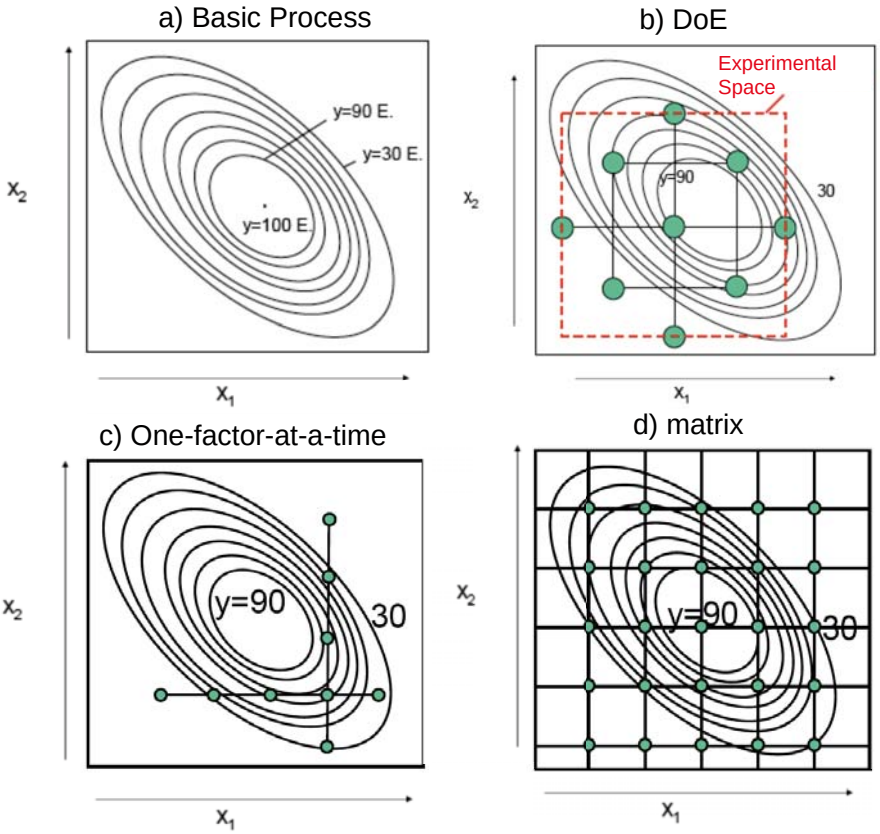

Figure 3.12: Common experimental strategies for examining the influence of parameters x_1 and x_2 on y. The unit E quantifies the closeness to optimum yield in percent [ADAM (2012)].

The “one-factor-at-a-time”-method is exemplified in graph c). The input factors are subsequently varied along their scales. The first factor is kept at the setting at which it delivers the optimal response. Following that the second factor is examined. This procedure is simple, yet leads to a strong interdependence of the factors (effect of x_1 is based on selection of x_2 and v.v.). It also fails to deliver information on the remaining experimental space, which decreases the informational value of a possible system equation.

The opposing extreme is given through the experimental matrix of graph d). In this case the complete experimental space is covered with measurements, which allows for precise modelling of the process. However, the number of required experimental runs is extensive.

A factorial is based on varying the factors independently between specified single levels (see green marks in graph b). This way a large experimental space can be covered and individual as well as interdependent effects are considered simultaneously. The results at the individual levels are employed

for regression modelling. This way the uncovered areas are quantified with help of interpolation.

In its simplest form the design consists of two levels whose values are typically normalized to +1 and -1 (upper and lower level). For three examined factors this can be modelled three dimensionally as shown in Figure 3.13. The matrix shows the complete set of possible factor level combinations and the combinations position in the three-dimensional model. These combinations determine the necessary amount of experimental runs as well as the data amount available for regression. In addition to examining the single factors, the analysis can be expanded by considering their interactions. This is achieved by multiplying the signs of the factors for each possible combination. The purpose of this step is to determine to which degree a factor depends on the level of another one. Commonly this is limited to two-factor first order interactions since other interactions are rarely significant [SCHMITT 2012].

A	B	C	AB	AC	BC	ABC	y
−	−	−	+	+	+	−	y_1
+	−	−	−	−	+	+	y_2
−	+	−	−	+	−	+	y_3
+	+	−	+	−	−	−	y_4
−	−	+	+	−	−	+	y_5
+	−	+	−	+	−	−	y_6
−	+	+	−	−	+	−	y_7
+	+	+	+	+	+	+	y_8

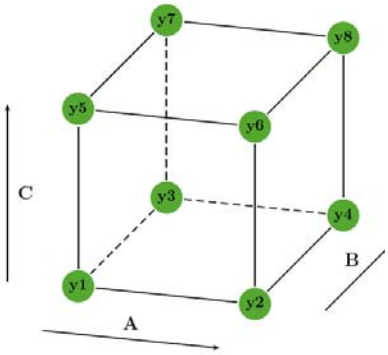

Figure 3.13: Three factor two-level design (according to [SIEBERTZ 2009])

For a two level design only linear relations can be derived. If more factor levels are included nonlinearity can be considered. The relation of number of factors, number of levels, combinations (necessary experimental runs / available data sets for regression) and unknowns for different models is summarized in Table 3.2. The number of unknowns is composed of constant, linear and quadratic terms as wells as the terms regarding interactions (see coefficient b_3 in equation 8). A generalized expression of a linear respectively nonlinear polynomial model is given below.

$$y = b_0 + b_1 \cdot x_1 + b_2 \cdot x_2 + b_3 \cdot x_1 \cdot x_2 + e \quad (7)$$

$$y = b_0 + b_1 \cdot x_1 + b_2 \cdot x_2 + b_3 \cdot x_1 \cdot x_2 + b_4 \cdot x_1^2 + b_5 \cdot x_2^2 + e \quad (8)$$

The variable ‘e’ can contain random errors as a well as systematic errors due to poor fitting of the model [BLAU & HAN 2007].

Number of factors	Number of levels	Combinations	Linear Model No. of unknowns	Quadratic Model No. of unknowns
z	l	z^l	z+1+z·(z-1)/2	2z+1+z·(z -1)/2
2	2	4	4	6
	3	8	4	6
3	2	9	7	10
	3	27	7	10
4	2	16	11	15
	3	64	11	15

Table 3.2: Characteristics of factorial designs regarding the number of factors and levels.

The combinations from three factors onwards indicate that nonlinear modeling (3-level design) becomes unfeasible if a basic amount of repetitions is to be included. An alternative is the application of central composite designs. These designs combine a basic two-level core with one central and several star points (see below).

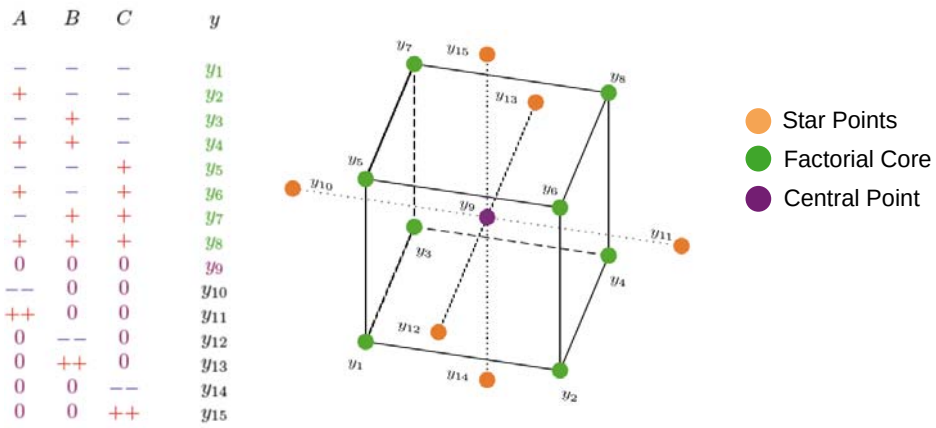

Figure 3.14: CCD-design for three factors (according to: [SIEBERTZ 2009]).

Central points can commonly be applied to check for an expected nonlinearity. For doing so the results actually obtained at central point settings are compared to the results predicted by fitted model. If the difference is larger than the confidence region of the effects (see ANOVA) a linear modelling is insufficient [ADAM (2012)]. In addition can repeated measurements at the central points deliver an estimation of the standard deviation.

Star points provide data for calculating the curvature of a polynomial. The distance of star point to factorial core determines the statistical properties of the design. The best properties are reached when the design is orthogonal as well as rotatable. Orthogonality exists if the levels are set independently of each other (common case for basic factorial designs). Rotatability is reached at dedicated distances of star-points to center-point depending on the number of factors. As a result, equal precision of estimations throughout the experimental space is given. To avoid correlations of the curvature terms several runs of the central point are necessary. The respective relations and required distances and repetitions for CCD-plans are given e.g. in [BLAU & HAN 2007].

The examples described so far full factorial designs. This means that all linear as well as interaction terms are determined. If an interaction is regarded to be negligible it can be replaced with another factor which is varied with the respective setting instead. This strategy is applied if a simple “screening” of the parameters to determine the most influential ones suffices. On the downside does the quality of the results decrease depending on the amount of substituted terms. This is because effects for single parameters become increasingly confounded with other factors or interactions.

The key figure “effect” compares the change of a quality characteristic when varying a factor from upper to lower level. Its computation is simple for two-factor designs and can directly be read from the experimental results. For more factors an ANOVA has to be carried out as discussed at the end of this section.

Regression:

Based on the experimental results multiple linear regression is carried out by applying the least square method. The term linear is applied since all polynomial coefficients are assumed linear [RELIASOFT 2008]. The data sets retrieved from e.g. a two-factor factorial design scatter around an area in the x_1-x_2-y coordinate system as illustrated below. This area is the actual regression model which is to be determined during the analysis.

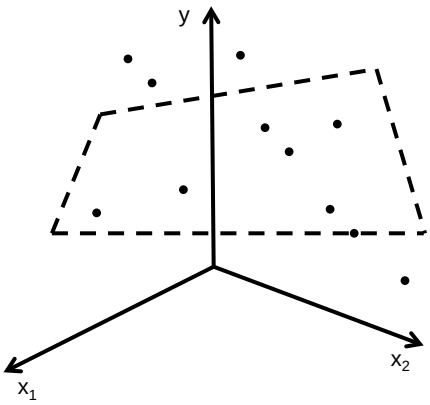

Figure 3.15: Fitted regression plane with scattering data sets for a random example.

In least square fitting a system of equations relating y and x is derived from the acquired data sets. An error quantity r (residual) is defined which describes the difference between actual data and fitted model as a function of the unknown polynomial coefficients. The number of variables is p. The number of observations is n. This is expressed through the following equation:

$$r = X \bullet b - Y \quad (9)$$

with

$$r = \begin{pmatrix} r_1 \\ \vdots \\ r_n \end{pmatrix} \quad X = \begin{pmatrix} 1 & x_{11} & \cdots & x_{1p} \\ \vdots & \vdots & \ddots & \vdots \\ 1 & x_{n1} & \cdots & x_{np} \end{pmatrix} \quad b = \begin{pmatrix} b_1 \\ \vdots \\ b_n \end{pmatrix} \quad Y = \begin{pmatrix} Y_1 \\ \vdots \\ Y_n \end{pmatrix}.$$

An optimal choice of the coefficients minimizes the residuals. Hence a minimization problem is given in the form:

$$\min_{b_1 \ldots b_n} \sum_{i=1}^{n} r_i^2 \quad (10)$$

The residuals are squared to emphasize strong outliers. Summing the squared residuals leads to an equal consideration of all data points and thus overall best fit. For the minimization problem explicit solutions exists depending on the degree of the model (see e.g. [CRAMER & KAMPS 2007]).

As a concluding step, the residuals for the calculated best fit need to be evaluated. In a typical residual plot the difference between real data and fitted polynomial are contrasted. One typically checks the feasibility of the fit by evaluating the amount of strong outliers (distorting effect) and a potential systematic distribution of the residuals (wrong model / polynomial degree, trends over trial population). The fit of the model can be evaluated the by considering the coefficient of determination R^2 as defined by the equation

below. The variance SS_{tot} of the accumulated data is considered by summing the squared difference of single observations (y_i) to grand mean ($\bar{y}$). This is divided by the error quantity SS_{err}, which sums the squared difference of observations and data predicted by the model (f_i).

$$R^2 = 1 - \frac{SS_{tot}}{SS_{err}} = 1 - \frac{\sum_i (y_i - \bar{y})^2}{\sum_i (y_i - f_i)^2} \quad (11)$$

An ideal congruency results in a R^2-value of 1. For far lower values must the model be reconsidered. In the same way does the confidence interval of the fitted model allow for an estimation of quality of regression. Typically a band at a confidence level of 5 % according to Working-Hotelling is constructed. The less wide the confidence band, the better the fit. Figure 6.8 and Figure 6.10 show respective examples.

In order to identify outliers a test according to Grubbs is applied. A graphical illustration of this procedure is given in Figure 6.10 in form of a normal probability plot. The residuals are plotted against the cumulated frequency of the complete population. If normally distributed, the data points lie along a straight line with the most data points around 0 (residual) and 50 % (cumulated frequency). Outliers are identified depending on their distance to the expected straight line and marked red in the plot. For more examples please consider [HART & HART 2012].

ANOVA:

The ANOVA method is applied to determine whether potential factor effects are statistically significant at given levels of confidence. By eliminating insignificant factors can the system equation be rendered more precisely.

At first the factor effects are determined. The experimental data are grouped for each factor according to its levels (e.g. A- and A+). As initial step the variances (or “sum of squares”) are calculated. These are in principle residual values which compare an individual data point of a group to a mean. Two sums of squares are considered. The sum of squares within groups (SSW) adds the squared residuals between group data and the groups’ mean. The sum of squares between groups (SSB) sums the residuals between group mean and mean over all measurements for each data point. The results are added to form the “total sum of squares” (SST). The discussed expressions are defined by the equations below. The index i refers to a single data point. The index j to a single group within the data. The combined form ij stands for the i-th measurement within the j-th group. Averages are marked with an

overscore, the grand mean $\bar{\bar{x}}$ with a double overscore. The experimental population consists of n observations and k groups.

$$SST = SSW + SSB = \sum_{j=1}^{k}\sum_{i=1}^{n}(x_{ij} - \bar{x}_j)^2 + n\sum_{j=1}^{k}(\bar{x}_j - \bar{\bar{x}})^2 \quad (12)$$

The sum of squares SSB represents the fraction of total variance that can be attributed to a changing factor level. This represents the actual effect. In the SSW the factor level remains constant. Thus, the occurring variance is interpreted as error or noise [SIEBERTZ ET AL. 2010]. Comparing the SSB for all main and interaction factors results in a hierarchic overview of factor influences with reference to the normalized coordinates.

The final assertion of the factor effects is achieved through considering the mean squares (MS). These divide the measures SSB and SSW by the available degrees of freedom (DOF). In case of the SSB the DOF amount to number of groups (=available factor levels) minus 1. For the DOF of the SSW the number of groups is subtracted from the total amount of observations – see equation 13 below. Practically does the MS reward factors which require less levels to reach a certain effect. It is thus a more precise measure when judging the effect of a factor [SIEBERTZ ET AL. 2010].

Eventually, a statistical hypothesis test is carried out to judge whether an effect is significant. This is especially relevant for eliminating factors with low SSB-values. The zero hypothesis: “the factor has no significant effect” is tested by considering the quantity F:

$$F = \frac{MS(SSB)}{MS(SSW)} = \frac{SSB/_{k-1}}{SSW/_{n-k}} \quad (13)$$

The quantity F will show a probability distribution depending on DOF in denominator and numerator (typically identical for the considered factorial designs). In case the 0-hypothesis is true the effect measure MS(SSB) and the no-effect measure MS(SSW) are equal and F will be one. Based on this distribution a confidence interval is defined for the actually received F value. Hence, a probability value (p) can be determined for having mistakenly assumed the significance of a factor. Throughout this thesis a threshold of 5 % is set as maximum for the p-value. Factor effects with larger values are regarded as insignificant.

All in all does the ANOVA render possible the elimination of those factors whose effects are low (SSB-value) or by a high possibility produced by chance (F-probabilty test).

In the previous sections the theoretical foundations of the thesis were introduced. Starting with the investigation on pulse-shaping capabilities, the experimental work is discussed in the following.

4 Investigation on Pulse Shaping Capabilities

Systematic comparisons between set and actual values of pulse shapes are examined for the laser system in use. At first the experimental set-up is verified and suitable measurands for quantifying occurring deviations are defined. The deviations found to be most relevant are examined in dedicated experiments. Eventually criterions are derived to evaluate the expected quality of set-point following.

4.1 Background and Motivation

It is known from experience that the set-point following of lasers typically applied in the given context is not ideal. Figure 4.1 displays a spectrum of possible pulse shapes as set by a user. The main geometric elements are (rectangular) edges, constant power levels or slopes as defined by the programmed set-point sequence. In order to guarantee a high informational value of the results the real pulse shapes should not critically deviate from the intended ones. Therefore, a criterion is needed to judge whether correct shaping can be achieved for each of these elements. The set-point spectrum can then be constricted accordingly to guarantee a satisfying performance.

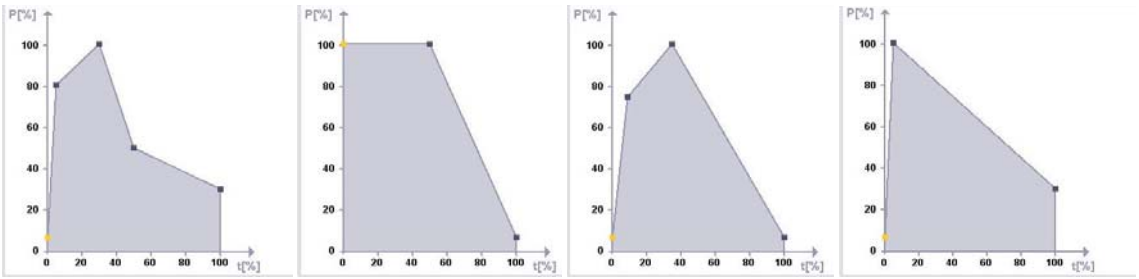

Figure 4.1: Pulse shapes containing various geometric elements (single shapes according to [KAMENZ 2010])

The limitations in achieving precise set-point following result from various non-linearities within the control loop (compare section 3.2.2). Figure 4.2 shows the power trace of a flash lamp's power supply and the resulting laser beam for a rectangular pulse. Typical deviations can be observed in form of non-perpendicular slopes at the edges. The systems show also a slight inertia when being switched on. Furthermore does a dead time occur in form of a delayed begin of the laser activity. When switching off, the resonator's activity decays slower than that of the lamp's power supply. Consequently will the laser pulse persist longer than set. This is an indication of ongoing oscillations within the resonator.

In the following such deviations are systematically examined and quantified.

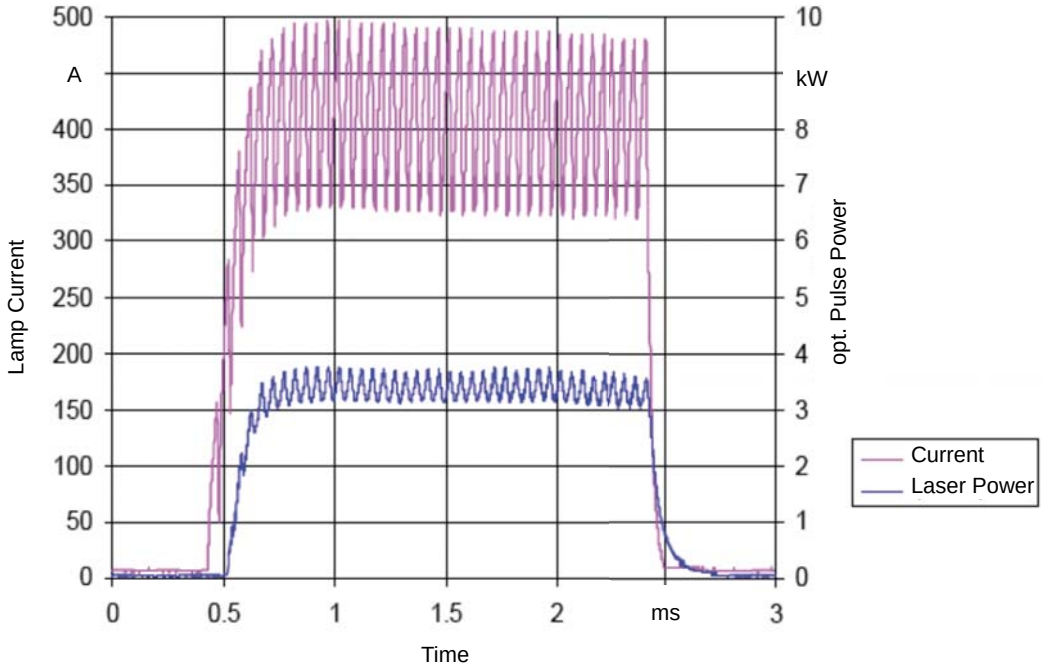

Figure 4.2: Comparison of lamp current and generated laser power in a Nd:YAG system (adopted from [DÜRR ET AL. 2006])

Contrary to the non-ideal performance along the time scale is the capability of the laser system to deliver the correct absolute power levels considered to be acceptable. Possible wear of e.g. the flash-lamp is equalized by closed loop measurements and adjustments of the power supply. The system generates an automatic warning in case the adjustments exceed a threshold and the lamp must be exchanged. Furthermore has the intensity been confirmed to show a top-hat profile in an internal study by the company (applied measurement system: “Primes BeamMonitor”).

Thus the main focus of the experiments lies on the relative course of power over time. This remains a major unknown characteristic of the laser system in use, which could cause discrepancies between expected and actual pulse.

4.2 Experimental Design and Set-Up

The limitations in set-point following are observed with help of a rectangular, triangular, trapezoidal and a “double-step” pulse. These pulses are programmed relatively (see Figure 3.8) and varied over time and peak power. The combination of time and power level determines the set-point position and hence the demanded control action from point to point. Large steps in power during short periods of time are e.g. expected to be critical tasks.

This procedure allows for an observation of possible deviations over continuous scales while maintaining a reasonable amount of experimental runs. The results cannot be extrapolated to the remaining experimental space (see one factor-at-a-time method in section 3.5). This is mainly because interdependencies of the factors power and duration are not considered. However, from experience and from observations throughout the following experiments the results seem representative for the uncovered areas as well.

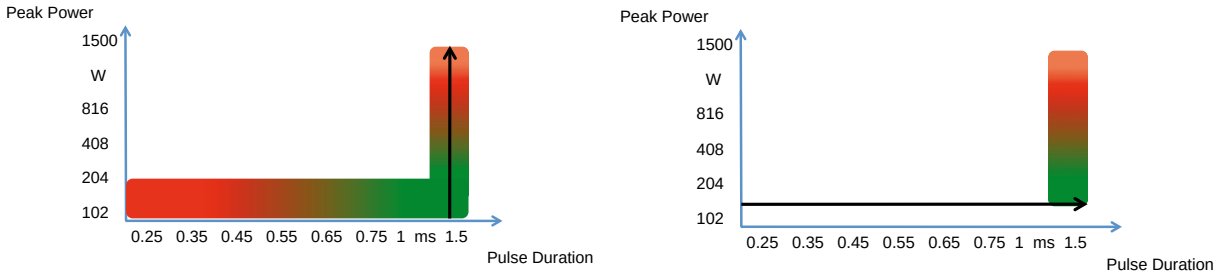

Figure 4.3: Experimental procedure for examining pulse shaping capabilities for a rectangular pulse. The "power series" is displayed on the left; the "time series" on the right. The colouring of the axes is adapted to the regions expected to be critical for pulse shaping due to high control demands.

The set-up consists of a laser of the type Trumpf TruPulse 21 which is applied to a highly reflective brass foil. A photo-diode with high sensitivity for light in the wavelength range of Nd:YAG lasers is pointed at the brass surface to record the reflected radiation. The sensor signal is amplified with different settings to control the maximal signal strength. Thus the absolute values of power- and time series are not comparable even though they cross at 102 W and 1.5 ms. The recorded data are visualized with an oscilloscope and converted into comma-separated values (.csv). This allows for the analysis in Matlab (Version: R2010b). The complete set-up is shown in Figure A1.1. For this experimental series the working height is reduced so that the beam hits the metal surface strongly out of focus. This prevents coupling.

At first the lowest possible power level at which stable pulse generation is observed is determined for each pulse shape. The system-inherent lower bound is 102 W. Following that the pulse duration is varied from 0.25 ms to 1.5 ms at this minimum level (referred to as "time series"). In lower time regions smaller steps are applied. This is due to the high interest in regions of low pulse energy, which are especially relevant for many applications. In the second measurement series ("power series") the duration is kept at 1.5 ms and the peak-power is raised stepwise to 1500 W (system-inherent upper

bound). In each case the measured pulse signal is analysed qualitatively and quantitatively with help of measurands introduced below.

The most relevant observations made during this first stage are further examined in dedicated investigations with a higher number of repetitions.

To quantify the observed deviations the following measurands are introduced.

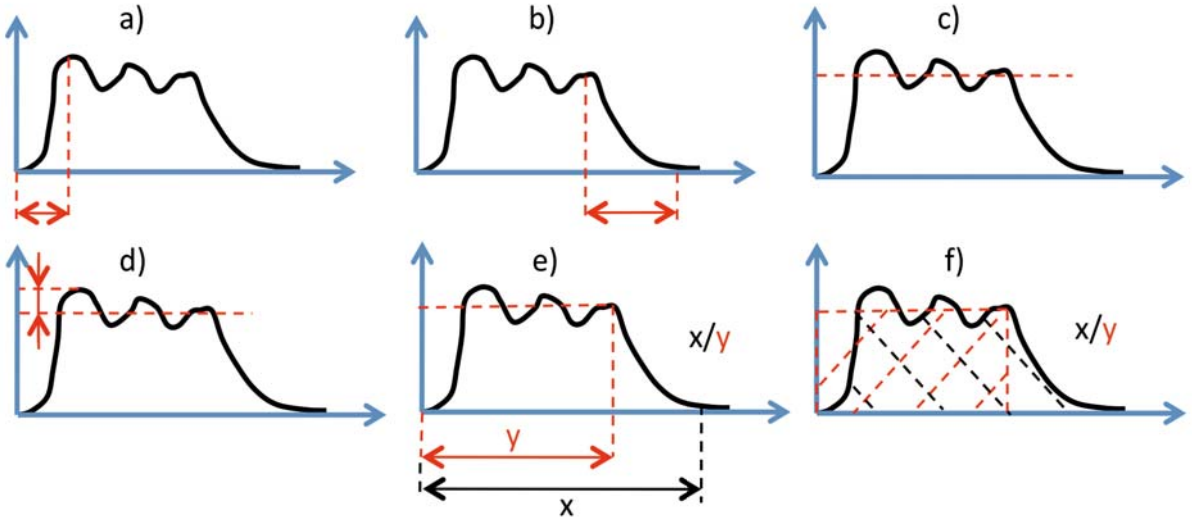

Figure 4.4: Quantities for judging set-following quality during pulse shaping.

From a) to f) the definitions are as following:

a) *Delta On* [s]: Time from start of the pulse until first point of inflexion (only relevant for rectangular edges).

b) *Delta Off* [s]: Time from the point of inflexion at the off-edge until reaching the basic level.

c) *Mean of Peak Level* [mV]: Mean level of sensor signal taken for all points between first and last point of inflexion at the peak level. For triangular shapes only the peak point is considered.

d) *Overshoot* [%]: Relative excess of the peak mean by the maximum of the sensor signal.

e) *Duration Ratio* [%]: Time between start and end of the pulse divided by the set time.

f) *Area Ratio* [%]: Area under the sensor's signal curve divided by programmed area. This represents the ratio of action and set energy.

These definitions may also be applied to intermediate steps within pulses e.g. the Delta On can also be taken for the second rising edge of a double-step pulse. The area ratio is calculated automatically by comparing the ideal shape

to the area under the csv-data (trapz-function in Matlab). All other values are based on the manual selection of the characteristic points.

Note that the area ratio is the result of the interactions of various other deviations. In this case it is extremely significant to compare the mere figure to the qualitative result. A ratio of 1 (meaning 100 % congruency) does not automatically guarantee sufficient shaping. Instead two unacceptably large deviations may neutralize each other to produce a zero effect on the area (see 4.4.1).

By applying the quantities defined above one can determine whether a deviation is constant, produced by chance or shows a trend along the scales. In combination with the qualitative analysis the existence of unacceptably large deviations can be determined. A deviation is deemed unacceptable in e.g. the following cases:

- Dominating Overshoots - meaning that over large period the actual intensity is higher than set.
- Large Duration Ratios - meaning that the time for energy coupling at a given power level may be too short or long.
- Large Deviations in Slopes - meaning that the desired heating or cooling gradients are not achieved. This can also lead to not reaching the desired peak level on time if the produced slope is too small.

In all of these cases will the pulse show a strongly biased outcome.

4.3 Capability Analysis of Measurement Equipment and Methods of Analysis

In order to evaluate the informational value of the available measurement data a rectangular pulse is measured repeatedly five times at 102 W and durations of 0.25 ms, 0.5 ms and 0.75 ms. The qualitative result is shown in below.

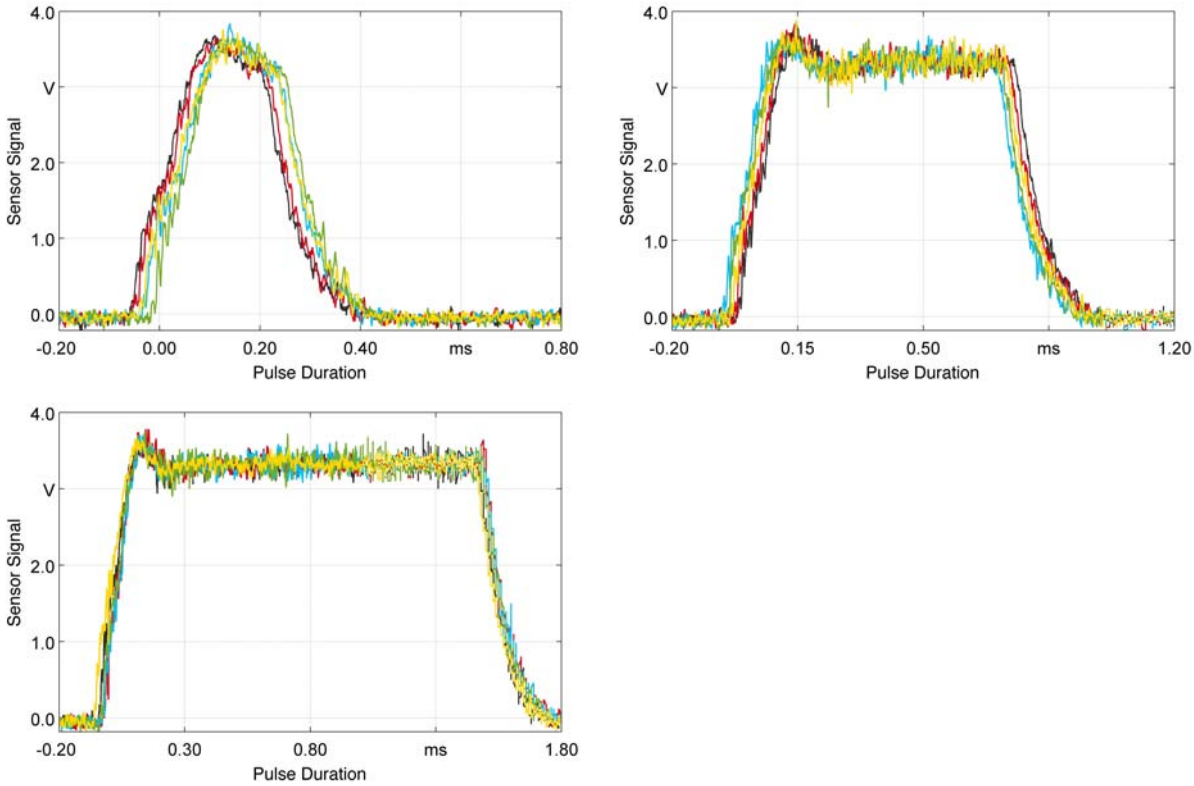

Figure 4.5: Five repeat measurements for a 102 W rectangular pulse at 0.25 ms, 0.75 ms and 1.5 ms

It can be seen that the measurements show large congruency in relevant regions (start, stop, overshoot etc.). A slight offset is observable between the individual slopes of rise and fall. This can be attributed to variances in the triggering of the oscilloscope due to noise. The trigger level is the lower signal bound at which the measurement is automatically started. Overall, the repeatability of the sensor signal is sufficiently accurate. This is confirmed when considering the observed scattering of the “area under pulse” in form of a boxplot as shown below. Boxplots are a graphical mean for displaying the scattering of a data set. The mean, first and third quantile are combined to form a box. So-called whisker are added to show the extent of the remaining data. The width of these sections indicates the level of scattering (see [MATHWORKS 1999] for additional detail).

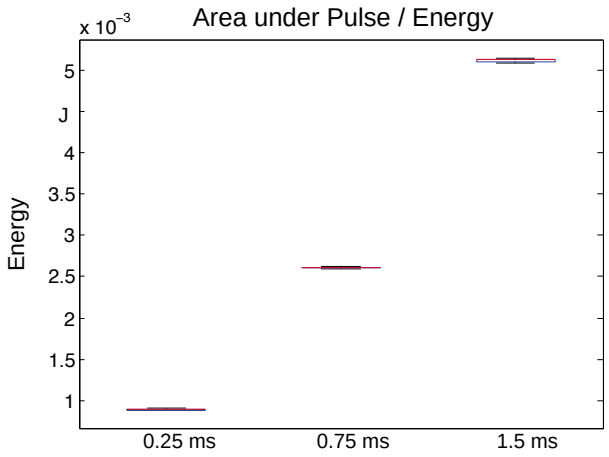

Figure 4.6: Boxplot for the area under the pulse (energy) for the repeat measurements of Figure 4.5.

Clearly, little or no variance is observable. This means that the generated pulses respectively the measurements deliver continuous and repeatable results.

From the measurement series illustrated in Figure A1.7 the peak means are measured and plotted in Figure 4.7. It can be seen that the sensor signal is proportional to the set power. It is therefore possible to calculate expected values of the sensor signal at any power level for measurements carried out under the same settings. This is employed for set-action comparisons of triangular and trapezoidal pulses. In all other cases the peak means are taken as expected set values (for the time-series the peak mean at 1.5 ms was chosen). These are needed to calculate the “Ratio”-measurands defined above.

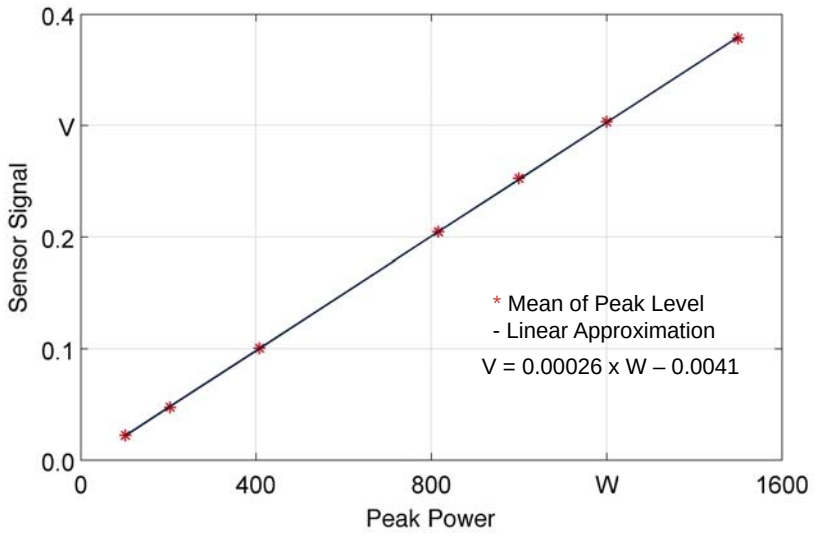

Figure 4.7: Linear relation of sensor signal and set-power derived from measurements of the rectangular power-series.

Figure 4.8 summarizes the variances of the introduced measurands for the repeat measurements in form of boxplots. Large scattering occurs in case of measurands which depend on the manual selection of relevant points. For values that are merely based on single points (e.g. Delta On) the scattering of repeat measurements is especially critical. Quantities which are based on averages perform better even though they may depend on manually selected boundaries (e.g. Mean of Peak Level). Especially at low durations this selection is complicated by comparatively poor shaping (compare e.g. Figure A1.10). Above 0.75 ms the measurements can be generally regarded as representative based on the scattering displayed below.

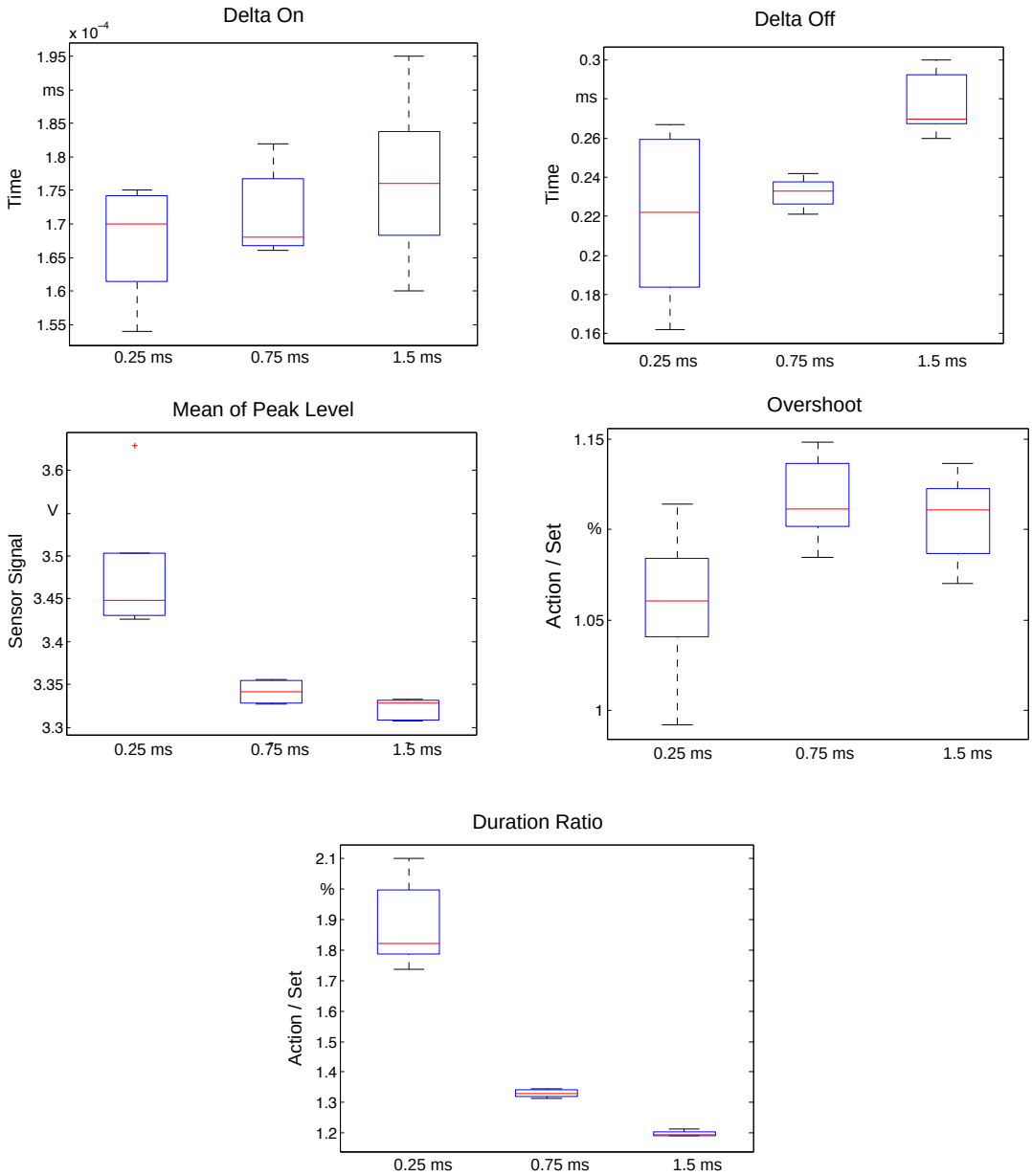

Figure 4.8: Boxplots on measurands taken at five repeat measurements of a 102 W rectangular pulse with varying duration.

In summary one can say that the measurement system's accuracy is satisfying. Yet, the quantitative analysis may be limited in its repeatability in the case of time-based values and for durations below 0.75 ms.

4.4 Results of the Measurement Series

Starting with a basic rectangular pulse the experimental results found to be relevant for defining operating ranges are compiled in the following. The complete sets of measurement graphs are included in appendix A section A1.

4.4.1 Rectangular Pulse

The qualitative analysis of the time series as shown in Figure A1.4 shows that a constant overshoot occurs following the rising edge. From the quantitative measurements in Figure A1.5 it is found that the desired power level is exceeded by around 10 % on average.

With help of the quantitative examination it is further found that the slope at the rising edge is constant with a Delta-On value of ca. 175 ms. At the falling edge the time of decay appears to rise with longer durations. This can be confirmed when considering the boxplots in Figure 4.6, which are based on the same parameter settings. The area ratio is rather stable and low. This is because the amount lost by the slow rise is equalized by excess energy from the overshoot and the delayed decay.

The power-series shows that the overshoot is significantly reduced at higher power levels (see Figure A1.8).

4.4.2 Double-Step Pulse

The minimum power level for generating a double-step pulse with equal power steps is 204 W since the intermediate step must lie above the system's lower bound of 102 W. The pulse duration is divided equally between the three vertical rectangular segments. The purpose of this design is to judge whether the application of further edges can e.g. limit effects such as overshoot. Furthermore it is to be examined whether higher rise times can be expected when starting above the initial lower boundary of 102 W.

In the analyses the indices one and two refer to first and second rising respectively falling edges. The three peak levels are equally numbered from one to three along the time axis. As shown in Figure A1.13 an overshoot occurs at the on-edge as known from the common rectangular pulse. At the second edge this is not the case. It can furthermore be seen that even though

the same step size is applied the Delta On is much smaller for edge 2 (see Figure A1.14). This is because the initial rise to 102 W is quite slow.

All in all very accurate set-point following along the time axis can be observed. Yet, due to the non-ideal rise time the top levels are severely reduced in duration. Consequently does the central power level not even reach 80 % of its desired duration (see duration ratio in Figure A1.11). The levels following a falling rectangular edge are equally reduced in duration since the fall time is non-ideal as well.

4.4.3 Triangular Pulse

The measurement series show that almost arbitrary slopes can be achieved at both edges. On the other hand does a fixed step response become apparent when starting the pulse. This refers to the initial jump to the minimum level of 102 W under roughly 45° (see Figure A1.19). Only after this jump is the power directed towards the desired peak value. This can be attributed to the application of a simmer trigger circuit and correlates with the ionisation curve of the flash lamp [KOECHNER 1992]. Such an initial response also takes place in case of the rectangular edges but becomes more obvious for non-perpendicular slopes. In lower power regions does this deviation from the ideal triangular shape result in a significantly large area ratio (see Figure A1.26).

An upper bound of the angle of inclination becomes apparent when considering the peak levels of the time-series in Figure A1.16. Instead of the expected constant peak of around 0.21 V a shortfall of up to 15 % can be observed at short durations. Similar to the observations on the duration ratio for double-step pulses does the control rate appear to be too small to reach the desired power level on time.

4.4.4 Trapezoidal Pulse

The pulse duration is divided equally between rising edge, peak level and falling edge. The observation of a limited rise time can be confirmed as well as the observation of a constant initial step. Other than that it was found that transitions from slopes to horizontal levels and vice versa can be achieved without problems.

4.5 Conclusions

Three noticeable deviations with the potential to decisively bias the pulse shape were identified above:

1) overshoots at rectangular edges for low power levels.

2) a general upper-bound for rise and fall times.

3) a fixed initial step to 102 W.

For each case limits are to be defined above or below of which the deviation is considered negligible. The remaining spectrum defines the range of possible set-point sequences for the following investigations.

Overshoots:

To limit the possible influence of overshoots on the resulting weld, it is defined that the minimum duration of a constant level following a rectangular step is to exceed the time until the overshoot fades out by a factor of two. The amount of overshoot was observed to be a function of the step height. Hence, a special measurement series is carried out with two runs per setting (n=2). Steps from 102 W to 1500 W are set off and the level of overshoot is measured (see below).

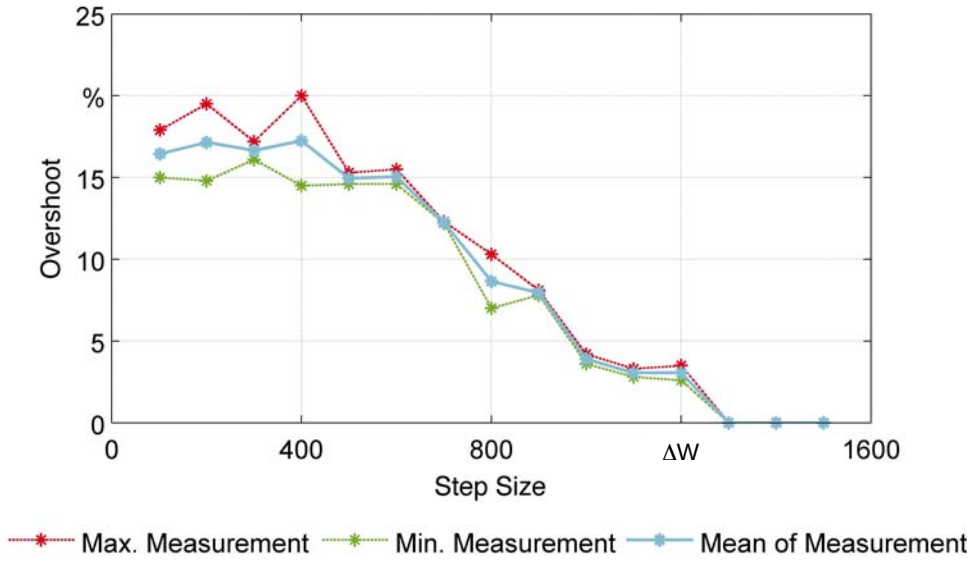

Figure 4.9: Overshoot following rectangular edges for different step sizes (n=2).

As expected, the overshoot is very critical in lower regions of the power spectrum. Above 900 W the overshoot can be regarded as negligible. The minimum durations necessary to equalize the overshoot are compiled below. Rectangular pulses are raised in their duration in increments of 0.05 ms until the duration suffices to fulfil the criterion defined above. Due to the size of the increments no scattering was observed. The determined duration defines the minimum time for rectangular edges applied in the following.

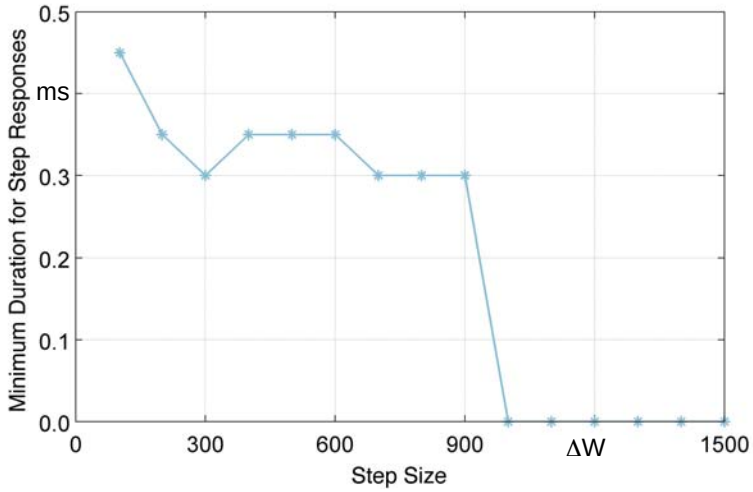

Figure 4.10: Minimum time to exceed the duration of the overshoot by a factor of two (n=2).

Rise and Fall Times:

The minimum rise time of a system is by definition determined from its step response. Hence, rectangular pulse edges are measured at increasing step heights. The time to reach the set-point level is measured and plotted below. As observed during the series on double step pulses, higher rise times can be expected for actions above 102 W. Therefore edges from zero and from above 102 W are measured independently. The responses show a linear increase of minimum time over step height. For steps from zero the response time decreases at first before showing a linear increase (compare e.g. Figure A1.7). For these measurements the scattering as expressed through the coefficient of variation (CoV= standard deviation/mean) was found to be negligible at around 5 %.

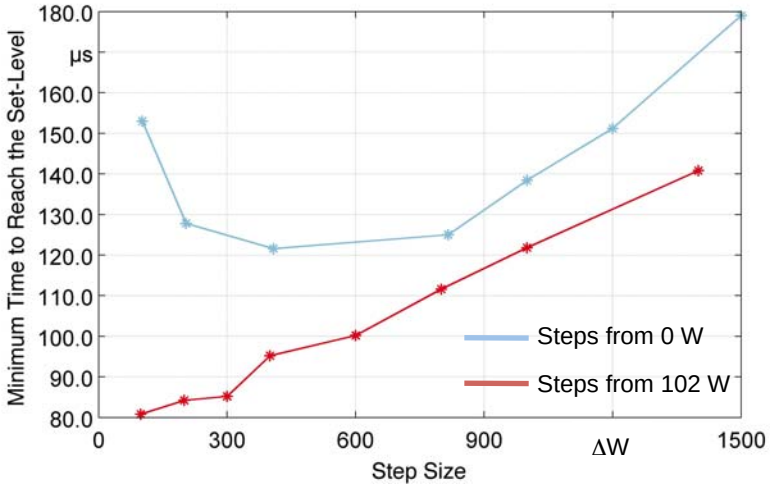

Figure 4.11: Minimum time to reach a given set-point level for rectangular steps (n=5).

When dividing the set-point level by the required minimum time the available rate-of-rise for the respective step height can be derived. As shown Figure 4.12 does the available rate increase almost linearly before it slowly flattens. This behaviour can be approximated with a second-degree polynomial (see Figure A1.27 and Figure A1.28). The curve can be applied to judge whether two set-points are too close too each other for carrying out a given step. The resulting loss of duration for a succeeding constant level can be equally estimated.

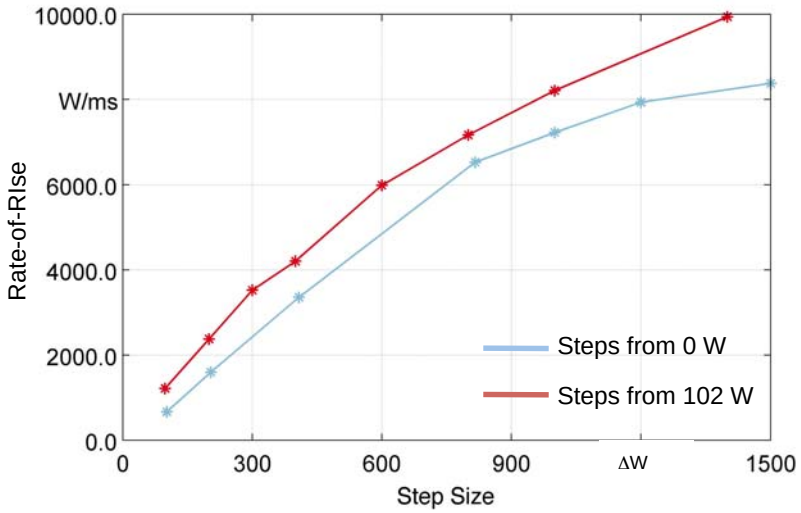

Figure 4.12: Rates-of-Rise for given step heights (n=5).

For this measurement series the time values are determined “by hand” similar to the Delta On measurements (applied oscilloscope software: FlukeView). Rectangular (steps from 0 W) respectively double step-pulses (steps from 102 W) are programmed with a duration of at least 2 ms. The step’s end point is defined as the first point of time at which the set-level is reached. Figure 4.13 shows a decrease of the slope at around 5 % below set-level. This was observed for steps from 102 W to 1000 W and above. The end point was in this case defined as the last point up to which the steep slope was maintained.

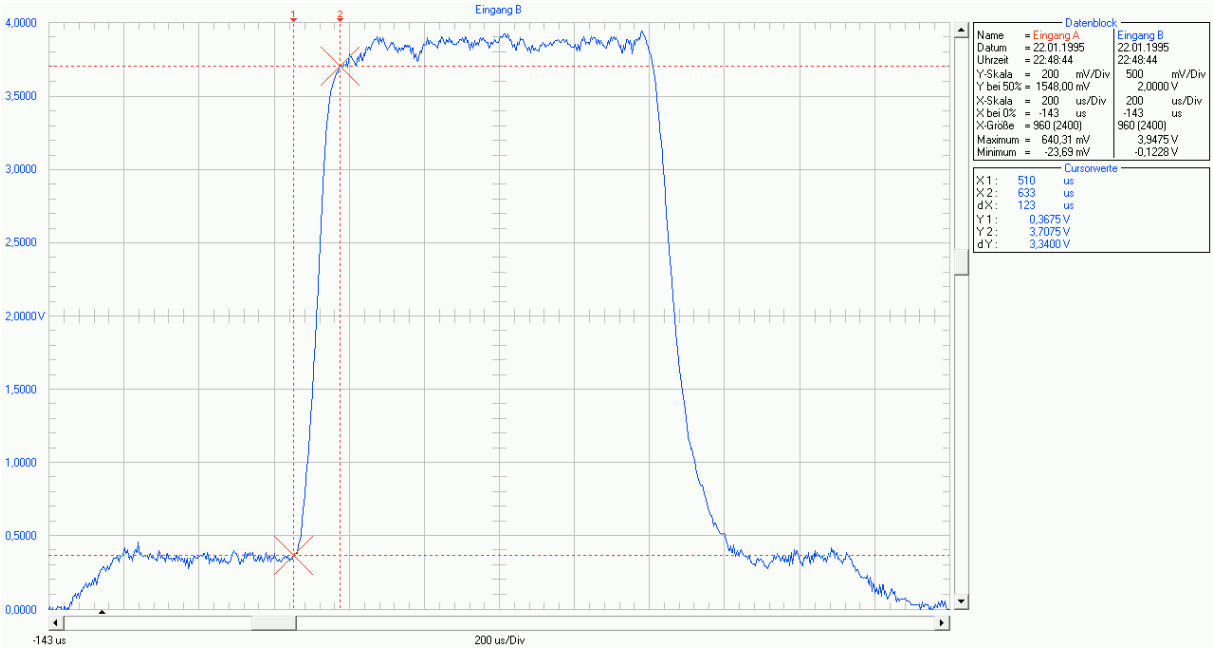

Figure 4.13: Screenshot of the oscilloscope's software showing the selection of relevant points as well as the occurring undershoot (1000 W double-step pulse). The horizontal line of the upper cursor should normally approximate the median of the peak level.

Falling rectangular edges generally consists of a steep decay followed by a slow fading out (see above). The fall times for double step pulses are therefore significantly longer (compare Figure A1.29 and Figure A1.30). Similar to the observed undershoot for rising edges a threshold of e.g. 5 % above the end level could be defined. This limits the influence of the slow fade out on the estimated fall time. However, in the following experiments only falling edges to 0 W are considered. In this case the fading out takes places in low power regions, which are not assumed to affect the welding process decisively. Therefore, no elaborate evaluation of fall times is carried out.

Initial Step:

The initial step is considered through the laser system's pulse programming tool by a pre-definition of first and last set-point (see Figure 3.8). Note that a different laser system with a basic level of 402 W is depicted. A delay along the time axis is not considered. The large area ratios for triangular and trapezoidal pulses indicate that the modelling of the pulse with an ideal triangular shape is not feasible. Instead the initial step must be considered.

Depending on the pulse programming method the initial step is modelled in different ways. For absolute programming a basic block of 102 W is assumed.

For relatively defined shapes a block is defined with a power level of 6.8 % of the overall peak (compare Figure 3.8).

In order to consider the initial delay a third alternative seems plausible. In this case the initial block is modelled as a trapezoid with a non-perpendicular slope. For determining the duration of the on- and off- section a series of triangular pulses at increasing durations and peak levels is analysed. The results as compiled Table 4.1 show an average step duration of 83 µs.

Peak Power W	Duration ms	Initial Step µs
150	0.25	63
150	0.35	85
200	0.45	85
250	0.55	108
300	0.65	78
350	0.75	90
350	0.85	93
400	0.95	78
400	1.05	95
450	1.35	93
1500	1.50	86
	Mean	86.73
	St. Dev	11.54
	CoV	0.13

Table 4.1: Duration of Initial Step measured at various slopes

The scattering of around 13 % (coefficient of variance) results from the difficulty to identify critical start and end points in low power regions. The general procedure is depicted in Figure A1.31. Similar to rectangular pulses, the off-section is marked by a slow fading out. This can be employed for positioning the cursors. For the moment only the duration of the on-section is determined and assumed to be an acceptable measure for both edges.

The three alternatives for modelling the initial step are compared in Figure 4.14 below. The expected sensor signals are quantified with help of Figure 4.7. The measured area (action value) is computed with help of the Matlab “trapz”-function.

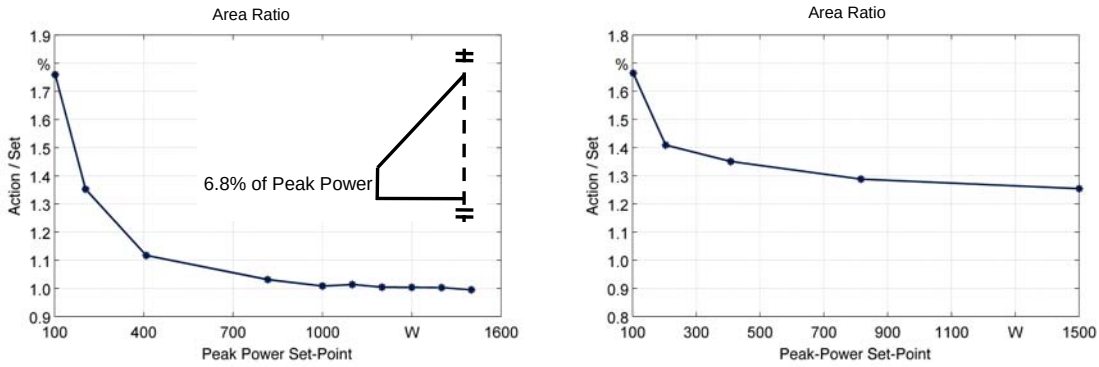

$$A_{set,tri} = 0.5 \cdot t_D \cdot 0.922 \cdot P_P + 0.068 \cdot t_D \cdot P_P$$

$$A_{set,tra} = (0.5 \cdot t_1 \cdot t_D \cdot 0.922 \cdot P_P + 0.068 \cdot t_1 \cdot t_D \cdot P_P) + (0.5 \cdot (1 - t_2) \cdot t_D \cdot 0.922 \cdot P_P + 0.068 \cdot (1 - t_2) \cdot t_D \cdot P_P) + (t_2 - t_1) \cdot t_d \cdot P_P$$

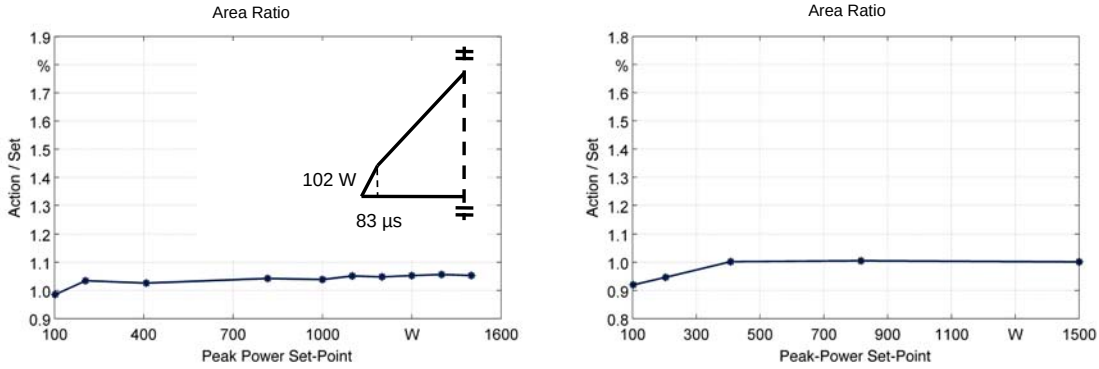

$$A_{set,tri} = 0.5 \cdot (t_D - 83\mu s) \cdot (P_P - P_{102}) + (t_D - 2 \cdot 83\mu s) \cdot P_{102} + 83\mu s \cdot P_{102}$$

$$A_{set,tra} = 0.5 \cdot t_1 \cdot (t_D - 83\mu s) \cdot (P_P - P_{102}) + 0.5 \cdot (1 - t_2) \cdot (t_D - 83\mu s) \cdot (P_P - P_{102}) + 0.5 \cdot (t_2 - t_1) \cdot (t_D - 83\mu s) \cdot (P_P - P_{102}) + (t_D - 2 \cdot 83\mu s) \cdot P_{102} + 83\mu s \cdot P_{102}$$

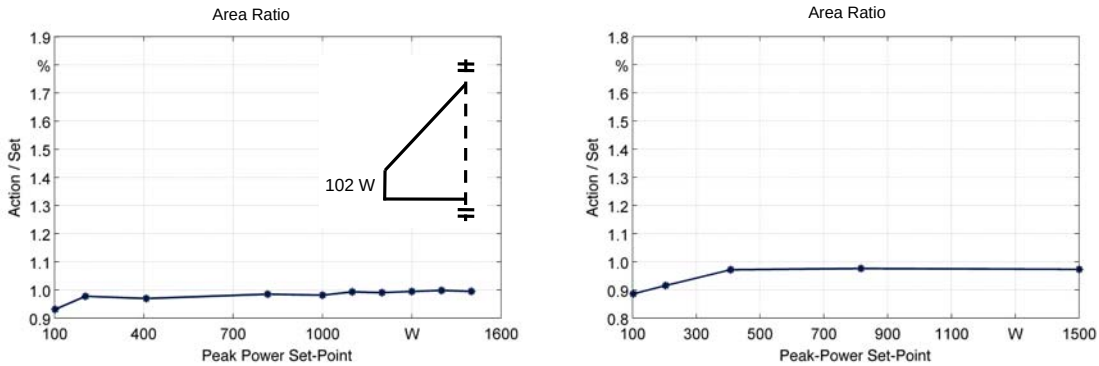

$$A_{set,tri} = 0.5 \cdot t_D \cdot (P_P - P_{102}) + t_D \cdot P_{102}$$

$$A_{set,tra} = 0.5 \cdot t_1 \cdot t_D \cdot (P_P - P_{102}) + 0.5 \cdot (1 - t_2) \cdot t_D \cdot (P_P - P_{102}) + (t_2 - t_1) \cdot t_D \cdot (P_P - P_{102}) + t_D \cdot P_{102}$$

$A_{set,tri}$: set area triangular shape $A_{set,tra}$: set area trapezoidal shape

t_D: pulse duration t_1: relative position of set point one t_1: relative position of set point two

P_P: sensor signal at peak power P_{102}: sensor signal at 102 W

Figure 4.14: Comparison of various models to calculate the set area for triangular (left column) and trapezoidal pulses (right column).

An ideal modelling of the set area would result in an area ratio of one, since the model would be as close to reality as possible. The comparison shows that the relative consideration of the initial step does not produce better results. The area ratio for a basic rectangular block model of 102 W is very stable and close to one. The consideration of an initial step duration of 83 µs further improves this accuracy and appears to be the best model. The poor performance in low power regions can be attributed to the large peak duration ratio (trapezoidal) or too low peak level (triangular) within these regions. Such shapes are however automatically avoided when considering the limited rise and fall times.

As a conclusion the initial step needs to be considered when determining the area of a pulse. This is essential when calculating the actually applied energy of the pulse. In this respect the modelling of the on and off edge as a non-perpendicular slope of 83 µs in duration appears to be the best solution.

Coming back to the initial motivation, Figure 4.1 can now be expanded with the criteria derived above. For each typical element of a pulse shape a decision rule or functional relation has been defined. On this basis it can be judged wheter acceptable shaping is possible within the scope of made assumptions and subjectively defined thresholds. Note that the rise and fall times were partially determined in reference to the basic level of 102 W. It can not be outruled that steps e.g. from 400 to 500 W might differ in required rise time. Such steps are however not going to be applied in this work.

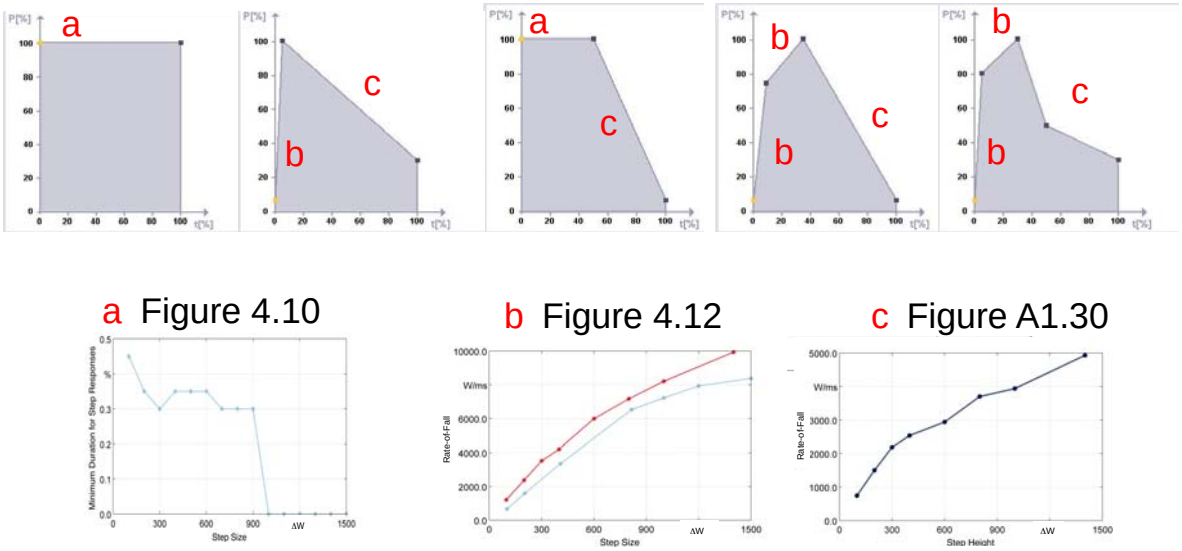

Figure 4.15: Application of derived graphs for judging the possibilities of acceptable pulse shaping (pulse shapes according to [KAMENZ 2010]).

The most relevant deviations between set and action value could be identified. The applied set-up as well as the methods of analysis were verified to ensure the validity of the investigation. The eventually retrieved results define the range of applicable pulses in the subsequent welding experiments. In addition an equation for calculating the applied pulse energy was derived.

5 Investigation on Welding with Rectangular Pulses

In order to prepare the application of DoE-methods a reference experiment with rectangular pulses is carried out. The experimental space is examined to derive a basic process window. In addition are surface-bound measurands evaluated and selected to effectively quantify the quality characteristics. The selection of factors for the subsequent experiments is supported by an ANOVA and the evaluation of the factors' effects.

5.1 Objectives of the Experimental Series

Four steps are essential before applying a DoE:

1. the selection of factors.
2. the selection of quality characteristics and ways to quantify them.
3. the acquisition of a basic knowledge on the experimental space.
4. the definition of boundaries for the experimental space.

Point one refers to the interdependency of the factors describing a pulse. As shown in Figure 3.10 four parameters exist (shape, energy, duration, peak power), of which only three can be varied independently. It is thus to be determined, which of these parameters will not be regarded as a factor in the following experiments. This less significant variable is going to be constantly adapted to the discrete variations of the other three.

Coming back to the basic process model of Figure 1.2 two major quality characteristics (strength, spatter) need to be quantified for evaluating the potential effects of pulse shapes. The occurrence of spatter is assumed to correlate with high melt pool dynamics. Such dynamics have a major effect on the solidified weld's surface structure. Quantities to evaluate the surface may thus permit conclusions on melt pool dynamics and thus on the risk of spatter. Hence, measurands prevalent in technical surface description are examined regarding their capability to indicate surface unevenness.

Regarding the experimental space it is to be examined whether a clear differentiation between KW and HCW is possible. This is necessary to determine the expected degree of nonlinearity of the measurands. A transition between these unlike regimes within the experimental space requires the application of more precise and complex methods of DoE.

In this context a basic process window can be defined which acts as a reference and basic characterization of the examined process. When considering a complete matrix of power and duration for a rectangular pulse (each combination defining the specific energy content) an upper limit of possible parameter combinations is given through the occurrence of spatter. On the other hand may too low energies result in poor coupling and insufficient weld dimensions. This defines a lower boundary based on which a process window can be defined (see below).

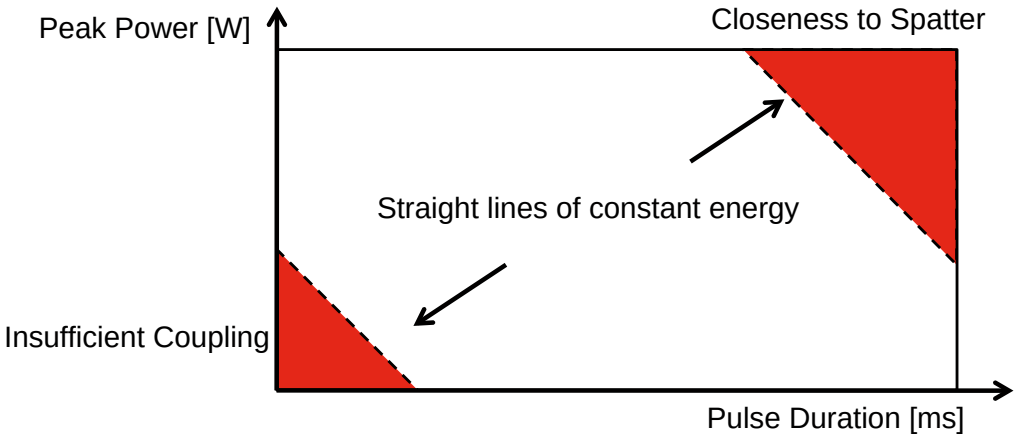

Figure 5.1: Principal design of a process window for rectangular pulses

Such a process window serves as a basic orientation on which regions are of interest when e.g. considering minimum demands for weld dimensions. In addition can the HCW or KW regimes be possibly associated with typical areas within the process window.

5.2 Methodology

Being a reference experiment, the characteristics of interest are desired to be observed over continuous scales. Thus a complete matrix of pulse power and duration is welded for rectangular pulses. The matrix ranges from 102 to 1000 W and 0.4 to 3 ms (see Figure 5.4). A rectangular pulse is chosen as it represents the most basic shape.

The overall set-up is similar to that of the experiments on pulse shaping capabilities. The material samples are round dies that measure 1 mm in thickness and 9 mm in diameter. They are turned from round wire and partially polished on one side. The polishing occasionally results in an inhomogeneous surface as depicted in Figure 5.2. Hence, the turned side is preferred. Through measurements with a white-light microscope an average maximum height of the roughness profile (R_z) was determined for 5 randomly selected samples (see section 5.7 for backgrounds). The measured values lie below “threshold-

values" as given by [HÜGEL & GRAF 2009] (fig. 3.16: peak of absorption at ca. 3.5 µm]). These refer however to different metallic materials. [VDI-TPT 1995] shows that for aluminium a R_z of 9 µm accelerates the beginning of vapourization by 40 µs compared to a surface with a R_Z of 3 µm. For the given samples the R_z-values are even lower. With applied pulse durations of 500 - 3000 µs the roughness' influence can be expected to have little significance. This assumption can however not be verified for the moment as different materials are applied and dedicated experiments would be necessary. Therefore, randomization is applied if more than one sample is used in an experimental series. This is mandatory due to the large scattering of R_z as listed below. Through randomization a potential effect of roughness is spread over the experimental population by chance.

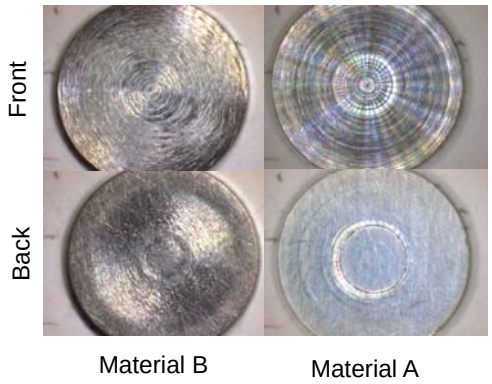

	Material B	Material A
R_z (mean)	1.98 µm	1.33 µm
St. Dev.	0.56	0.33
CoV	0.28	0.25

Figure 5.2: Surface roughness of the applied material samples.

The samples are defatted and positioned on a plastic piece. With help of a XY-Table a matrix of 5 by 5 spots is welded in randomized sequence. A typical result is displayed below.

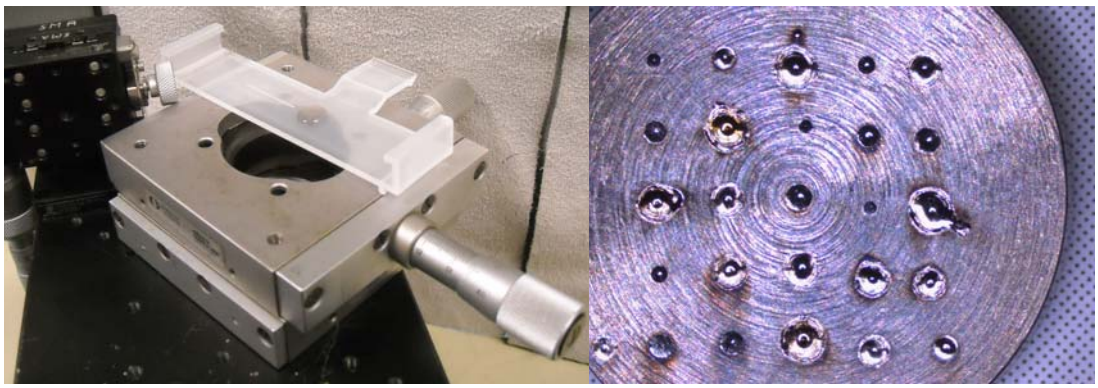

Figure 5.3: : Positioning of a material sample on a XY-table and matrix of spot welds on material sample

To limit the efforts of execution for the experiments and following analyses no repetitions are carried out (n=1). The welds are at first analysed two-dimensionally with a stereo microscope. In a second step a white-light microscope is applied for a three-dimensional analysis of the topography. Alongside is the reflected laser radiation measured with a photodiode (see chapter 3). In each case a qualitative and quantitative analysis is conducted.

5.3 Two-Dimensional Analysis – Qualitative Results

During the execution of the experiments observations such as spatter or heavy spill are noted. Figure 5.4 includes the result with respectively coloured markings. When comparing the bottom left corners it is obvious that the coupling is less efficient in Material A. The upper right half of the matrices indicates increasing spill and spatter. The defects start at lower energies in the case of Material B.

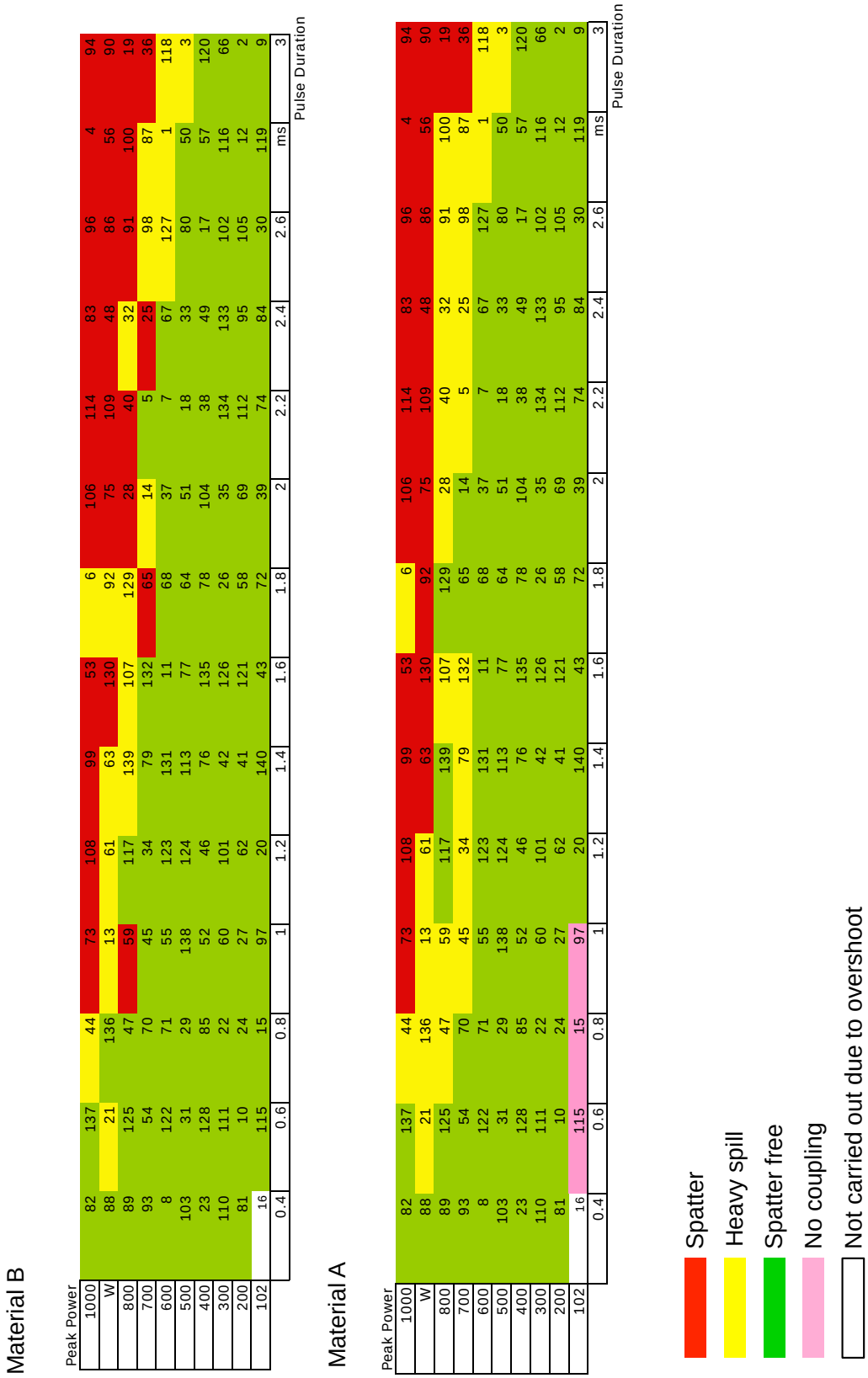

Figure 5.4: Experimental power-duration matrix for rectangular pulse experiments. The numbers inside the matrix stand for the randomized experimental sequence.

From pictures taken during the stereomicroscopic examination these “on-line” observations can be confirmed from the solidified surfaces. In general do the asymmetry as well as spill and waved surfaces increase with higher energies. The complete set of photographed spot welds is compiled in Figure A2.1 and Figure A2.2. The black appearance of some spots is the result of an incomplete illumination. When slightly tilted, all spots show a bright metallic reflection.

In some cases does discoloration occur which indicates poor gas shielding. As a reason the simultaneously triggering of laser and gas pulse was identified. In the systems applied for production the gas supply is set off prior to the laser pulse and maintained for a short duration after welding. This cannot be realized in the given set-up. Therefore, in the following experiments the gas is set to continuous flow at the same settings (0.5 bar initial pressure, 1 l/min flow rate). This may limit the transferability of the results between the single experimental series. Yet, the positioning of the gas nozzle remains an uncontrollable parameter for all experiments (compare Figure A1.1). This leads in any case to an unknown influence of the gas. The nozzle is iteratively positioned before each series until no soot and discoloration occurs. To which degree this non-repeatable positioning affects the results would have to be determined in dedicated studies. This is not further pursued due to a lack of time.

In the following various graphs are introduced based on the single analyses steps. For reasons of readability only the graphs on Material B are included in the following section. The plots on Material A can be found in appendix A2.

5.4 Two-Dimensional Analysis – Quantitative Result

The following quantities are measured via a stereomicroscope and the respective software analysis tool “µsoft Analysis – Version 5.1.1”:

- Spot-weld core diameter D_{min}:

  A circle is drawn from the centre point up to the largest diameter at which the area completely covers the welded area. If the centre point cannot be determined optically, a circle is constructed with help of three points along what is perceived to be the largest diameter. In Figure 5.5 the left picture illustrates the latter case, whereas the centre point of the right weld can sufficiently be estimated by vision.

- Melt Overspill D_{Diff}:

  A circle is drawn from the centre point of the previously carried out D_{min}-measurement (see below). It is extended up to the last point at which it touches part of the weld. This diameter is referred to as D_{max}. Substracting D_{min} from D_{max} gives the measure D_{Diff} for melt overspill.

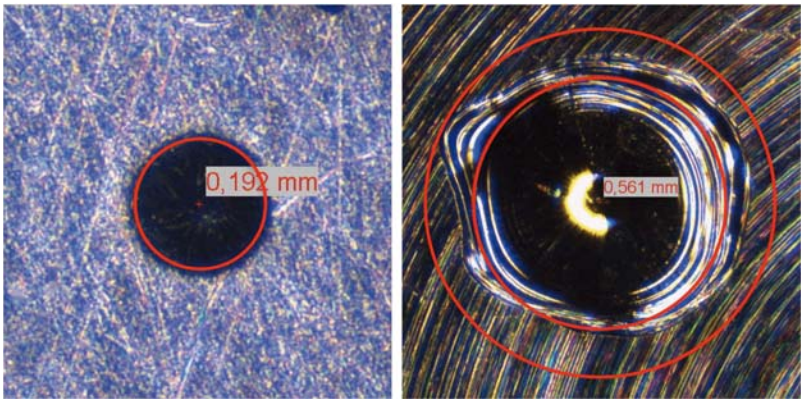

Figure 5.5: Stereomicroscopic measuring of relevant diameters. Left: 3-point circle construction for a weld of Material B at 102 W and 1.2 ms. Right: Centre point detected by vision for a weld of Material A at 800 W and 1.4 ms.

The measurements as determined above are plotted in Matlab. The results are displayed below. Corresponding to the qualitative observations do the values increase towards regions of high energies.

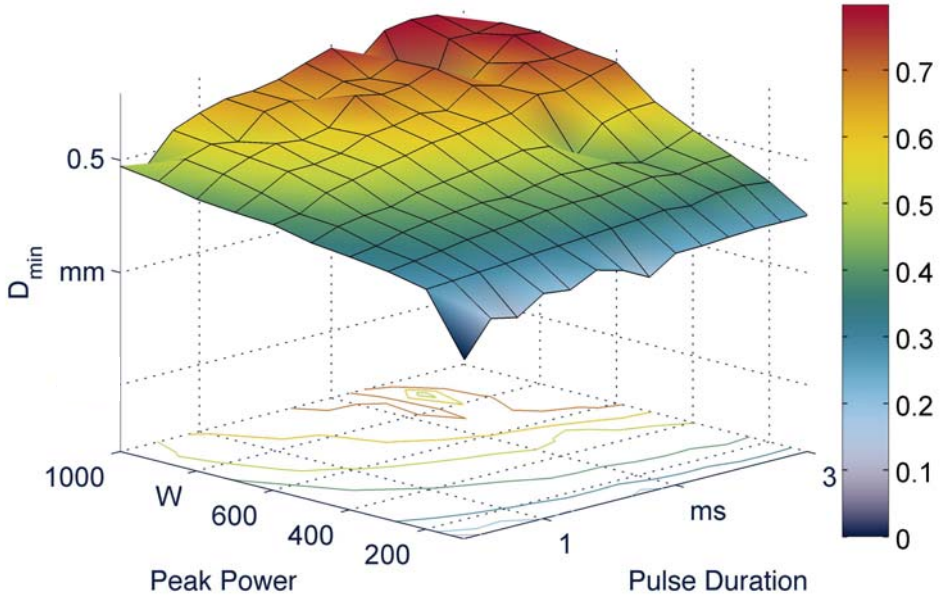

Figure 5.6: D_{min}-measurements from the stereomicroscopic analysis of Material B welds

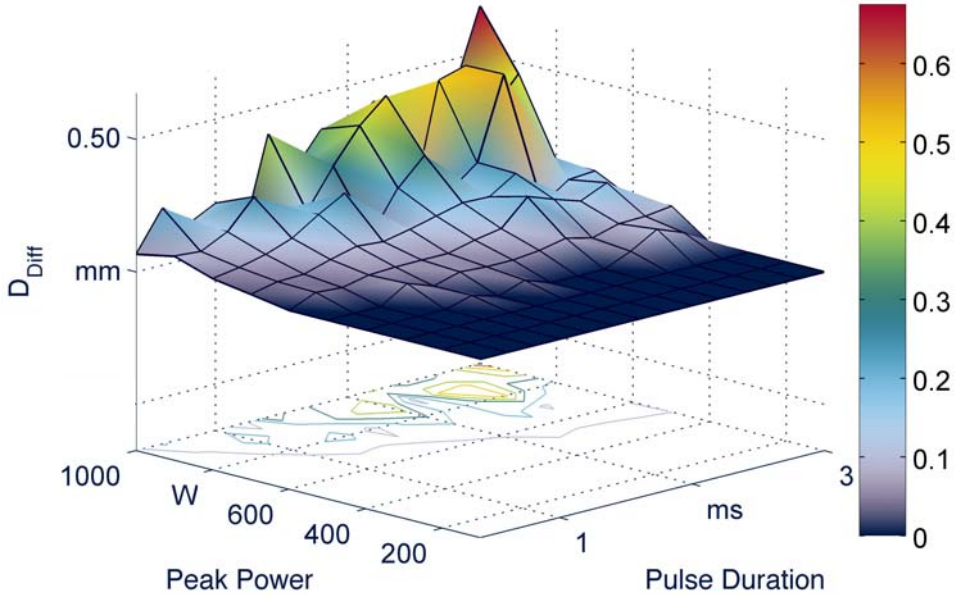

Figure 5.7: D_{Diff}-measurements from the stereomicroscopic analysis of Material B welds

From these graphs a first process window can be defined. For doing so the basic coordinate system of power and duration is maintained. The contour line of D_{min}= 0.3 mm is used as a lower boundary. This is because sufficient coupling is assumed to be only the case if the weld diameter exceeds that of the laser spot (300 µm). For the upper boundary the D_{Diff}-contour with a value of 0.1 (meaning 100 µm overspill) is chosen. The welds along this boundary subjectively appear to be a suitable upper limit. Both contours are approximated with a third degree polynomial and plotted below.

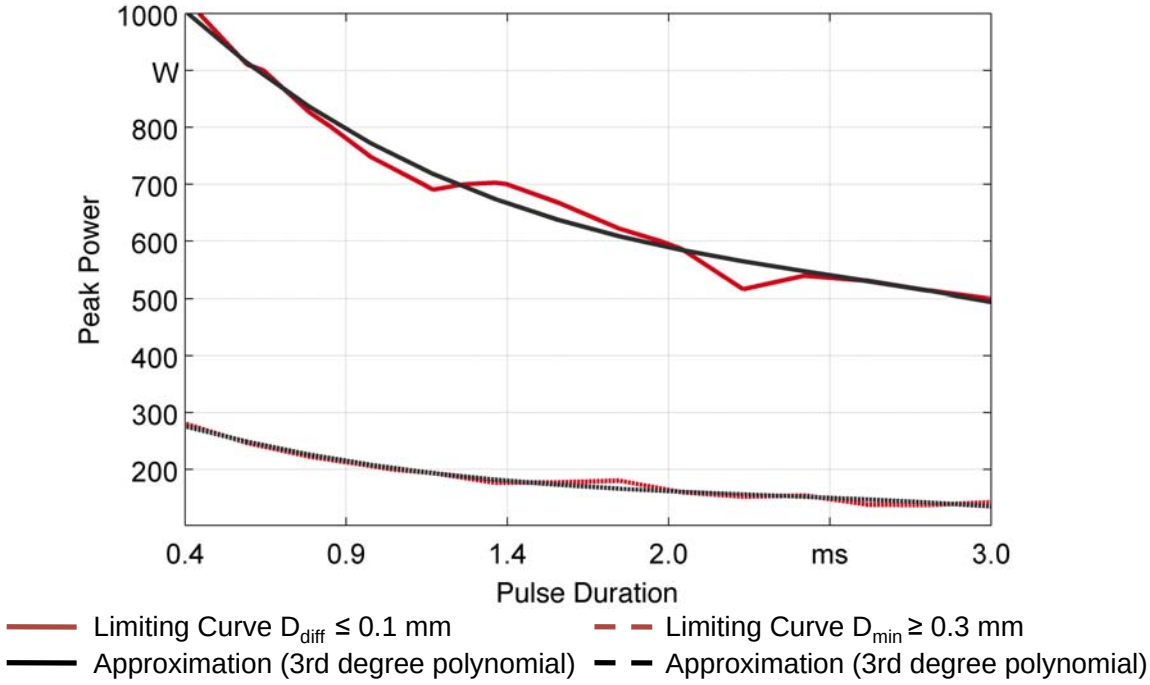

Figure 5.8: Approximation of critical contours to define a process window for Material B

To add more informational value to the process window the D_{min}-contours of Figure 5.6 are added (see below). It becomes obvious that with the current upper boundary one reaches a maximum core diameter between 0.5 and 0.6 mm for Material B and roughly 0.5 mm for Material A (see Figure A2.6).

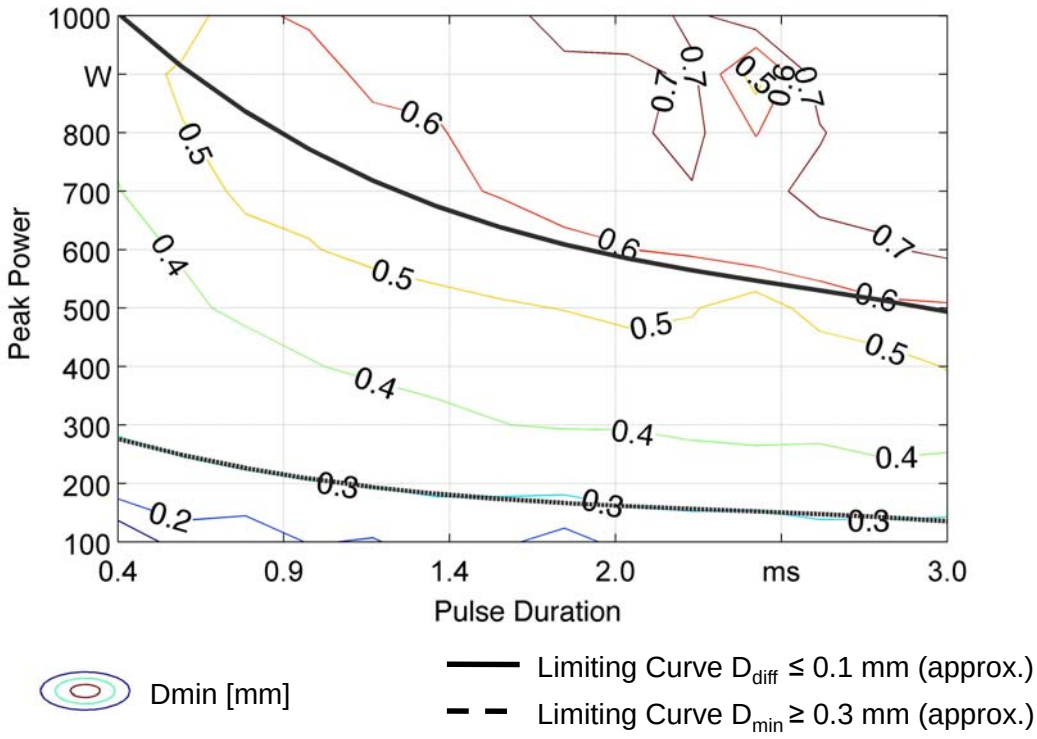

Figure 5.9: Addition of D_{min}-contours to the process window for Material B

5.5 Transition from HCW to KW

As has been shown in chapter 3 a photodiode can be applied to record the reflected intensity of a laser pulse over time. If the laser is applied to a reflective surface without coupling, the photodiode's signal resembles the pulse as generated by the system. However, if coupling occurs part of the laser radiation is absorbed. Furthermore, if a vapourisation of material takes place or even a steady vapour plume forms (as inherent to KW) characteristic fluctuations in the sensor's signal can be observed [GARTHOFF ET AL. 2008]. This is because part of the incoming radiation is diffusively reflected. Figure 5.10 shows a typical sensor signal for a weld in the KW regime. Starting from a gradual increase an eruptive increase occurs. As a measurement the time from the start of the laser activity (red signal of PEM taken as reference) to the base point of the eruption is measured. This quantity is referred to as "time to vapour plume (t_{2vp})".

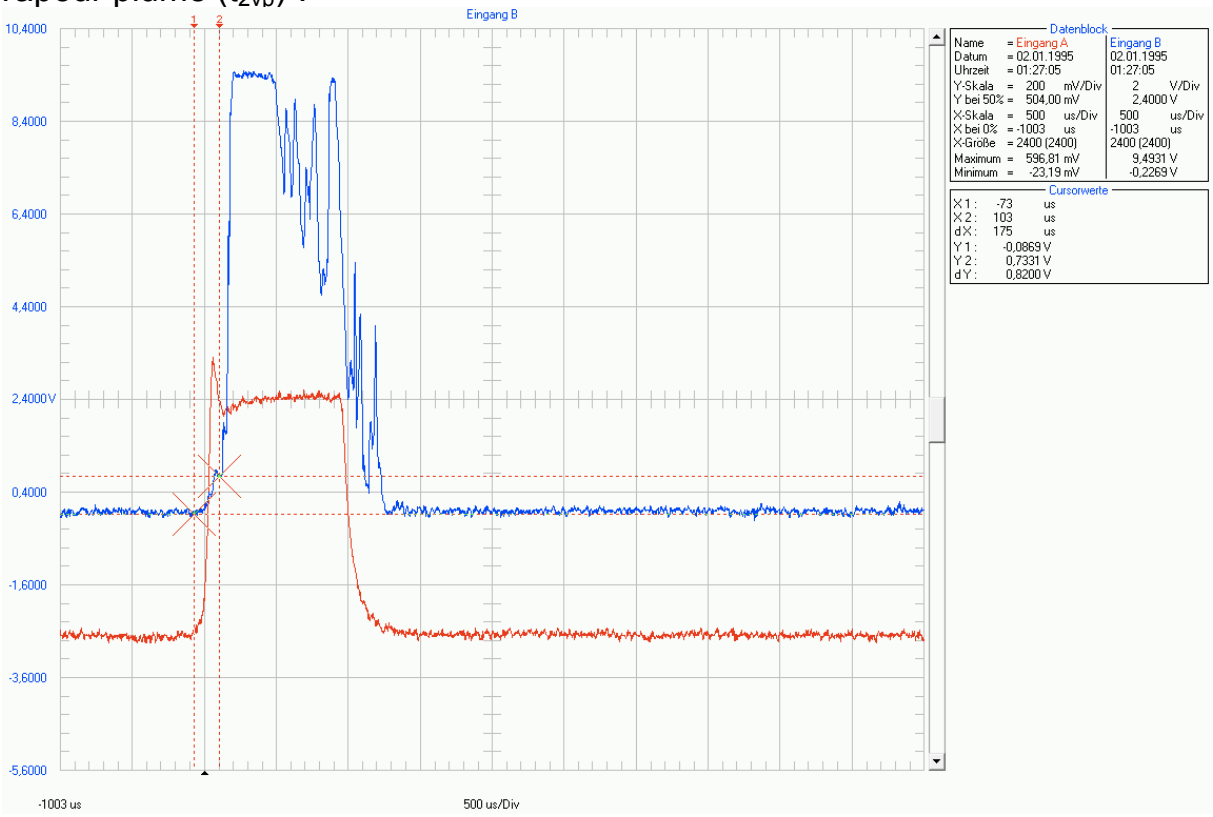

Figure 5.10: Complete screenshot of the measuring of the photo diode's signal (blue) via the oscilloscope. The displayed signal was measured for a rectangular pulse of 900 W and 0.8 ms. The PEM signal (red) is not further evaluated.

In Figure 5.11 further examples of sensor data throughout the experimental matrix are given (contrasted with the PEM signal). Example three shows the phenomena of an early spike, which indicates high reflection due to poor

coupling efficiency. Following that a phase of absorption takes place until the eruptive signal occurs. Example five shows a late spike, which may not correlate with a complete and stable KW-phase. Nevertheless, it indicates that vapourisation has begun and that a transition is imminent.

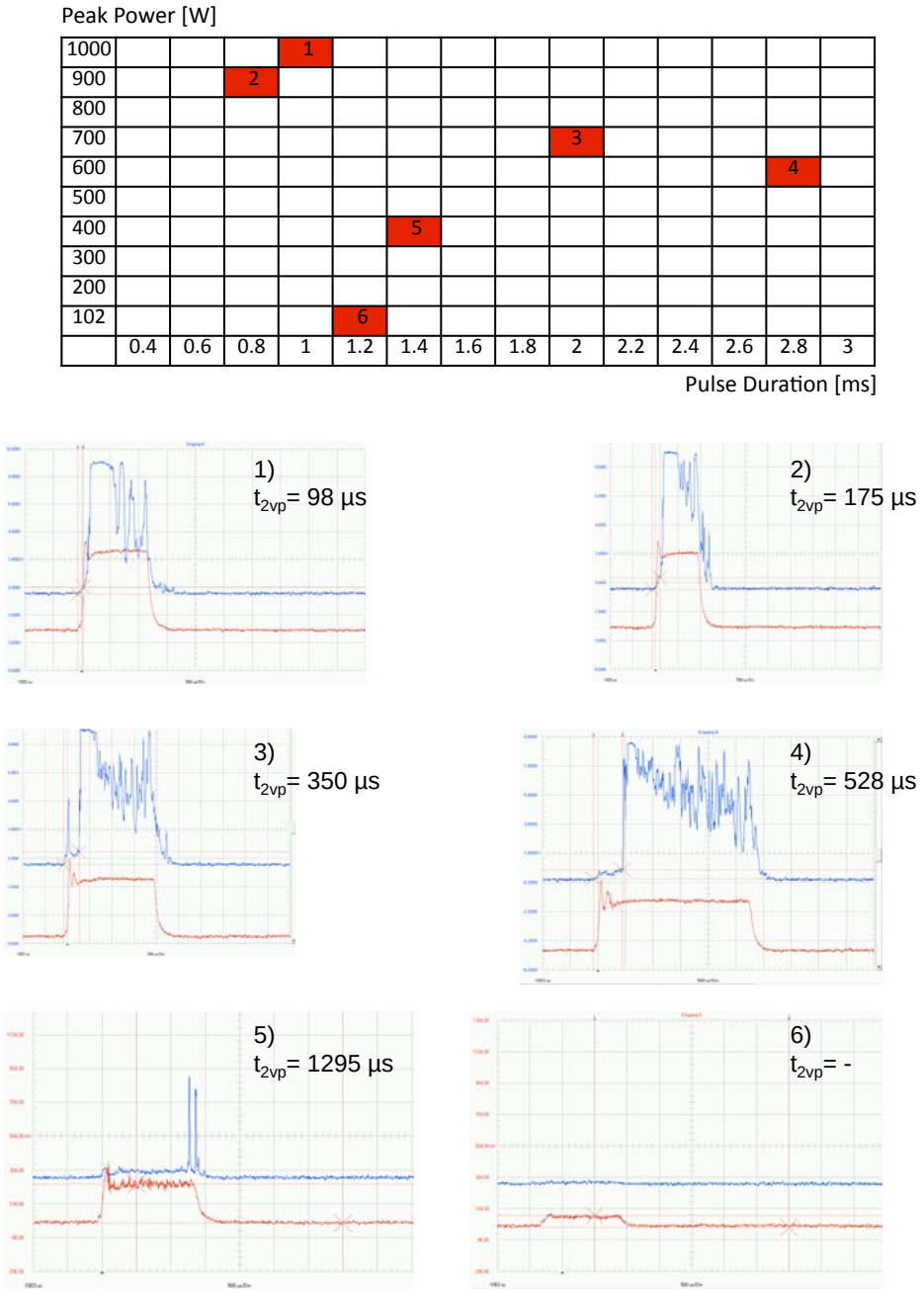

Figure 5.11: Exemplary graphs of the photodiode signal indicating the occurrence of a vapour plume. The scaling along the horizontal time axis is constant at 500 µs per box.

The t_{2vp}-measurements taken throughout the experiment are given in Figure 5.12. An almost constant value of t_{2vp} along the power levels can be observed.

This indicates the existence of a threshold amount of absorbed energy for each applied level of intensity.

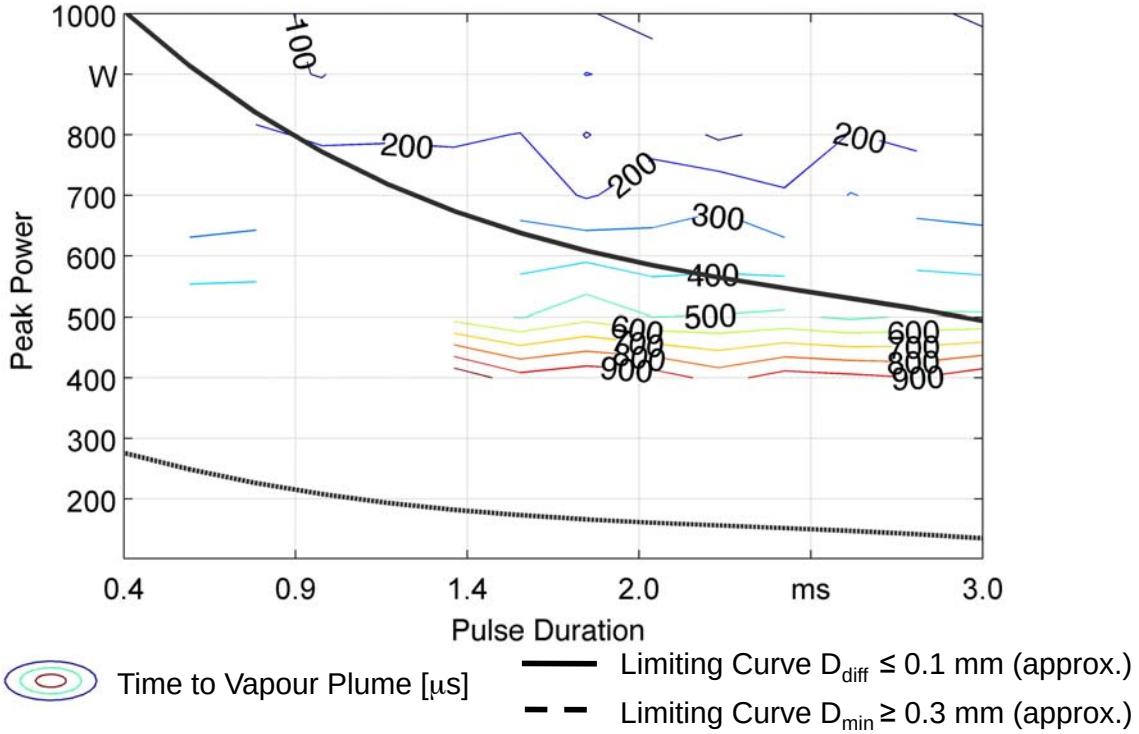

Figure 5.12: Measurements on time to vapour plume occurrence added to the process window for Material B.

The measurements are averaged for each power level and plotted in Figure 5.13 below. A first nonzero is obtained value at 400 W. Below that no characteristic sensor signals are found. The peak power threshold must therefore lie somewhere between 400 W and 300 W. To generate a more informative process window the last measurement is continued linearly to 350 W. The plot shows that e.g. at a pulse duration of 0.5 ms a transition to KW is to be expected for peak powers of 500 W and above.

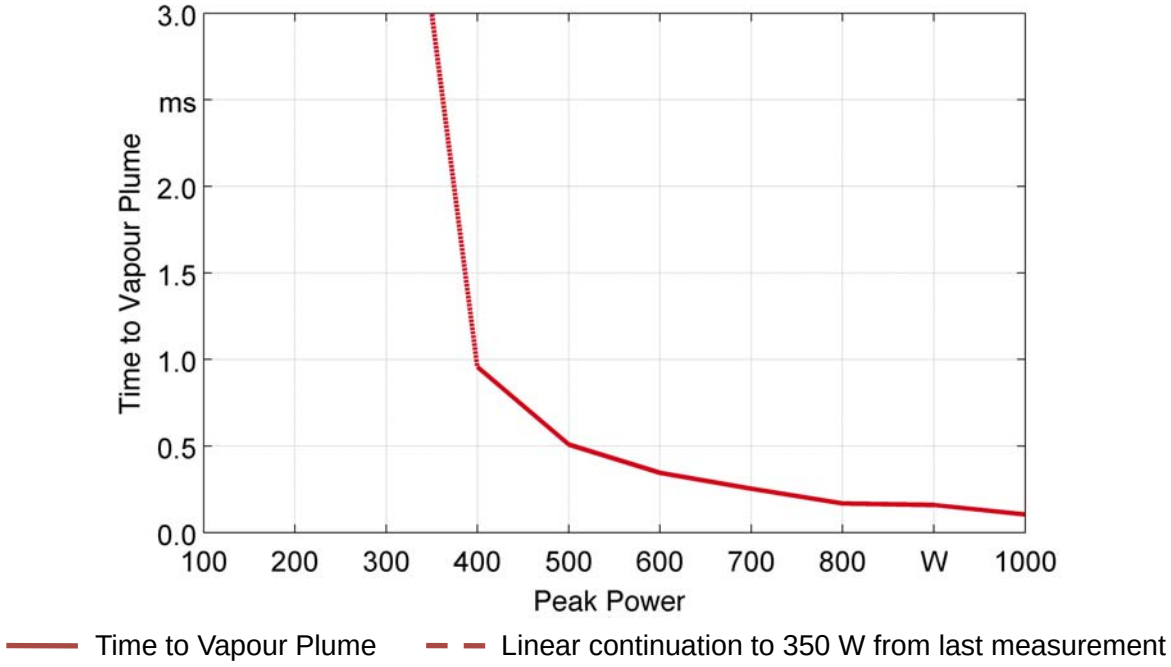

Figure 5.13: Time to vapour plume measurements as a function of applied peak power for Material B.

The threshold intensity for directly achieving keyhole welding amounts to $1x10^6$ W/cm^2 for steel [DAUSINGER 1995]. In the given case the measurements for 1000 W pulses may equally be interpreted as complete transitions from the start (compare example one in Figure 5.11). Hence, a threshold intensity of $1.415x10^6$ W/cm^2 (1000 W for a 300 µm top-hat spot) can be estimated for the Material B samples.

With the results of the measurements discussed above a complete process window can be defined. For doing so Figure 5.9 and Figure 5.13 (with switched axes) are combined. The resulting plot below shows that the transition to KW roughly splits in the existing process windows in two halves. Regarding the D_{min}-contours one can estimate which core diameters can be reached above and below the transition line to KW. In theory does the penetration depth of the weld correspond to half this diameter in the HCW regime (ideal gas shielding assumed). If the KW-phase is entered the penetration can be expected to rise significantly in relation to D_{min}.

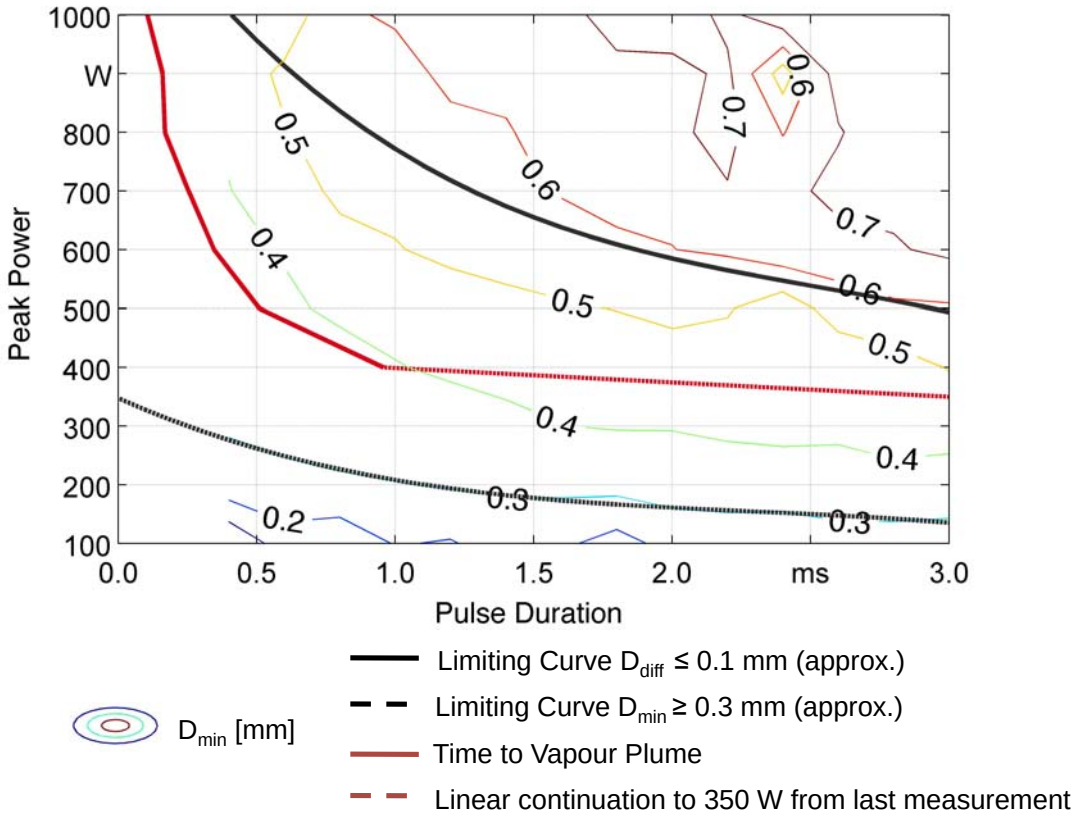

Figure 5.14: Complete process window for Material B welds

All in all the does the transition show that different physical phenomena are present within the experimental space. This means that the measurands are likely to show a nonlinear behaviour and that respective DoE-models are required (3-level design or CCD – see section 3.5).

5.6 Three-Dimensional Analysis – Qualitative Analysis

With help of a white-light microscope the topography of the spot welds is examined. This serves to confirm and expand the qualitative observations of the two-dimensional analysis. Due to the amount of spot welds the examination is constricted to the Material B samples. The applied measurement systems consists of a microscopic unit (nanofocus µsurf, twentyfold magnification, resolution / step-size 0.1 µm) and a software analysis tool (µsoft Premium 3). The results are compiled in Figure A2.10.

[BERTRAND & POULON-QUINTIN 2011] present a classification of typical spot weld irregularities as shown in Figure 5.15 below. Three main surface-bound irregularities are identified: undercut, curved spot and pit crater. Apart from these classifications of the global shape, it also regarded as significant to examine the local unevenness in form of the waviness along the surface.

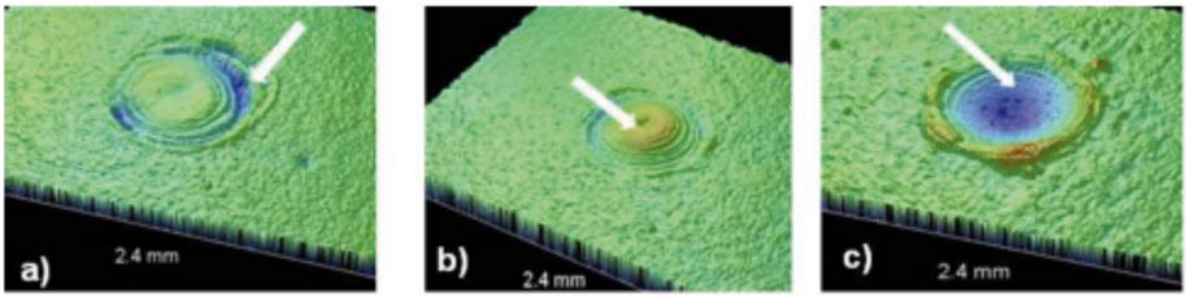

Figure 5.15 Classification of surface-bound spot weld irregularities according to [BERTRAND & POULON-QUINTIN 2011]: a) undercut, b) convex spot, c) pit crater.

Figure A2.11 compiles cross sections of the analysed welds. It can be seen that the mentioned irregularities occur mostly in a combined from. Starting from the bottom left corner, the spot welds show a pit crater-like shape, yet without the bulged edge. The central funnel-shaped depression is quite narrow in relation to the overall spot diameter. From 400 W and 2.2 ms onwards, the spots begin to show a waved surface. From 500 W and 1 ms undercuts and bulged edges occur. Progressing towards higher energies convex shapes with undercuts are observed in irregular frequencies (e.g.: 600 W, 2 ms).
Figure 5.21 includes the three most typically observed cases: pit crater (no bulged edge), convex shape and combination of undercut, bulged edge and slight convexity.

5.7 Three-Dimensional Analysis – Quantitative Analysis

Based on the received three-dimensional data the occurring height variations can be calculated with standard parameters according to [DIN EN ISO 4287 2009].
The measurement sequence as illustrated in Figure 5.16 begins with the definition of the zero level by choosing three points assumed to lie on that level. Following that an area for a vertical cross section is defined. The generated height profile (referred to as primary profile P) is further split into a low-frequency part (roughness profile R) and high-frequency part (waviness profile W). The separation is achieved by applying a Gauß-filter with a “cut-off” or threshold wavelength of 0.08 mm (settings in accordance with [DIN EN ISO 4287 2009]). Based on the generated profiles various measurements can be taken. The waviness profile describes the global basic shape of the spot, whereas the roughness profile shows the height variations along the basic shape’s surface.

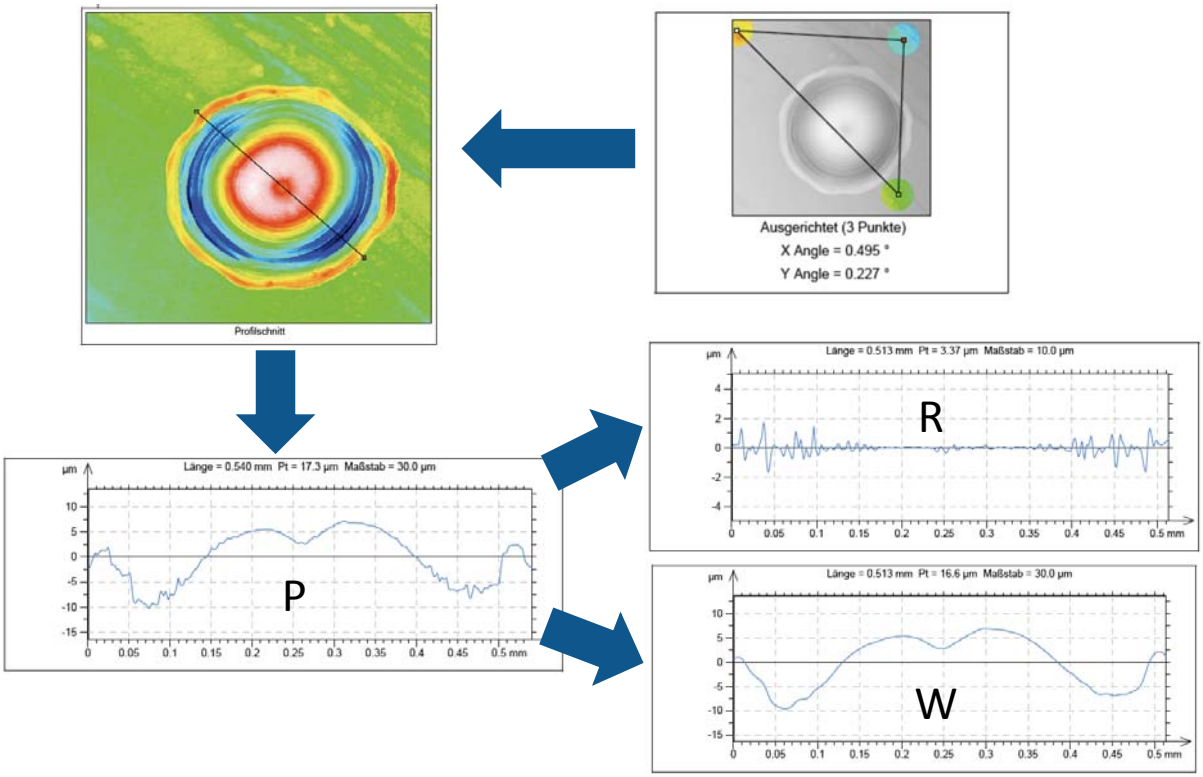

Figure 5.16: Working sequence for analysing the height profile. Primary roughness and waviness profile are marked with respective letters. Note that the x-axis has its origin at the average height value P_a. The first and last points mark the zero-level of the surface.

An alternative to working with a single cross section is considering the height profile along the complete spot weld surface (marked S in [DIN EN ISO 4287 2009]). Yet, this requires the measurement to be very accurate (e.g. without widespread interpolation). Such requirements raise the measurement effort by a critical degree as the microscope has to be constantly adapted. This not applied for the moment but taken up in the main experiments on partial penetration welding. The examined cross sections (P-profile) are compiled in Figure A2.11.

5.7.1 Preselection of Parameters for Surface Evaluation

The range of possible parameters for surface evaluation as defined in [DIN EN ISO 4287 2009] is judged according to their capability to indicate surface unevenness. This is considered for the basic shape itself (P-profile) as well as the unevenness along it (R-profile). Furthermore is the ability to indicate the type of the predominant surface distortion evaluated (e.g. notch or irregularities according to [BERTRAND & POULON-QUINTIN 2011]).

All values are based on accumulating the z-data (vertical axis) or amplitudes of each point along the measuring length (l_r). Points above the zero level are referred to as heights or peaks – points below as depths or valleys. An exemplary profile with the respective coordinate system is given below.

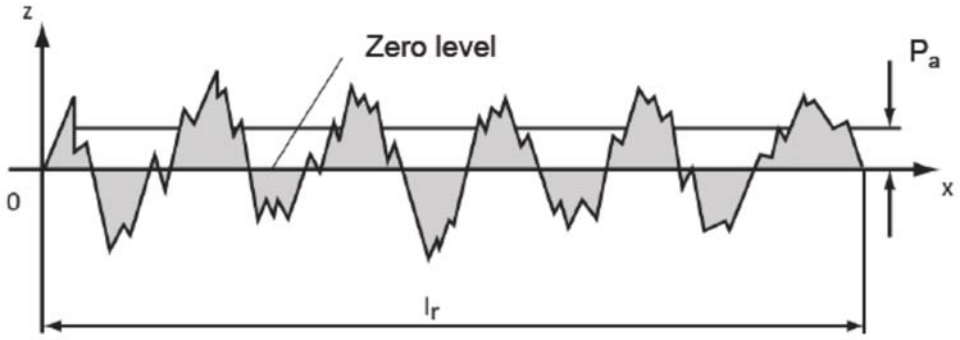

Figure 5.17: Primary Profile along x with depths and heights along z. The total measuring length is referred to as l_r (adapted from [JUNG 2011]).

From the range of possible parameters the ones listed below are preselected. Based on their definition they are regarded to bear the highest potential for providing the desired information.

- P_t [µm] (Profile depth): difference between highest peak and deepest valley. It represents the absolute range of z-values.
- S_z [µm]: difference between highest peak and deepest valley for a complete surface area
- P_a [µm]: arithmetic mean of z-values along the measuring length
- S_a [µm]: arithmetic mean of z-values for a complete surface area
- P_q [µm]: Root mean square of z-values which reacts stronger to large values due to squaring.
- P_{sk} [-]: skewness of the amplitude density curve of z-values
- P_{ku} [-]: kurtosis of the amplitude density curve of z-values
- R_a[µm]: arithmetic mean of z-values of the roughness profile. In this case the profile is measured as a sequence of single sampling lengths with l_r equal to the cut-off wavelength.

The parameters are discussed in more detail in the following. For further information please consider the respective standard or [ASME 2011]. The individual equations are given below.

$$P_a = \frac{1}{l_r}\int_0^{l_r} |z(x)|\, dx \qquad (14)$$

$$P_q = \sqrt{\frac{1}{l_r}\int_0^{l_r} z^2(x)\, dx} \qquad (15)$$

$$P_{sk} = \frac{1}{P_q^{\,3}}\left[\frac{1}{l_r}\int_0^{l_r} |z(x)^3|\, dx\right] \qquad (16)$$

$$P_{ku} = \frac{1}{P_q^{\,4}}\left[\frac{1}{l_r}\int_0^{l_r} |z(x)^4|\, dx\right] \qquad (17)$$

$$S_a = \frac{1}{A}\int_A |z(x,y)|\, dx\, dy \qquad (18)$$

$$R_a = \frac{1}{l_r}\int_0^{l_r} |z(x)|\, dx \qquad (19)$$

Figure 5.18: Equations of the examined surface parameters. The single data points are referred to as z. The measuring length along the x-axis is named l_r.

Note that the waviness profile is not considered as the parameters can equally be determined from the primary profile.

5.7.2 Profile depth P_t

As can be seen from Figure 5.19 below the profile depth shows a clear trend from low to high energies. It is thus a suitable measurand for indicating surface unevenness. Yet, it is based on sole extreme values. Therefore a broad scattering can be expected.

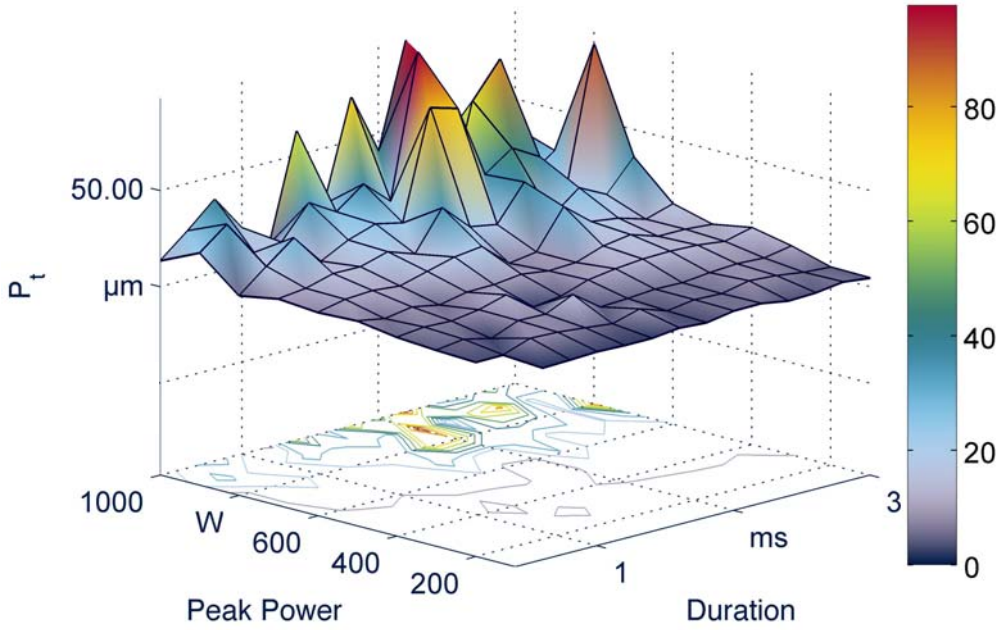

Figure 5.19: P_t-measurements for Material B welds

As no sign is given the profile depth cannot be applied to differentiate between the potential sources of irregularities. However, it is in any case a direct measure of the largest occurring notch. In this context does a potential sign play a subordinate role. For the expected mechanical effect it can be assumed irrelevant whether the maximum difference of heights and depths occurs due to a pit crater, undercut or even convex shape. The latter case is typically caused by pores, which act as inner notches.

5.7.3 P_a and P_q

Both quantities are a measure of the average amplitudes of heights and depths from the zero level. The measurements as shown below show the expected trends with slightly larger absolute values in case of P_q. Due to the obvious correlation only P_a is considered in the following. P_q does not produce linear results since it squares the measurements. This emphasizes extreme values and is not regarded to be necessary or advantageous in the given context.

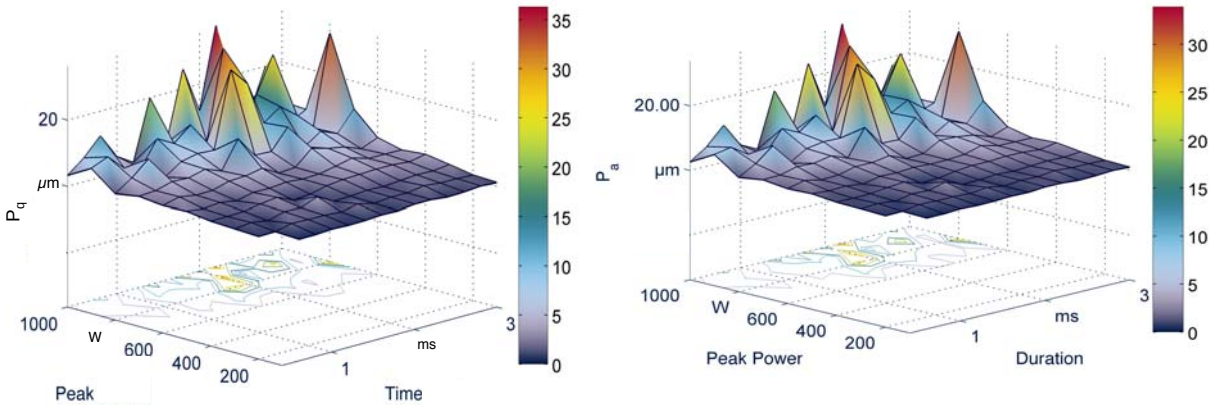

Figure 5.20: P_q- and P_a-measurements for Material B welds

In any case does a lack of signs not allow for inferences on the direction of the average amplitude (e.g. predominance of valleys or convex shape). However, the absolute value is a clear indication of surface unevenness as it implies to which degree the spot weld disrupts the plain surrounding surface. In contrast to P_t does this value not depend on sole extreme values and could hence be accompanied by less scattering.

5.7.4 P_{sk} and P_{ku}

The quantities of skewness and kurtosis describe characteristics of the amplitude density curve. This curve is derived from a histogram as illustrated in Figure 5.21 (note: envelope of the histogram is depicted). The frequency of amplitudes can be divided by the total amount of taken measurements to

derive the density curve. The shapes will however be equivalent. The vertical axis of the primary profiles has its origin at $P_{q.}$ From top to bottom the most typical profile shapes are given: pit crater (no bulged edge), convex shape and combination of undercut and slight convexity.

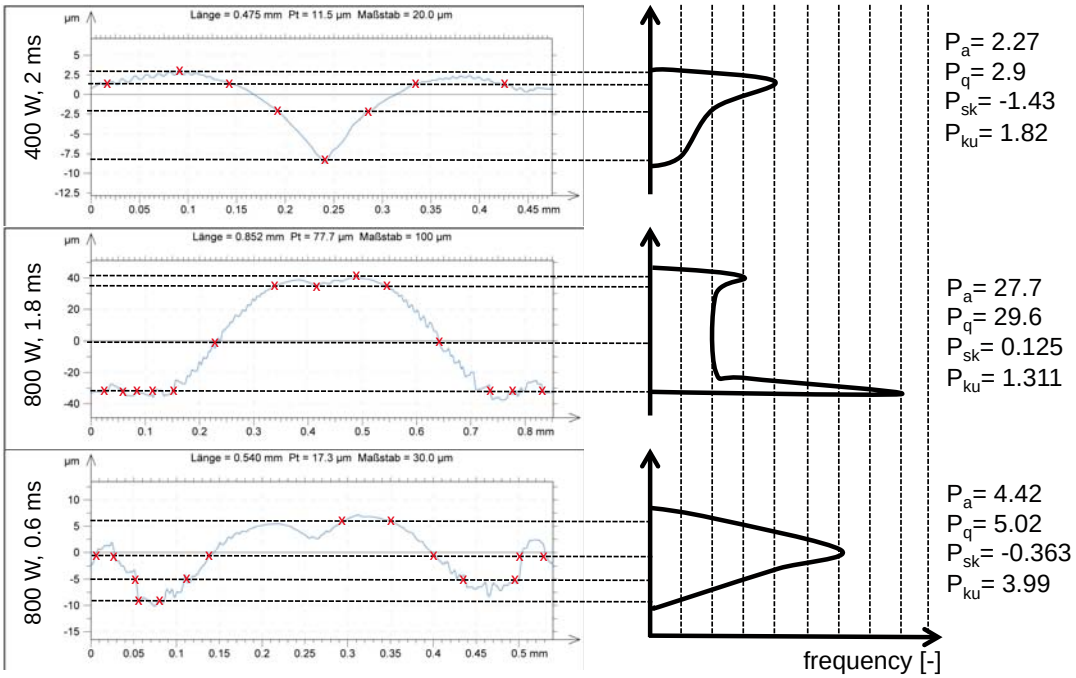

Figure 5.21: Derivation of amplitude histogram (similar shape to amplitude density curve) and comparison of related parameters.

The skewness describes the asymmetry of a distribution. It relates the position of the mode (value with highest frequency or probability) to the mean and median of the distribution. According to [DEAN & ILLOWSKY 2011] the mean (in this case P_q) has a higher informative value in this context. If the mode and mean coincide the curve is normally distributed (symmetric) and the skewness is zero. If the mode is shifted to the left of the mean (positive direction along the abscissa) the skewness takes on a negative value. If it is shifted to the right of the mean it becomes positive.

As exemplified above the distribution for pit crater-shaped profiles is typically negatively skewed and for convex profiles positively. If a combination of undercut and convexity occurs, the distribution is close to normal and the sign may change based on which effect dominates. Note that for the given convex profile the application of the skewness-measure is critical as the distribution is bimodal (“two peaks”) instead of unimodal [CRAMER & KAMPS 2007]. However, the positive sign corresponds to the results found by [BERTRAND & POULON-QUINTIN 2011] for convex profiles.

The skewness measurements compiled in Figure 5.22 are compared to the qualitative results of Figure A2.11. Absolute values larger than one indicate the expected shape correctly (see e.g. valley between 200 and 400 W or single positive peaks indicating convexity). However, most welds show combined irregularities. Their values are close to zero and do not provide the desired information (e.g. 1000 W and 0.8 ms was expected to be positive). Thus the skewness value does not contribute consistent and reliable insight for the examined welds.

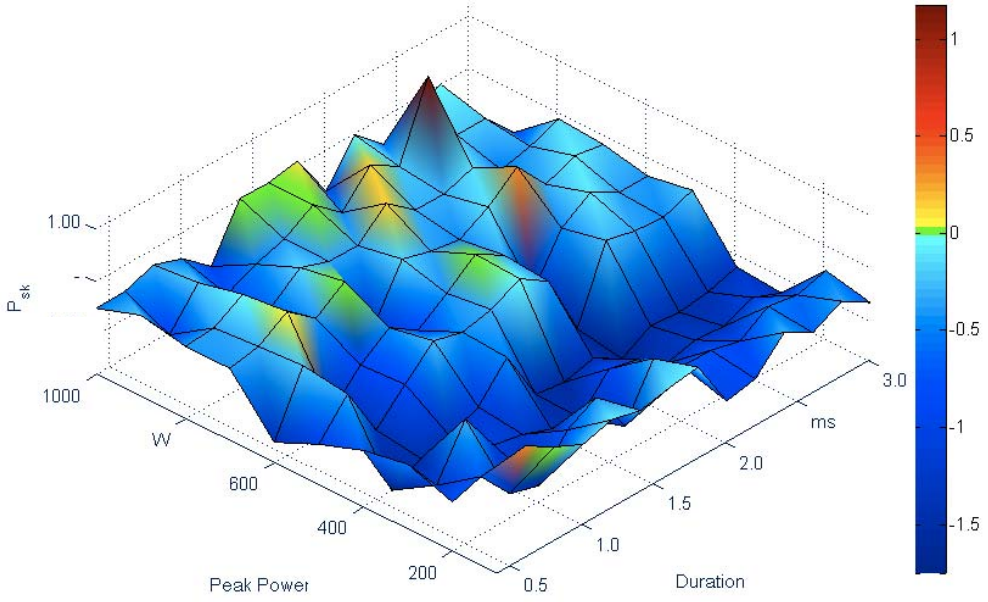

Figure 5.22: P_{sk}-measurements for Material B welds.

The kurtosis characterizes the scattering of the values of a distribution around the mean. A normal distribution has a kurtosis of three, whereas larger spreading due to outliers results in a stronger peakedness. The kurtosis of such distributions is larger than three. For distributions that are less outlier-prone the kurtosis is less than three [MATHWORKS 1999]. The results shown below indicate the existence of pit craters with values above three. Combined irregularities take on low values. Convex shapes cannot be identified.

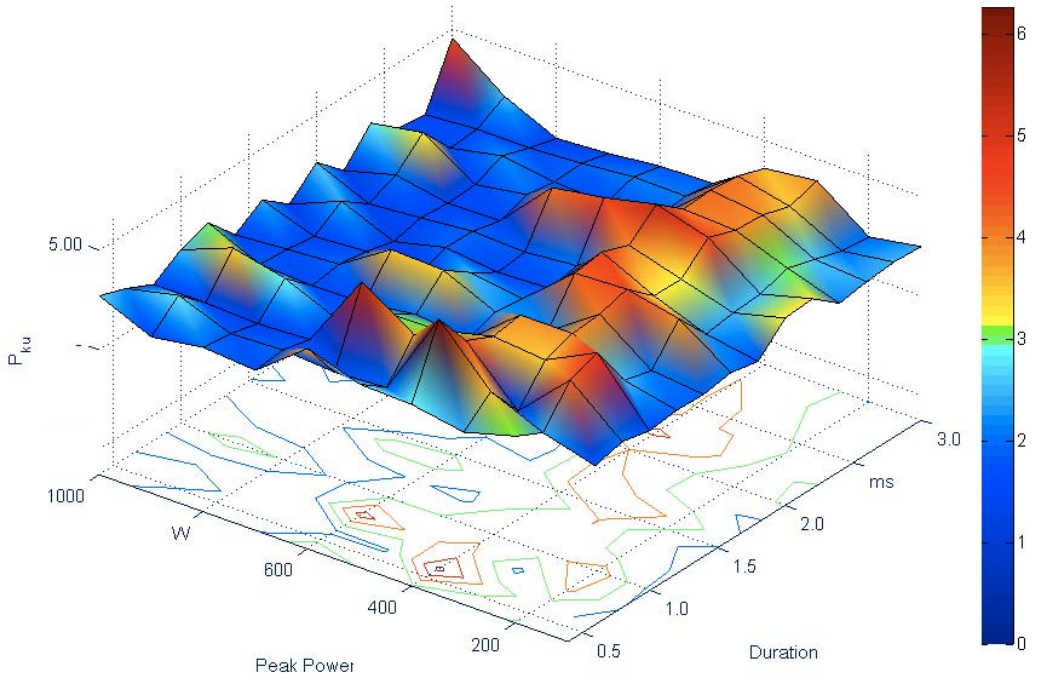

Figure 5.23: P_{ku}-measurements for Material B welds

Overall do neither skewness nor kurtosis provide unambiguous information on the kind of dominant irregularity. They can be employed as additional threshold criteria. The skewness should e.g. take on absolute values below one. Otherwise dominating craters or convex shapes appear likely. The kurtosis should not be far above three to avoid significant outlying regions as e.g. deep craters.

5.7.5 R_a

The roughness profile describes the observed wave pattern along the surface. Throughout the measurements it was observed that strong changes in the slope of the surface (e.g. craters or undercut) are included in the roughness profile as local peaks. These lie significantly above the surrounding values. The R_a-measurements compiled in Figure 5.24 show a moderate trend towards increasing energies. Yet, numerous outliers occur in low power regions.

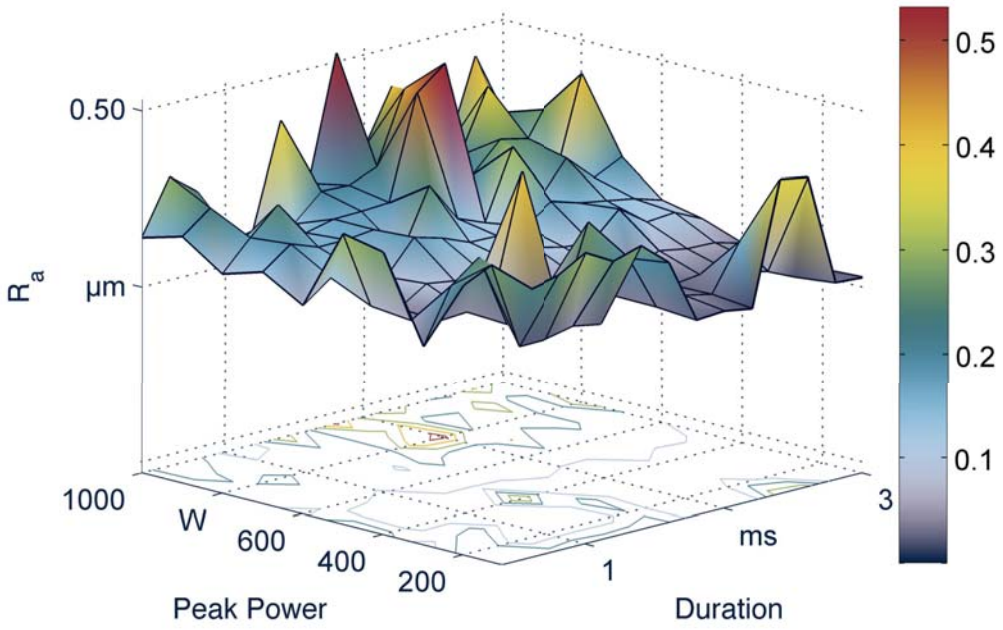

Figure 5.24: R_a-measurements for Material B welds

When compared to the R_{ku}-values below these cases frequently coincide with amplitude density curves that are outlier-prone. This indicates the significant influence the local distortions mentioned above.

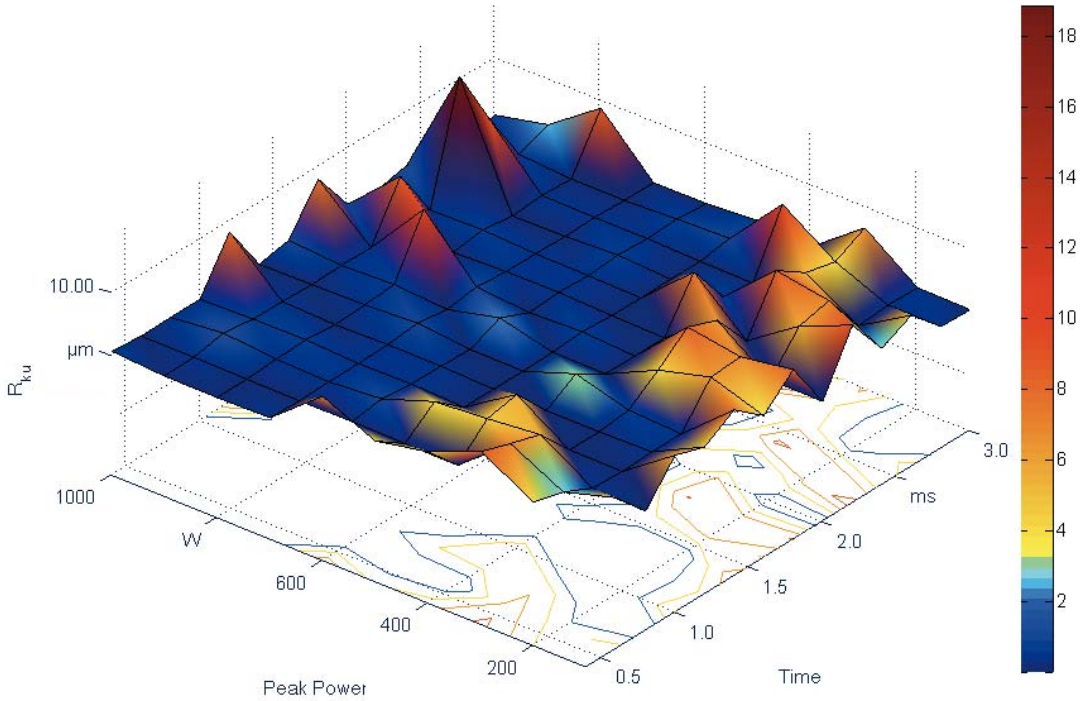

Figure 5.25: R_{ku}-measurements for Material B welds

Measurements of R_a should hence only be considered when they do not include such distortions. This complicates the analyses however decisively.

5.7.6 Repeatability of Examined Measurands

For evaluating the repeatability of measurements welds from trapezoidal pulses of the same settings are examined. The results are listed in Table 5.1 below. The observed scattering is a combined result of process instability as well as non-ideal measurement equipment and methods. All in all is the average scattering of roughly 10 % deemed acceptable for further analyses. The manual influence when measuring with help of self-drawn circles appears to be especially low (see D_{min}).

Note that the measurements are based on the whole of the surface instead of a single cross section (S-index instead of P). This strategy delivers more representative results and is applied throughout the subsequent experiments. The scattering of S_z (which corresponds to P_t) was expected to be higher than the scattering of the average-based value S_a. This will be further examined in the main welding investigation.

	D_{min}	S_q	S_{sk}	S_{ku}	S_z	S_a
	0.267	1.140	-1.550	7.150	9.790	0.850
	0.272	1.430	-2.180	8.920	9.950	0.990
	0.267	1.530	-2.070	8.220	10.300	1.060
	0.270	1.200	-2.120	9.200	9.010	0.850
CoV	**0.009**	**0.140**	**0.147**	**0.109**	**0.056**	**0.112**

Table 5.1: Scattering of measurements for a trapezoidal pulse of 465 W and 2.26 ms (ramp-up and -down 26 %, middle section 48 % of duration).

The examined pulse lies roughly in the middle of the observed energy spectrum. The scattering can be expected to decrease towards regions of lower energy and increase towards higher values. This is however rather a result of the changing process dynamics than of the applied measurement equipment and methods.

For selecting the surface, the applied software offers either a circular or a polygonal tool as shown in Figure 5.26 below. The discrepancy of the measurands' values between both cases is listed in the figure's table as ratio of circular to polygonal measurements. The average-based values (S_a and S_q) as well as the histogram-based values (S_{sk} and S_{ku}) show slight deviations. This is because in the circular measurements additional surface area is added. These sections do not alter the maximum values of heights and peaks (see S_z). The amount of deviations is however confined to 5 %. Therefore for close to circular circumferences the circular tool is regarded as sufficiently precise. For the exemplified case and cases with even stronger asymmetry the polygonal tool is applied.

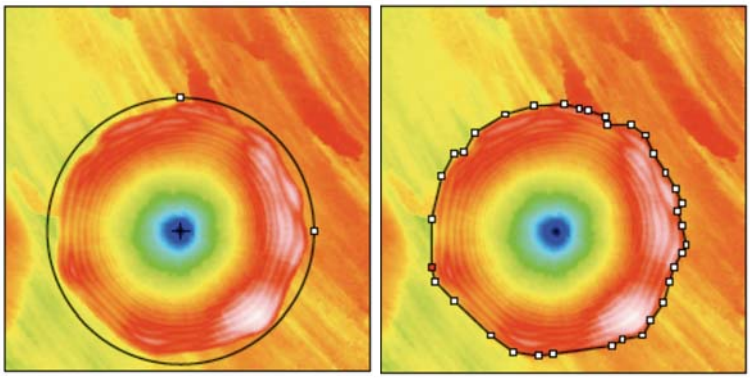

Measurand	Circle/Polygon
S_q	0.96
S_{sk}	0.99
S_{ku}	1.05
S_z	1.00
S_a	0.95

Figure 5.26: Circle- (left) and polygon-tool (right) for selecting the surface of interest

5.7.7 Conclusion on Surface Quantification

The preceding discussions are summarized in form of table. The single measurands are evaluated regarding their ability to indicate the various types of unevenness or typical irregularities.

Measurand	Global Unevenness	Unevenness along basic shape	Indication of notches	Indication of pit craters	Indication of convexity	Indication of undercut	Indication of waves
D_{diff}	XX						
P_t (S_z)	X		XX				
P_a (S_a)	XX						
P_{sk}				O	O		
P_{ku}				O			
R_a		O					O
XX: very good indication X: good indication O: restricted indication							

Table 5.2: Evaluation of measurands for surface quantification. Empty fields mark no potential for indication.

From comparing the respective graphs in appendix A2 a strong correlation of P_t and P_a and even of P_t, P_a and D_{diff} is obvious. However, each is thought to be associated with or represent a different phenomena. P_t is applied to evaluate notches. P_a is chosen as an indicator of global unevenness. D_{diff} is regarded as especially relevant since the melt pool dynamics caused e.g. by a rectangular pulse edge can possibly be alleviated by following ramp-downs. The momentarily higher melt pool dynamics may thus not be observable in the

solidified surface. An overspill is on the contrary not reversible and can indicate high temporary dynamics. Therefore, all of these measurands are considered in the following even though they might show a strong correlation.

The remaining measurands can be employed to refine the analysis. Yet, they are not regarded as capable of providing decisive and unambiguous information and therefore left out in this work.

5.8 Evaluation of Experimental Results with Methods of DoE

The experimental data are summarized in form of a two-factor design and analysed with the software “Visual Xsel 11.0“. The number of possible levels is limited to seven. Hence, only part of the P-t-matrix is evaluated. For the sake of completeness all measurands examined before are chosen as quality characteristics. The respective process model is shown below.

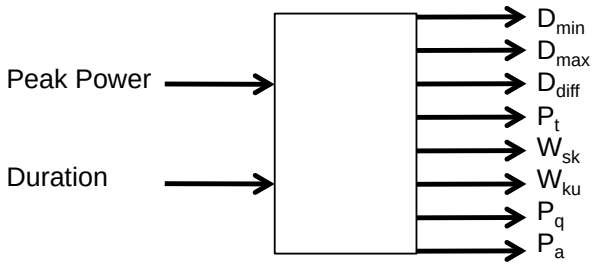

Figure 5.27: System model for DoE-analysis

The following factor levels are selected:

Level	Peak Power [W]	Pulse Duration [ms]
3	800	2.8
2	700	2.4
1	600	2.0
0	500	1.6
-1	400	1.2
-2	300	0.8
-3	200	0.4

Table 5.3: Selected levels for DoE-analysis

The determined effects from an ANOVA are compared below. Overall does the peak power show stronger and more effects than the duration. In theory this can be explained with the coupling efficiency, which directly depends on the peak power (see threshold intensity for KW-transition in section 5.5). The peak

power must therefore be regarded as the more decisive factor regarding whether and to which degree the KW-regime is entered. This finding is highly significant for the selection of factors in the following investigations.

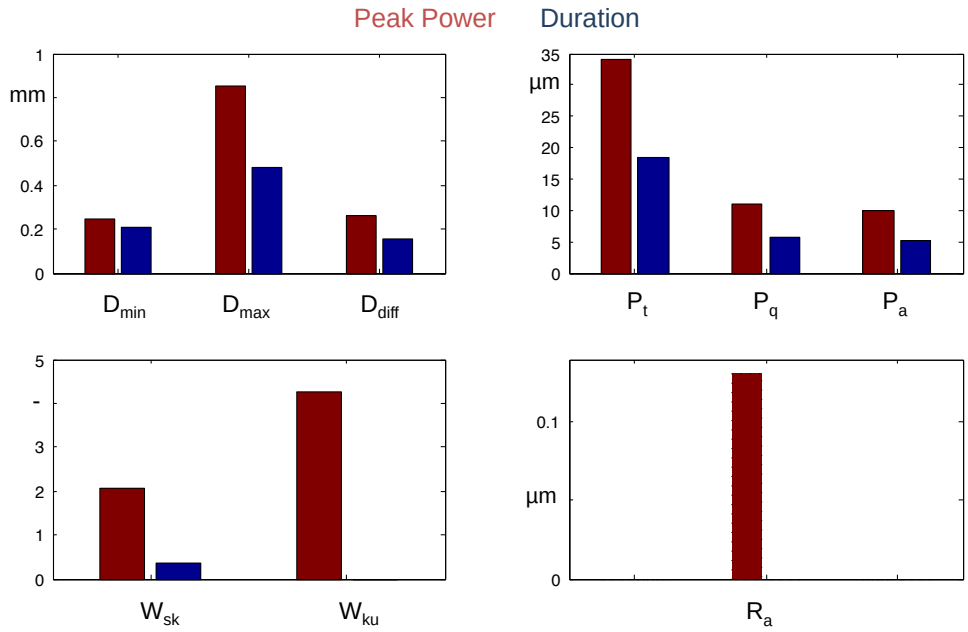

Figure 5.28: Effects of peak power and duration for Material B welds

The effect plot for Material A shows in principle the same hierarchy (no topography analyses was carried out).

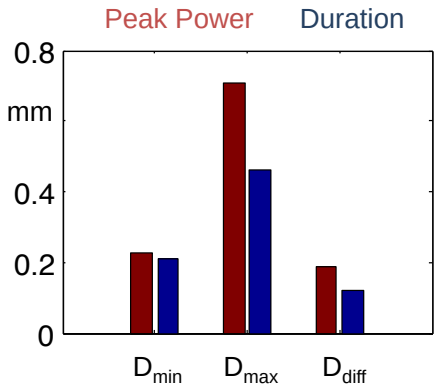

Figure 5.29: Effects of peak power and duration for Material A welds

The process was clearly found to be nonlinear regarding the observed physical phenomena. Basic process windows for both materials were defined. Measurands to indicate melt pool dynamics from the solidified surface were evaluated and selected. The influence of the peak power on the weld characteristics was found to outweigh that of the pulse duration. These results lay the foundation for systematically examining the influence of the pulse shape in the following main investigation.

6 Main Investigation on Partial Penetration Welding

An experiment to systematically investigate the effects of the pulse shape is designed and conducted. The produced welds are evaluated with surface-bound measurands as well as metallographic cross sections. The results are confirmed by studying the actual outcomes for each factorial level. A comparison to the results of known studies is included. Eventually, a concluding experiment gives an outlook on joining dissimilar materials and evaluating overlap welds in tensile tests.

6.1 Factorial Design

The proceeding experiment identified the measurands P_t, P_a and D_{diff} as suitable quality characteristics. To achieve more representative measurements the whole of the surface is selected as "primary profile" (S_z and S_a instead of P_t and P_a – see 5.7.6). The remaining diameter values D_{min} and D_{max} are considered alongside to achieve comparability to the prior investigations. Metallographic cross sections are applied to determine the welding depth W_D (see Figure 6.6). The respective process model is given below.

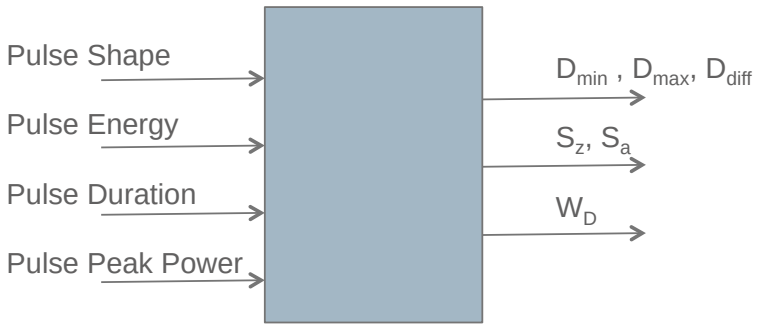

Figure 6.1: Process Model for the main welding experiments

As outlined in section 3.3.2 the depicted factors cannot be varied independently of each other. There exists a maximum of three degrees of freedom, which means that one factor has to be eliminated from the model. This factor will constantly be adapted to the settings of the other three.

The shape is the main factor of interest and must therefore be kept. To compare the shape's effect the energy must not vary arbitrarily. Systematically varying the shape entails a variation of the energy distribution between sections of ramp-up, -down etc. In order to solely focus on the shape's influence must the energy remain constant during these stages.

Consequently can only the duration or peak power be eliminated from the model. The ANOVA-results from the prior investigation clearly identified the peak power to be of higher influence. It is therefore chosen as the third factor.

The factor “shape” is further broken down into sub-factors to ensure a broad spectrum of variation. These factors should allow for the application of shapes “from rectangle to triangle”. Furthermore should ramping-up and -down be considered independently of each other. This can be achieved by applying two set-points, whose levels are the relative positions along the time axis. The complete process model is illustrated below.

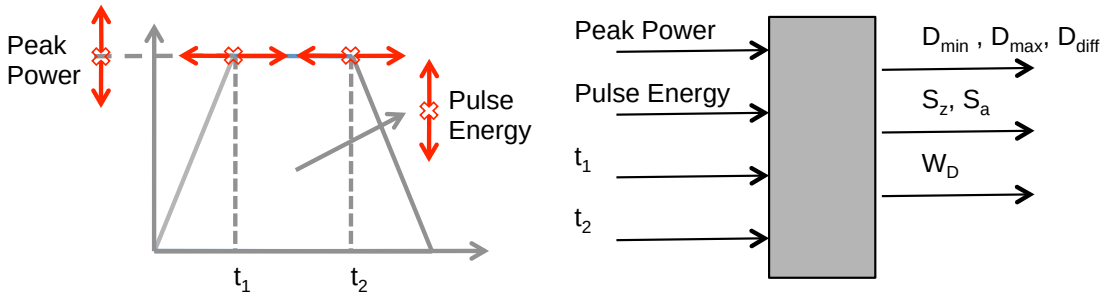

Figure 6.2: Process Model and chosen factors for the main welding experiments.

Being of a highly nonlinear nature, the process needs to be modelled by at least a second-degree polynomial. For four factors a CCD-design requires the least amount of runs (compare Table 3.2). The value of alpha is set to two in order to achieve the statistically most valuable results (see section 3.5).

The priorities when setting the factor-levels are to create shapes from “rectangle to triangle” and to cover both welding regimes. The upper limit for the applied power should not be far above 1000 W (significant deficiencies expected) and cannot lie below 102 W (system-inherent lower bound). Each shape must be verified regarding the required rise times. The fall times are not considered since no intermediate set-points exist along the falling edge (compare section 4.5).

The following settings fulfill the demands discussed above:

Level	Peak Power [W]	t_1 [%]	t_2 [%]	Energy [J]
2	1025	0.08	0.92	1.55
1	800	0.18	0.82	1.3
0	575	0.28	0.72	1.05
-1	350	0.38	0.62	0.8
-2	125	0.48	0.52	0.3

Table 6.1: Level settings for the main welding experiments.

The range of pulse shapes at these settings is depicted in Figure 6.3 below. The pulse shape at central point settings is given in Figure A3.1.

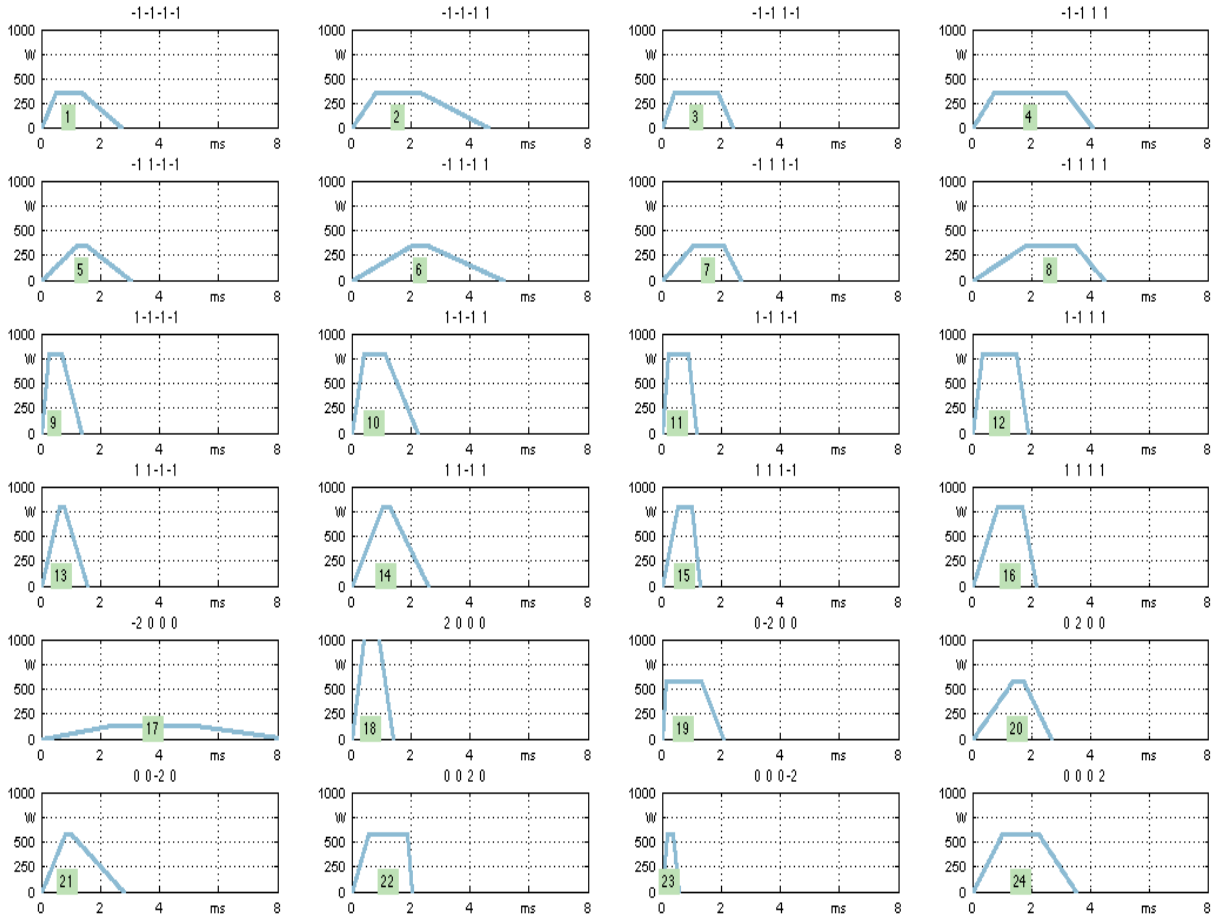

Figure 6.3: Range of applied pulse shapes. The title contains the factor settings in the sequence: Peak Power, t_1, t_2, Energy.

The pulse shapes with close to rectangular slopes (factor t_1 at level 2 or 1) are added to the process window of section 5.5. The duration for these pulses is limited to t_2 when added to the plot. This is because the section following the second set point is not assumed to contribute e.g. to the achievable D_{min}. This modelling is based on pure assumptions and only serves as a basic orientation

to verify the level setting. The resulting plot is shown in Figure 6.4. The numbering corresponds to that of the preceding figures. As can be seen, the factorial core is roughly adapted to the previously defined process window. The star points reach however further to the margin areas.

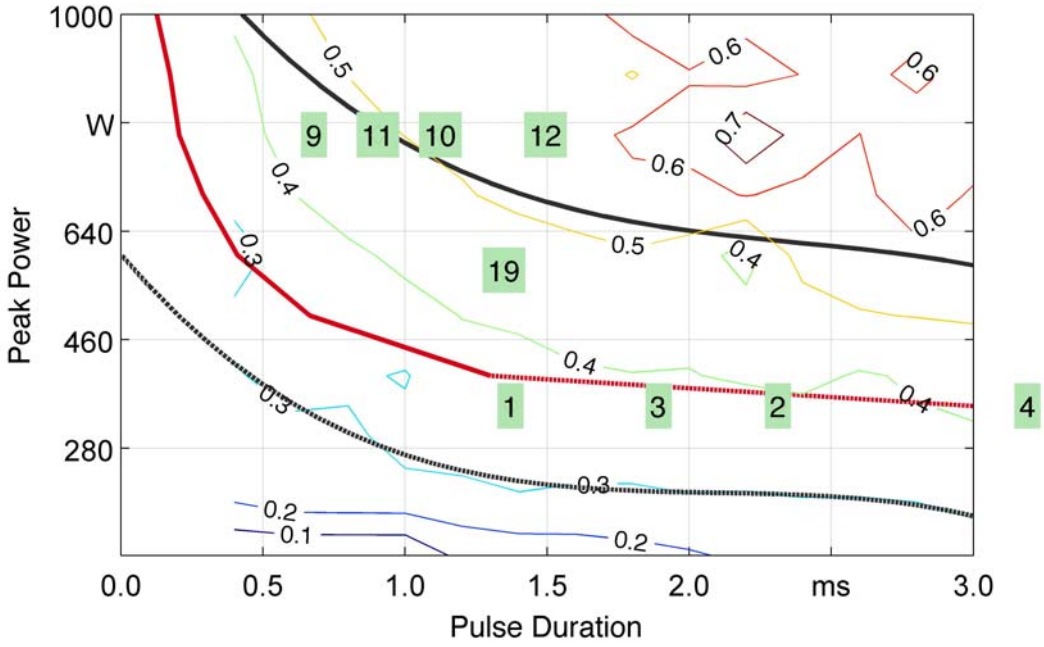

Figure 6.4: Process window with selected CCD-pulses.

6.2 Experimental Set-Up & Methodology

The basic set-up is maintained. The samples are halved by electric discharge machining. This is due to the necessity of a horizontal edge for the following metallographic grinding process. A row of spot welds is welded along this edge. For doing so the samples are arranged on a linearly guided plastic rail (slide rule) and fixed with adhesive tape (see below). This represents a change compared to the mere plastic piece applied before. However, the samples are still positioned on heat insulators, which are assumed to have the same effect on the resulting weld. The exact positioning of each sample is adjusted with help of the laser system's optical crosshair.

Figure 6.5: Positioning of halved samples on slide rule and embedded samples after producing metallographic cross sections.

The working sequence for producing the metallographic cross sections consists of embedding the samples in plastic, grinding the embedded sample to the centre-point line of the spot welds, polishing the plane of the cross sections and eventually etching this surface.

It is in this case extremely relevant to randomize the experimental sequence. On average 11 spot welds can be fitted on one sample. The overall population of 108 welds (n=4) is hence distributed over 10 samples. The grinding process is carried out manually and therefore prone to subjective influences (e.g. optical detection of centre-point line). It cannot be excluded that certain samples are grinded less accurately than others. These influences need to be distributed equally over the experimental population by randomization.

The topography of the welds is measured with the white light microscope prior to embedding (compare section 5.6). The diameter-related values are determined alongside from these measurements. The software measures only the radii, which is why the known values are marked with R instead of D in the following. For measuring the welding depth the metallographic cross sections are analysed with the stereo microscope and its respective software (see below).

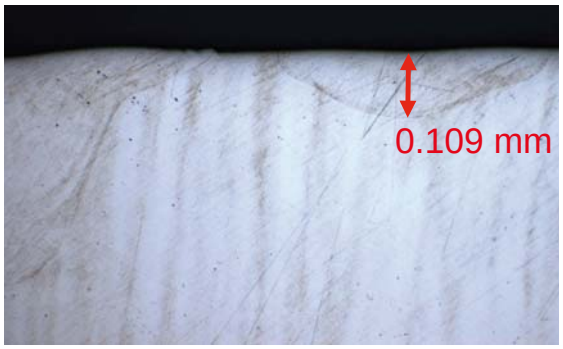

Figure 6.6: Measuring of the welding depth from metallographic sections. Left: weld from a 800 W pulse at 1.3 J, Right: 350 W at 1.3 J.

The duration is calculated by transposing the energy equation derived in section 4.5. The results are compiled in the overview on experimental settings in Table A3.1. At first only Material A is welded.

6.3 Experimental Results

The accumulated data are analysed with the software Visual Xsel. The derived system equations as well as the received R^2-values are listed below.

System Equations	R^2
Sa = 1.9889+1.9395•P+0.799333•E+0.91675•P•E+0.76895•P2	0.636
Sz = 16.77342+15.60396•P-0.22938•t2+7.136875•E-5.14938•P•t2+8.021875•P•E+5.800042•P2	0.770
Rdiff = 0.022583+0.04775•P+0.008333•t2+0.014917•E+0.024625•P•E+0.022292•P2	0.745
Wd = 0.1588+0.141208•P-0.00883•t1+0.021208•t2+0.079042•E+0.089125•P•E-0.035•t1•E+0.056067•P2	0.899
Rmax = 0.240486+0.265417•P+0.071917•E-0.09732•P2-0.1072•E2	0.851
Rmin=0.237817+0.074625•P-0.00525•t1+0.008792•t2+0.033125•E-0.01425•t1•E-0.0288•P2	0.905

Table 6.2: System equations derived through regression and ANOVA.

From the equations above it is obvious that the set-points and thus the shape are of comparatively little influence. This is given further evidence when considering the factor plot below.

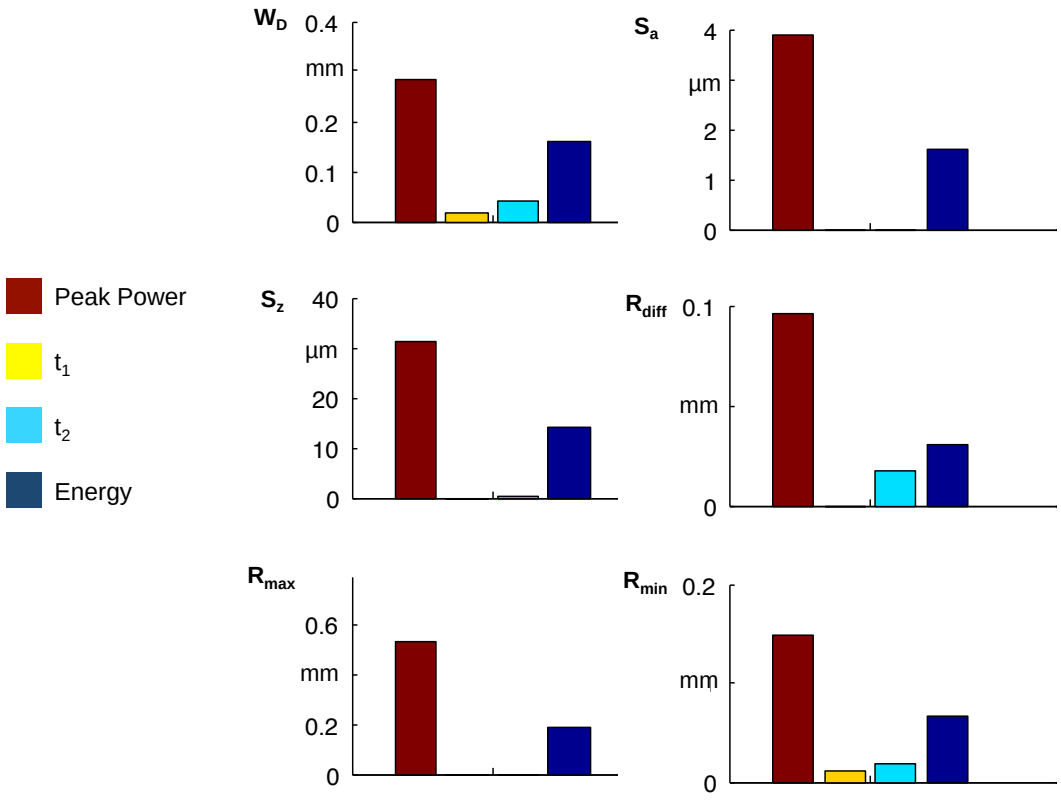

Figure 6.7: Effect plot for the main welding experiment.

Similar to the investigation on rectangular pulses is the peak power identified to be the most influential factor. The energy has about half the effect. Regarding the shape ramping-down shows higher and more frequent effects. However, both shape factors do not always pass the ANOVA (F-test) and are clearly of less significance.

The consistency of the results can be confirmed when considering the explicit results of the factorial core (Figure A3.2) as well as of the star- and centre-points (Figure A3.3). The figures compile the individual pulse settings with an exemplary metallographic cross section as well as the most relevant measurements and their scattering.

In Figure A3.3 the results are grouped according to the varied factor. From one to four these are: t_1, t_2, peak power and energy. The effects of the variation can be examined from left to right (or v.v.) with the central point as intermediate step. In case of t_1 and t_2 the mere shape is varied. It becomes obvious that ramping up by varying t_1 shows only very little influence on the achievable welding depth (ca. 10 %) and profile height (S_z). Stronger variances occur in case of the overspill (30 %).

When varying t_2 and hence the ramp-down stronger effects become noticeable. Steep ramps raise the welding depth by up to 60 % compared to lower level settings. The overspill increases however proportionally.

The shape or relative energy distribution between the single pulse sectors remains constant when varying energy and peak power (groups 3 and 4). In the latter case an increase in welding depth of 350% is reached at the same energy content. The overspill and profile height increase accordingly. Regarding the energy, similar yet less drastic effects can be observed. All in all, the hierarchy of the factor plot can clearly be confirmed.

It is also worth noting that the scattering of the average profile depth S_a is lower than that of the maximum value S_z. This was expected but could not be confirmed in Table 5.1. The CoV of the R_{diff}-values shows some strong outliers. In these cases an overspill was (subjectively) detected in only some of the four welds per parameter setting. Defining a quantified lower boundary for marking an overspill is an obvious challenge when applying this measurand.

With reference to Figure A3.2 it can be seen that the influence of the shape occurs independently of the welding regimes. The groups from one to four depict varying shapes for two energy contents (grouped in columns). The respective HCW or HCW-KW-transition welds can be found in groups one and three (see shapes of cross sections). When raising the peak power within one column the welds enter the KW-regime without changing the pulse energy. Again does the variation of the ramp-down show a higher influence than ramping up.

6.3.1 Curve Diagrams and Contour Plots

The equations listed in Table 6.2 can be visualized with curve diagrams. Each factor is varied along its scale whilst the remaining factors are kept at the 0-level.

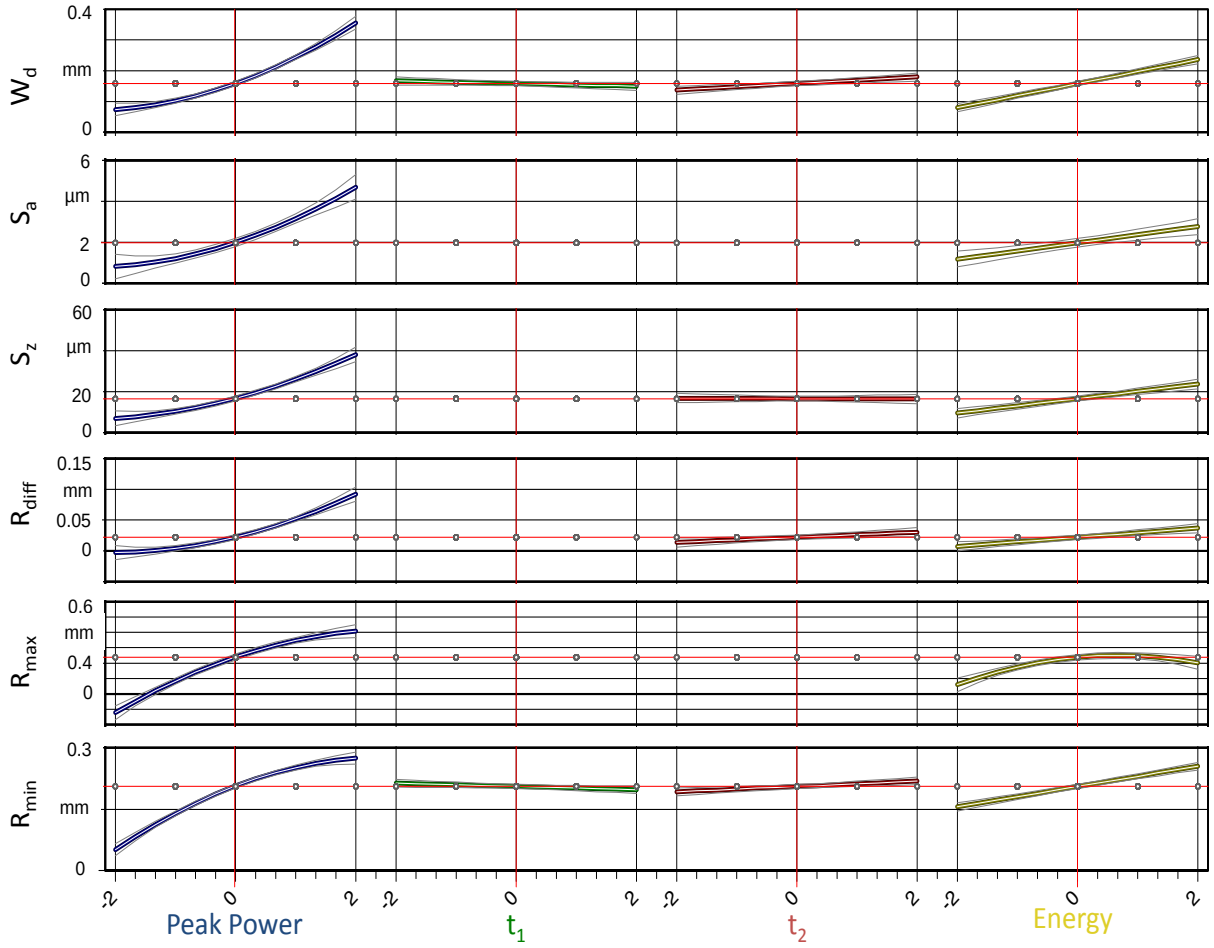

Figure 6.8: Curve diagrams for the main welding experiment.

For the central factor peak power one can see that no plateau is reached for the welding depth (unlike for the R_{min}-curve). This central quality characteristic can hence be significantly raised throughout the experimental space. On the contrary do R_{diff} as well as he S-values increase simultaneously. When varying the shape through t_1 and t_2 the same proportional relation of welding depth and surface irregularities can be observed.

Due to this proportional behaviour no optimization potential can be indentified. The conflicting goals of weld volume and quality cannot be solved by any of the factors as no relative gains between the measurands are achievable. The amount of tolerable surface irregularities therefore define the maximal achievable welding depth

In a contour plot two parameters are varied with respect to a given quality characteristic. This way the respective interdependencies can be considered. For such a plot the most influential factors of peak power and energy are chosen (t_1 and t_2 at 0-level). As shown below does the maximum achievable welding depth amount to 0.55 mm. From the previous discussions it is obvious

that this value can only slightly be raised by e.g. changing t_2 to a steeper ramp-down. Furthermore, it can be confirmed that advances in welding depth are almost proportionally accompanied by surface unevenness. This is obvious from the S_z contour plot below.

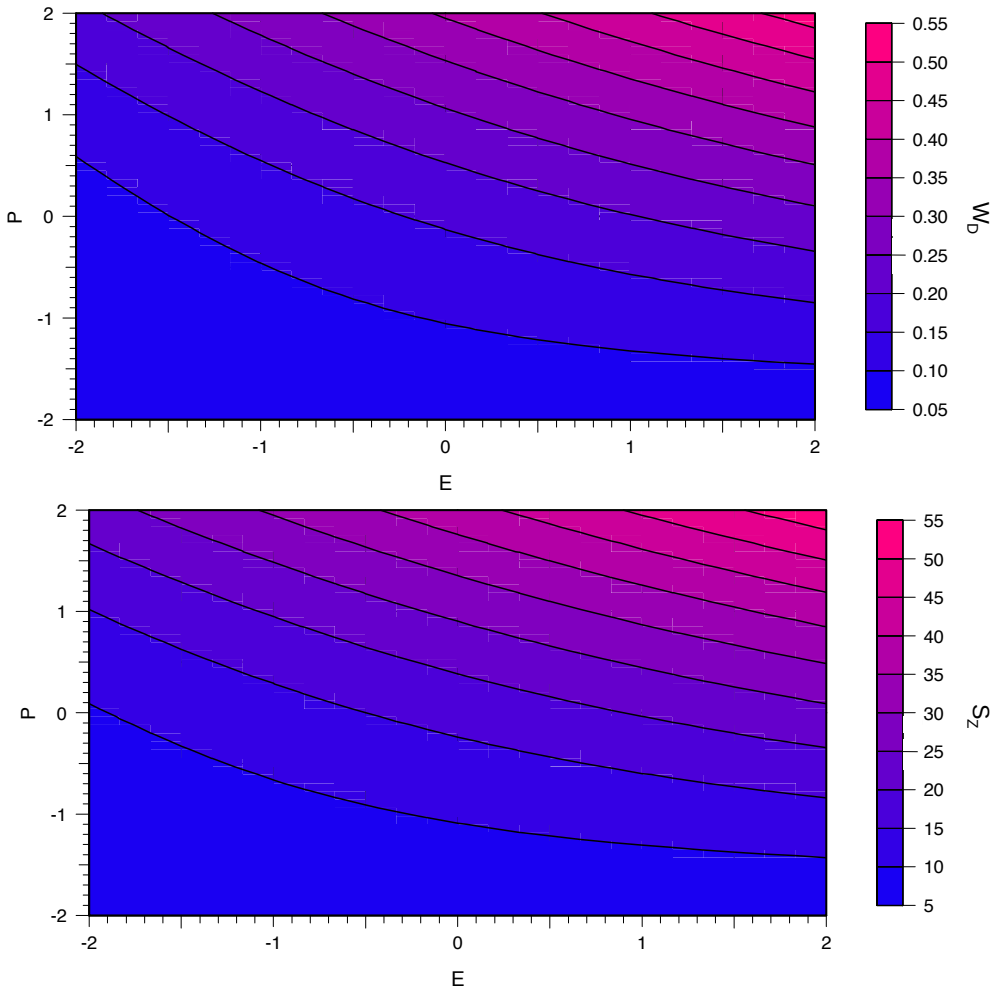

Figure 6.9: Contour plots for achievable welding depth (W_D) and profile depth (S_z) as a function of the most influential factors.

With respect to the global goal of avoiding spatter must the W_D-plot be limited in its applicability. Heavy spill is noted in one out of for welds for the peak power star-point. Furthermore, pores have been detected in one of four welds for a pulse with 800 W (power-level 1) and 1.3 J (energy-level 1) as well as for the energy star-point (level 2).

Hence, the possible parameter settings need to be restricted to avoid the top right corner of the plot (e.g. maximum settings of 1.5 for both factor levels). Reliable thresholds require however further verification through experiments.

For the moment no refinement of the system equations is carried out (e.g. by eliminating outliers). This is because the system models' main purpose is to

achieve a basic understanding of the factors' significances and influences on the process. If used for optimization purposes or for predicting possible outcomes a refinement should be considered. With regard to the curve diagrams in Figure 6.8 a potential for improvement of the models can be observed for the R_{diff}-equation (below zero at P-setting of -2) and the R_{max}-equation (decrease towards energy star-point is implausible).

The normal probability plot below identifies some welds to be outliers (compare section 3.5).

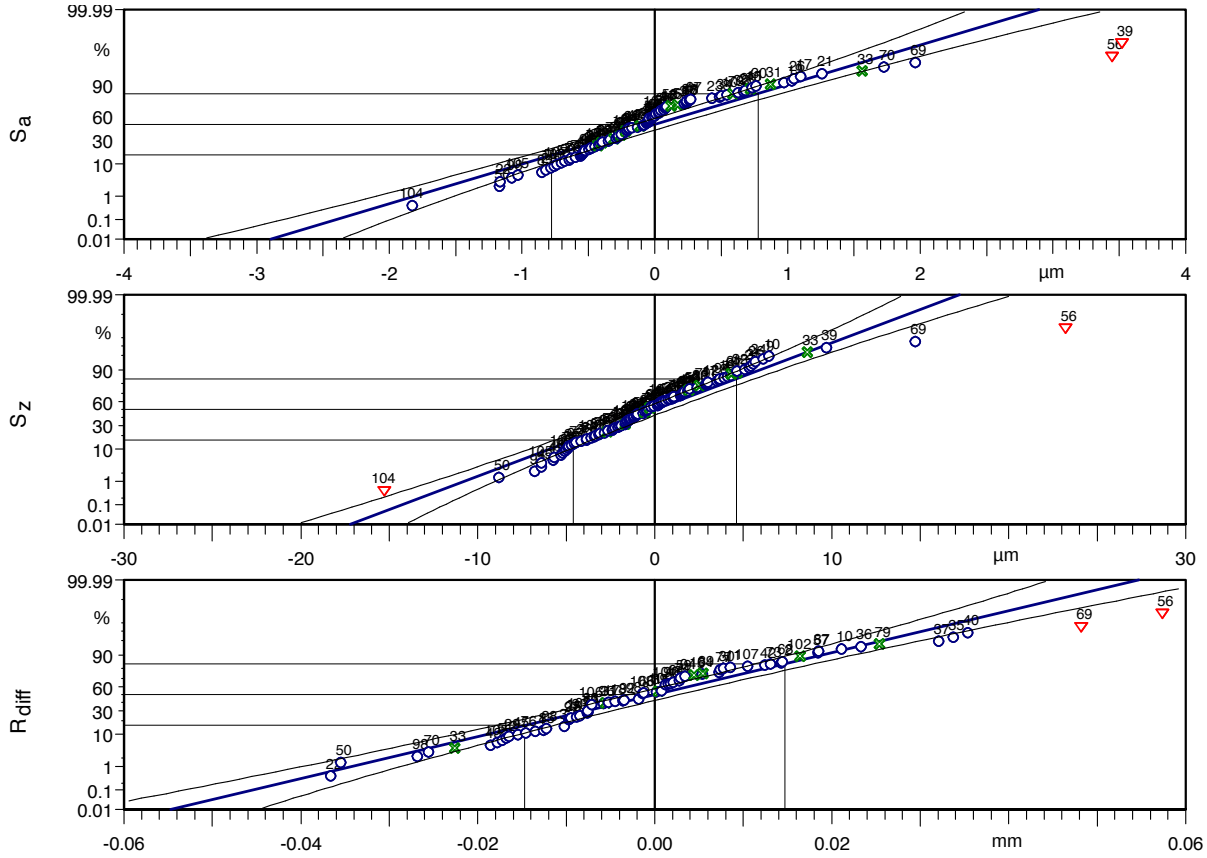

Figure 6.10: Normal probability plot of residuals

If these outliers are removed the R^2-values are raised and – in theory – the predictive quality is higher. On the other hand do the outliers result from actually observed process dynamics. This seems evident when considering the applied settings for the outliers (numbering corresponding to Table A3.1), which are exclusively in power regions of 800 W and above. These regions have already been identified to be very dynamic and prone to irregularities in chapter 5. If these welds were removed a stability of process is pretended that cannot be confirmed from practical experience. The welds in question are furthermore only marked as outliers for surface-bound measurands but not for the welding depth or R-values. This indicates that a systematic error in the set-

up or measurement equipment is unlikely. Instead, the models should not be applied for calculations in regions of high power and energies (e.g. above level 1.5) since the dynamics and thus the potential for outliers is critically raised. If this restriction is made, the outliers could also be removed without problems to raise the predictive quality within regions of lower power.

6.4 Confirmation of Factor Hierarchy for Material B

From a simple test run the factor hierarchy observed for Material A is confirmed for Material B. The level settings are slightly lower respectively closer together. This is because this series was carried out as a simple test run before choosing the final settings applied for the elaborate investigation of Material A. The level settings can be read from the table below.

Level	Peak Power [W]	t_1 [%]	t_2 [%]	Energy [J]
2	795	0.06	0.94	1.20
1	630	0.16	0.84	1.0
0	465	0.26	0.74	0.8
-1	300	0.36	0.64	0.6
-2	135	0.46	0.54	0.2

Table 6.3: Level settings for partial penetration welding on Material B samples.

The factor plot is given in Figure 6.11 (note: t_1 not included since it does not pass the ANOVA F-test for any of the quality characteristics). Only surface-bound characteristics are considered. In principle the same factor hierarchy is revealed. Since the results provide basically the same information it is not regarded as insightful to expand this investigation. The larger effect of energy on S_a can be attributed to the omittance of repetitions and therefore low precision of the results.

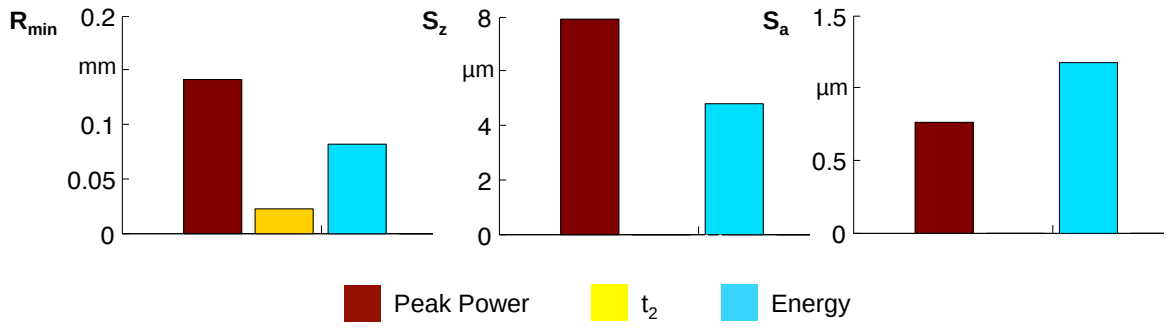

Figure 6.11: Effect plot for partial penetration welding on Material B samples.

6.5 Comparison of Experimental Results and Results in Literature

The experimental results of this work cannot fully confirm the rules of thumb on pulse shape influences as compiled in section 2. In addition can contradicting experimental results be found in literature as detailed below. With regard to these studies the following differences are apparent:

- The pulses applied in this work are comparatively low in terms of energy, power and duration.
- Different Materials are examined. No studies on the materials applied in this work are known.
- The applied process models deviates from the one at hand. It is mostly not explicitly mentioned how the factors pulse power, energy and duration behave when the shape is varied. This is denoted as “unknown process model” in the following. In some cases this can also mean that the observed effects cannot be automatically attributed to the shape itself. Instead the result may have equally been caused by another factor, which was varied alongside.
- None of the studies provide information on whether the found influences of the shape help to solve the conflicting goals of quality and strength (except in parts [KAISER & SCHÄFER 2005]). It is frequently shown that e.g. ramp-downs improve surface quality. Yet, it is not examined whether this could equally be achieved by lower peak powers as the results above suggest. Furthermore, it is not mentioned to which degree these quality improvements take place at the expense of the achievable welding depth.

The table below lists some of the available studies and the major differences to the investigations of this work.

Reference	Results	Differences
NAEEM 2004	Confirmation of basic rules of thumb on pulse shape influences (stainless steel and Al).	Unknown process model, pulse energy appears to be excluded and varies when comparing shapes.
BERTRAND & POULON-QUINTIN 2011	Shape influence on quality confirmed (Pd-Ag-Sn alloys).	Examination of seam welds from spot weld chains Shape comparisons at different energy contents and with longer durations (6 ms)
KAMENZ 2010	Triangular pulse identified to be advantageous for Cu-Ni alloys.	Peak power excluded from process model, power levels vary when comparing shapes.
KAISER & SCHÄFER 2005	Confirmation of basic rules of thumb on pulse shape influences (steel, Ag, Al).	Higher energies (6,5 KW), peak powers (3 KW) and durations applied (10 ms). Process model partially unknown in terms of applied peak power. No systematic effect comparisons for the factors in question.
VDI-TPT 1995	Confirmation of factor hierarchy regarding (average) power and ramp-downs on penetration depth (Cu, steel). Confirmation of the influence of ramp-downs on quality (Al).	No consideration of optimization potential and conflicting goals of quality and strength.
KLAGES ET AL. 2004	Confirmation of the influence of ramp-ups and -downs on quality (Cu, steel).	Examination of seam welds from spot weld chains Process model unknown. Far longer durations applied (20 ms).

Table 6.4: Overview of relevant studies and their results.

[KAISER & SCHÄFER 2005] show that the pulse-shape can improve quality and maintain penetration at the same time (Ag and steel combination). Yet, as listed above the pulse data are far above the ones studied in this work. A sole KW-process must be assumed at around six times the energy.

In the light of the determined results these findings can obviously not be scaled down to the examined process dimensions.

On the other hand, influences such as workpiece geometry, coatings and gaps between join partners were not considered. For these cases pulse shaping may still proof to be a relevant parameter even in the scenario at hand. In addition the pulse shape was only modulated by ramping up and down and not by e.g. initial sparks as in [KAISER & SCHÄFER 2005].

6.6 Concluding Experiment: Outlook on Joining of Dissimilar Materials

As a concluding step an additional experiment is conducted in which dissimilar materials are joined and examined in a tensile test. The purpose of this investigation is to:

- confirm the results derived above for an example of joining dissimilar materials.
- examine the evaluation of overlap joins in tensile tests.

The examined material combination is Material C and Material A. The Material C samples are thin quadratic plates with a thickness of 0.1 mm. With help of a marking laser these plates are cut into strips of 2 by 10 mm. The Material A samples and the overall setup are similar to before. The Material C strips are positioned on the Material A dies and held down by ceramic tweezers. An example of a Material C sample after tensile testing is given below.

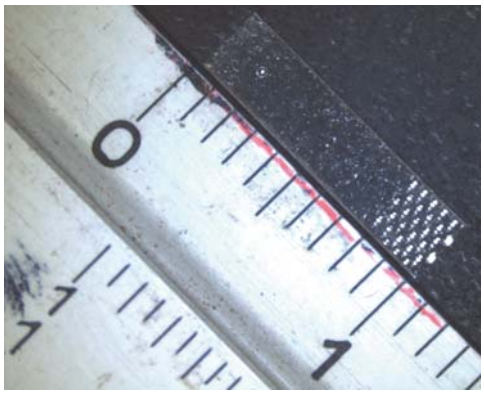

Figure 6.12:Material C sample after tensile testing. The profile at the bottom is caused in the clamping process.

The welded samples are clamped in a tensile tester (Zwick/Roell: zwicki-line) The tensile strength R_m is taken as measurement for evaluating the join. The clamping must in this case be regarded as not optimal because it is stiff a both ends. Ideally should a “soft-end” clamp be used at the Material C strip to avoid the introduction of torque into the weld. Such a soft-end typically consists of a clamp hanging from a metallic wire. This arrangement was initially tested but the clamp occasionally slipped from the samples. For more representative results such an arrangement should in any case be applied (e.g. use stronger clamps at soft-end). This could however not be arranged for in the shortness of time. Figure 6.13 shows a welded sample in the applied set-up.

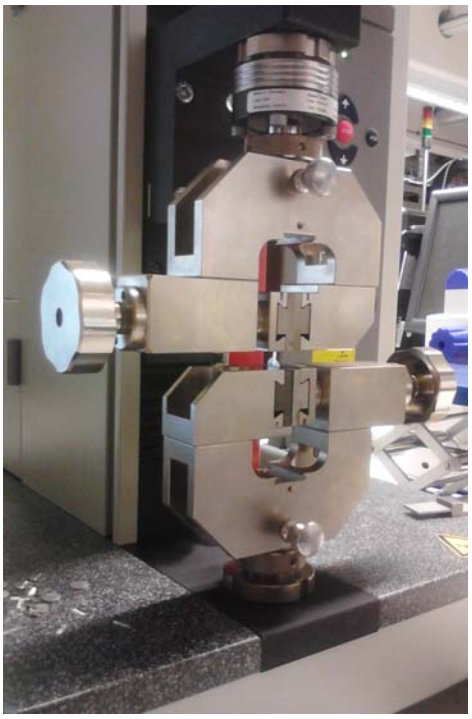

Figure 6.13: Welded sample in tensile test.

As an additional measurement the diameter of the weld at the Material A surface is measured after rupture (see below). This is thought to represent the join diameter.

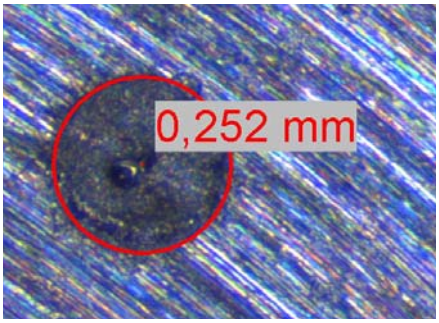

Figure 6.14: Join cross section on Material A sample after rupture and its measured diameter.

6.7 Experimental Design and Results

To reduce the number of runs the energy is kept constant at 1.5 J. Furthermore, the number of factor levels is reduced to two since only a hierarchic overview of the factors' influences is desired. The shape is again varied by the two set-points t_1 and t_2 and the duration is calculated as before. One repetition (n=2) is carried out. The following level settings are applied:

Level	Peak Power [W]	t_1 [%]	t_2 [%]
1	700	0.45	0.85
0	400	0.15	0.55

Table 6.5: Level settings for the concluding experiment.

The main effect plot below confirms the results of the main welding experiment.

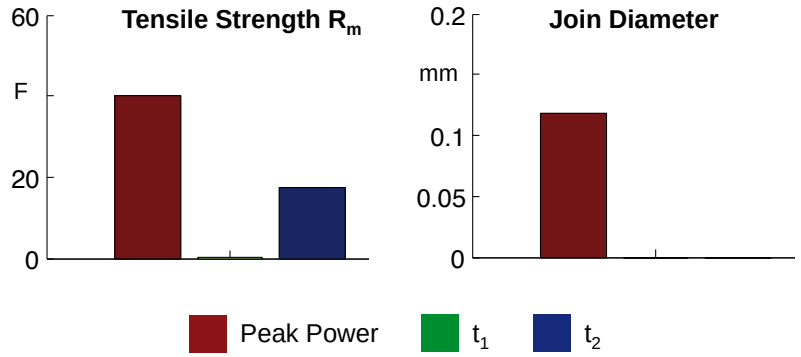

Figure 6.15: Effect plot for concluding experiment.

From this result no secured inferences on the relation of join cross section and transmittable force can be made. According to section 1.2.1 the cross section is a major parameter to resist shearing force on the weld. This is confirmed by [ZHOU ET AL. 2003] who found the diameter of spot welds (nuggets from resistance spot welding of steel) to be more significant than the overall volume. Yet, it does not seem plausible that the ramp-down has a large effect on the overall strength without having an effect on the (in theory) main parameter join cross section.

An explanation can be the measurement method of the join cross section and the occurrence of different failure modes. For low power settings the weld typically shows an interfacial fracture along the join cross section. At higher values the weld is torn out of the Material C strip completely and leaves a hole (compare [CHAO 2003]). Thus deformed material remains at the surface of the Material A sample, which can bias the measurement. The observed failure

modes are illustrated below. The weld from low power settings shows a bright metallic reflection in the center point. The weld from high power settings shows a dark hole, which indicates the pullout of the core weld.

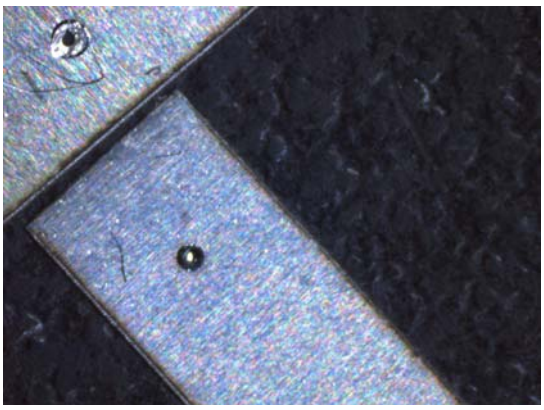

Figure 6.16: Different failure modes in tensile tests observed from Material C samples. Left: Pullout at high power settings, right: interfacial fracture at lower power.

The main welding experiment showed that the influence of the pulse shape is very low compared to applied peak power and pulse energy. It was furthermore shown that neither of these parameters bears the potential to improve the conflict between potential strength (weld volume) and spatter risk (surface quality). Instead a proportional development of these characteristics was observed. A comparison of the results to known studies showed that the influence of the pulse shape is only confirmed for far higher power and energy levels. In tensile tests the results were also found to be valid for a joining task of dissimilar metals. Yet, the applied set-up and measurement methods for tensile testing need further improvement.

7 Summary and Outlook

The work at hand examines the influence of the pulse shape on welds in laser beam micro joining of exemplary materials. For doing so different pulse shapes are systematically applied to produce partial penetration welds in an experimental design according to methods of DoE.

In order to guarantee a high informational value and a transferability of the results the pulse shaping capabilities of the laser system in use are studied at first. The non-ideal nature of the laser system leads to numerous deviations between set and action behaviour. These are observed and quantified. Based on these results criteria are defined to judge whether a given pulse shape can be generated with sufficient accuracy.

In the next step a reference investigation with basic rectangular pulses is carried out. A complete matrix of pulse power and duration is applied to produce partial penetration welds. The welds' surfaces are measured to quantify irregularities, which indicate closeness to spatter formation. In a comparison between qualitative observations and quantitative results suitable measurands are identified. These are needed for the evaluation of welds in the following DoE-designs. By measuring the reflective signals of laser radiation with a photodiode the points of transition from HCW to KW are estimated. It is found that the examined process is highly nonlinear with a central transition between the two regimes. Furthermore, it can be shown that the pulse peak power has a stronger influence on the examined measurands than the pulse duration.

The results are employed for designing the main experimental investigation. A four factor CCD-design is developed to produce partial penetration welds. These are analysed from the surface as well as with metallographic cross sections. It is found that the influence of the pulse shape is very low when compared to the pulse's peak power and energy content. None of these factors bears the potential to solve the conflicting goals of quality (spatter, surface roughness, pores etc.) and achievable strengths. A systematic comparison of the investigation to known studies is carried out. This reveals the examined process dimensions to be far below the ones examined in literature. As a concluding step the main result is confirmed for the joining of a combination of dissimilar metals. In this case overlap joins are produced and evaluated in tensile tests.

For all materials and even for a combination of dissimilar metals the pulse shape was determined to be a factor of low significance within the scope of examined parameter settings. It can not be ruled out, however, that in case of coatings, real workpiece geometries, special material combinations or gaps the pulse shape may still be valuable parameter for process engineering.

Regarding the applied measurands for examining welds, the measure of overspill D_{Diff} proofed to be an efficient parameter. In comparison to measurands, which are based on height profiles of the surface, this value can be easily detected by vision. This is highly advantageous when considering standardized or even automated solutions for spot weld inspection.

References

ADAM 2012

Adam, M.: Skript zur Vorlesung: Statistische Versuchsplanung und Auswertung. Fachhochschule Düsseldorf (2012). Available at mv.fh-duesseldorf.de (Last viewed: 07.02.2012).

ASME 2011

American Society of Mechanical Engineers (ASME): ASME B46 Committee – Surface Texture – Panel Discussion. Online presentation (2011). Available at: http://cstools.asme.org/csconnect/pdf/CommitteeFiles/21763.pdf. Last viewed 15.01.2012.

BLAU & HAN 2007

Blau, G.; Han, S.: Response Surface Methodology. Lacture Slides (2007). Available at: pharmahub.org/resources/166/download/t6rsm.ppt. Last viewed (07.02.2012)

BERTRAND & POULON-QUINTIN 2011

Bertrand, C.; Poulon-Quintin, A.: Effect of temporal pulse shaping on the reduction of laser weld defects in a Pd-Ag-Sn dental alloy. Dental Materials (2011). Vol. 27. p. E43-E50.

BRASSEL 2002

Brassel, J.-O.: Prozesskontrolle beim Laserstrahl-Mikroschweißen. Dissertation Universität Erlangen. Bamberg: Maisenbach-Verlag 2002.

CHAO 2003

Chao; Y. J.: Failure modes of spot welds: interfacial versus pullout. Science and Technology of Welding and Joining (2003). Vol. 8. No.2. p.133-137.

CRAMER & KAMPS 2007

Cramer, E.; Kamps, U.: Grundlagen der Wahrscheinlichkeitsrechnung und Statistik. Berlin: Springer Verlag (2007). ISBN 978-3-540-36342-2.

DAUSINGER 1995

Duasinger, F: Strahlwerkzeug Laser: Energieeinkopplung und Prozesseffetivität. Habilitationsschrift. Stuttgart: Teubner-Verlag (1995).

DEAN & ILLOWSKY 2011

Dean, S.; Illowsky, B.: Descriptive Statistics: Skewness and the Mean, Median, and Mode. Online Article (2011). Available at: http://cnx.org/content/m17104/latest/. Last viewed: 15.01.2012.

DEY ET. AL 2009

Dey, V.; Pratihar, D. K.; Datta, G.L.; Jha, M.N.; Saha, T.K.; Bapat, A.V.: Optimization of bead geometry in electron beam welding using a Genetic algorithm. Journal of Materials Processing Technology (2009). Vol. 209, p. 1151-1157.

DIN EN ISO 4287 2009

DIN EN ISO 4287: Geometrische Produktspezifikation (GPS) – Oberflächenbeschaffenheit: Tastschnittverfahren – Benennungen, Definitionen und Kenngrößen der Oberflächenbeschaffenheit. Berlin: Beuth Verlag 2009.

DÜRR ET AL. 2006

Dürr, U.; Holtz, R.; Westphäling, T.: Industrielle Anwendungslösungen mit gepulsten Nd:YAG-Lasern. Presentation slides for the 5. Laseranwenderforum (2006).

EICHLER & EICHLER 2006

Eichler H.-J.; Eichler J.: Laser – Bauformen, Strahlführungen, Anwendungen. 6. Auflage. Berlin: Springer Verlag 2006. ISBN-10 3-540-30149-6.

FRITZ & SCHULZE 2008

Fritz, A. H.; Schulze, G. (Hrsg.): Fertigungstechnik. 8. Auflage. Berlin: Springer Verlag 2008. ISBN 978-3-540-76695-7.

GARTHOFF ET. AL. 2008

Garthoff,C.; Richter,K. ; Holtz.R.: Steigerung der Prozesssicherheit von Mikropunktschweißungen durch Real-Time-Prozessregelung. Düsseldorf: DVS Media GmbH 2008. DVS-Berichte Band 250. ISBN 978-3-87155-256-4.

GENERAL ATOMICS 2012

Genral Atomics: Pulse Forming Networks. Online Article (2012). Available at: www.ga-esi.com/EP/pulsed-power/pulse-forming-networks/index.php. Last viewed 13.03.2012.

GOßNER 2011

Goßner, S.: Grundlagen der Elektronik. 8. Ergänzte Auflage. Aachen: Shaker Verlag 2011. ISBN 978-3826588259.

GREF 2005

Gref, W.: Laserstrahlschweißen von Aluminiumwerkstoffen mit der Fokusmatrixtechnik. Dissertation. Technische Universität Stuttgart 2005.

HART & HART 2012

Hart, R. F.; Hart, M. K.: Testing for “Near-Normality”: The probability Plot. Online Article (2012). Available at: www.statit.com/support/quality_practice_tips/testingfornearnormality.shtml. Last viewed: 13.03.2012.

HÜGEL & GRAF 2009

Hügel, H.; Graf, T.: Laser in der Fertigung. 2. Auflage. Wiesbaden: Vieweg+Teubner 2009. ISBN 978-3-8351-0005-3.

IWB 2011

Slides on the course “Laser Technologies“. Technical University Munich – Institue for Machine Tools and Industrial Management 2011.

JUNG 2011

Jung, S.: Oberflächenbeurteilung – Rauheitsmessung. Unterlagen zum allgemeinen Praktikum Maschinenbau und Hauptfachversuch. Universität Stuttgart 2011. Available at: http://www.ima.uni-stuttgart.de/studium/dt/Hauptfachversuche/aktuell/HFV_Oberflaechenbeurteilung_2011.pdf. Last viewed 15.01.2012.

KAISER & SCHÄFER 2005

Kaiser, E.; Schäfer,P.: Pulse shaping optimizes the quality of pulsed seam- and spotwelds. Proceedings of the Third International WLT-Conference on Lasers in Manufacturing LIM2005. München 2005.

KAMENZ 2010

Kamenz, T.: Effects of pulse shaping on spot welding of copper nickel alloys with Nd:YAG laser. Bachelor Thesis. Beuth Hochschule für Technik Berlin 2010.

KELKAR 2011

Kelkar, G.: Pulsed Laser Welding. Online article 2011. Available at http://www.weldingconsultant.com/PulsedLaserWelding.pdf. Last viewed 24.11.2011.

KLAGES ET AL. 2003

Klages, K.; Ruettimann,C.; Olowinsky, A.: Laser Beam Micro Welding of Dissimilar Metals. From: Chen, X.; Laser Institute of America: ICALEO 2003, 22nd International Congress on Applications of Lasers and Electro Optics. Congress proceedings. CD-ROM. ISBN: 978-0-912035-75-8.

KLAGES ET AL. 2004

Klages, K.; Gedicke, J.; Olowinsky, A.: Pulse Forming at Laser Beam Micro Welding. Proceedings of the 23rd International Congress on Applications of Lasers and Electro-Optics. San Francisco 2004.

KOECHNER 1992

Koechner, W.: Solid State Laser Engineering. 3rd Edition. Berlin: Springer Verlag 1992. ISBN 3-540-53756-2 3.

MATHWORKS 1999

The MathWorks, Inc.: Statistics Toolbox User's Guide. Revised for Version 2.1.2 (1999). Available at: http://www.mathworks.com. Last viewed: 05.02.2012.

MATSUNAWA ET. AL

Matsunawa, A.; Kim, D.; Katayama, S.: Porosity formation in laser welding. Mechanisms and suppression. San Diego: Laser Inst of America (1997). Proceedings of the Laser Material Processing Conference ICALEO. Pages 73-82. ISBN: 978-0912035567.

NAEEM 2004

Naeem, M.: Controlling the pulse in Laser Welding. Online article 2004. Available at: http://weldingdesign.com/equipment-automation/news/wdf_11036/. Last viewed 21.03.2010.

NIEMANN ET AL. 2005

Niemann, G.; Winter, H.; Höhn, B.-R.: Maschinenelemente Band 1. Berlin: Springer Verlag 2005. ISBN 3540251251.

PROPAWE 2005

Propawe, R.: Lasertechnik in der Fertigung. 1. Auflage. Berlin: Springer Verlag 2005. ISBN 3-540-21406-2.

RELIASOFT 2008

ReliaSoft Corporation: Online User Guide for Software Package Doe++ (2008). Available at: www.weibull.com/DOEWeb/introduction.htm. Last viewed 07.02.2012.

ROTH 2011

Roth, T.: Homepage on the quality management software package “qualityTools” at the Technische Universität Berlin. Available at: http://www.user.tu-berlin.de/kalicete/qualityTools/qualityTools.html. Last viewed: 24.11.2011.

SAVARECHIEV & JIE 2004A

Safarevich, S.; XIe, J.: Pecularities of Micro Laser Welding of Medical Devices. ASM International 2004. Medical Device Materials: Proceedings of the Materials & Processes for Medical Devices Conference. Pages 31-36.

SAVARECHIEV & JIE 2004B

Safarevich, S.; XIe, J.: Laser Welding Processing for Medical Devices. ASM International 2004. Medical Device Materials: Proceedings of the Materials & Processes for Medical Devices Conference. Pages 25-30.

SIEBERTZ ET AL. 2010

Siebertz,K.; van Bebber,D.; Hochkirchen, T.: Statistische Versuchsplanung. 1. Auflage. Berlin: Springer Verlag 2010. ISBN 978-3-642-05492-1.

SCHMITT 2012

Schmitt, R.: Vorlesung Qualitätsmanagment. Lecture Slides. RWTH Aachen (2012). Available at: www.wzl.rwth-aachen.de. Last viewed 09.02.2012.

TRUMPF 1994

TRUMPF Laser GmbH: Technische Information – Laserbearbeitung YAG Laser. Dokumentnummer T223DO. Ausgabe 09/1994.

TRUMPF 2009

TRUMPF Laser GmbH: Technische Information - Gepulstes Schweißen. Dokumentnummer T637DE. Ausgabe 02/2009.

UPMC 2012

UPMC Medical Center. Online article. Available at: www.upmc.com/MediaRelations/PublishingImages/MRI_Safe_Pacemaker_Revo.jpg. Last viewed 20.03.2012.

VDI-TPT 1995

VDI Technologiezentrum Physikalische Technologien (Hrsg.). Schweißen mit Festkörperlasern. Düsseldorf: VDI-Verlag 1995. ISBN 2-18-401407-X.

WEBERPALS 2010

Weberpals, J.-P.: Nutzen und Grenzen guter Fokussierbarkeit beim Laserschweißen. Dissertation. Technische Universität Stuttgart 2010.

WIKIPEDIA 2011

Online article: Buck Boost converter (2012). Available at: http://en.wikipedia.org/wiki/Buck%E2%80%93boost_converter. Last viewed at 12.03.2012.

WILDEN 2009

Wilden, J.: Metallurgische Grundlagen zum Fügen mittels im Puls modulierbarer Laserstrahlquellen. Document collection available at: http://www.dvs-ev.de/fv/neu/index.cfm?Navigation=Forschungsergebnisse&PID=608&CFID=15759918&CFTOKEN=44076. Last viewed: 13.02.2012.

ZHOU ET AL. 2003

Zhou, M.; Zhang, H; Hu, S. J.: Relationships between Quality and Attributes of Spot Welds. Welding Journal. April 2003. Pages 72-77.

Appendix A

A1 Investigation on Pulse Shaping Capabilities

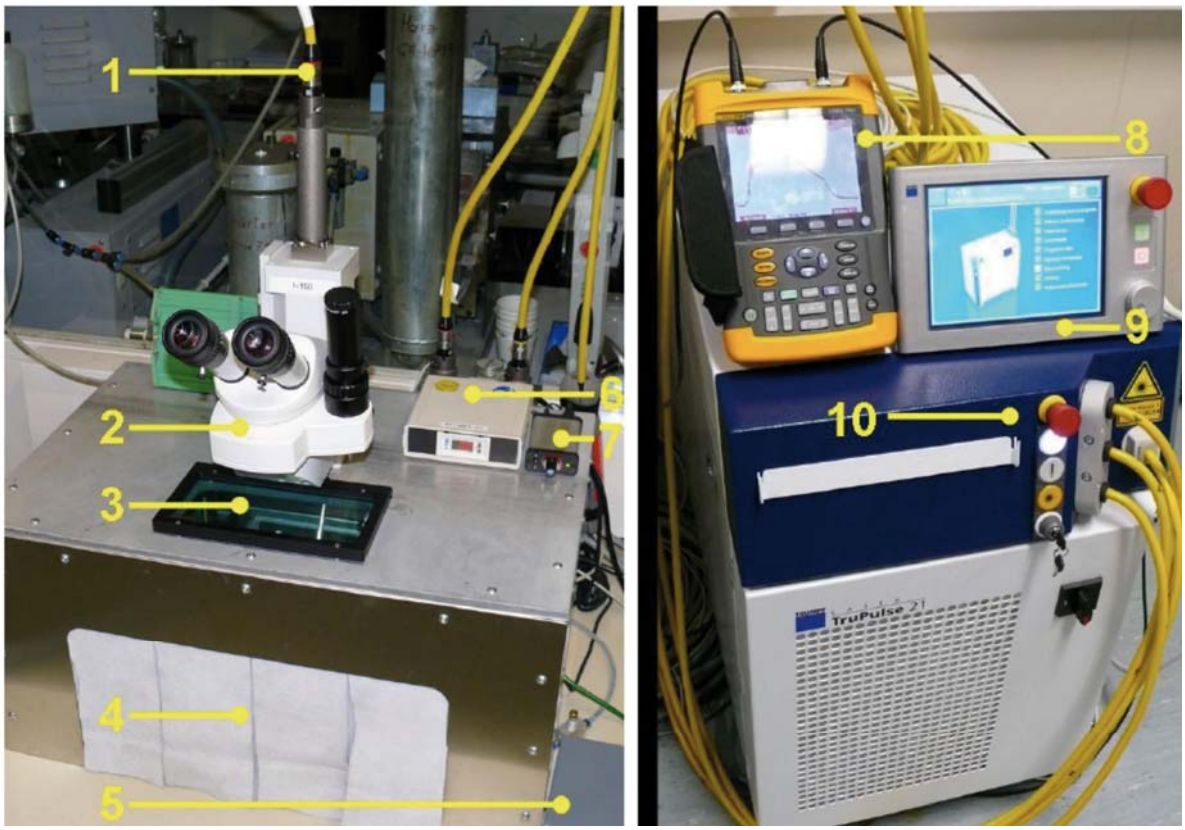

Figure A1.1: Experimental set-up (according to [KAMENZ 2010]).

Num.	Name	Properties
1	Light conducting cable (llc)	Core diameter dc = 400 µm
2	Optical unit	fc = 200 mm, f = 150 mm -> Focal spot size 300 µm
3	Protective glas	Low permittance of wavelengths in the Nd:YAG regime (1064 nm)
4	Protective covering	-
5	Amplifier for the photodiode	-
6	Gas flow meter	Max. pressure 100 kPa (1 bar) max. flow 1.5 l/min
7	Switch for ring light (see table B1.2)	-
8	Digital oscilloscope	Fluke Type 196c
9	Laser control panel	-
10	Laser (source)	Trumpf TruPulse 21

Table A1.1: Details of the experimental set-up (adapted from [KAMENZ 2010]).

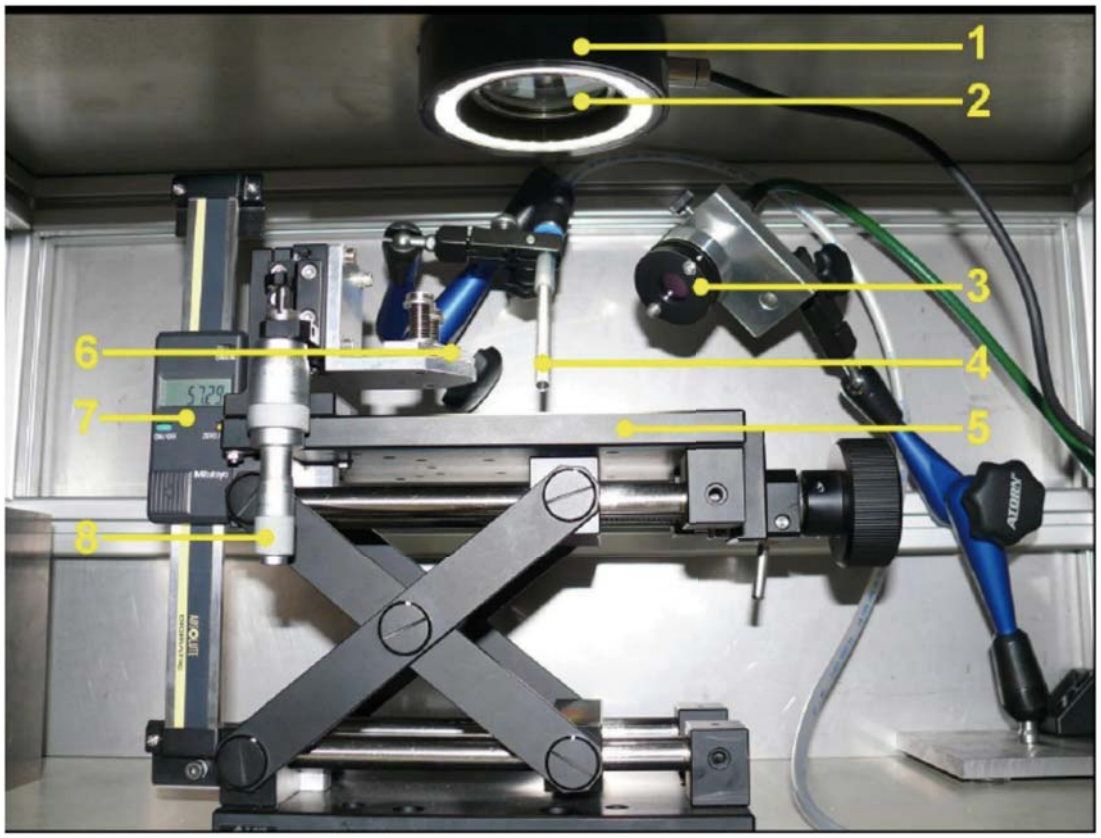

Figure A1.2: Experimental set-up inside the protective covering (according to [KAMENZ 2010]).

Num.	Name	Properties
1	LED ring light	-
2	Optical unit	-
3	Photodiode	Spectrum of sensitivity 1050 - 1070 nm
4	Gas nozzle	Argon gas with a pressure of 50 kPa (0,5 bar) and flow rate of 1 l/min
5	Lifting table (z-axis)	Ensuring correct working height
6	Optional fixture	-
7	Sliding Calliper	Displaying current height with a precision of 0.01 mm
8	Height adjustment of optional fixture	-

Table A1.2: Details of the experimental set-up inside the protective covering (adapted from [KAMENZ 2010]).

Rectangular Pulse

Time Series:

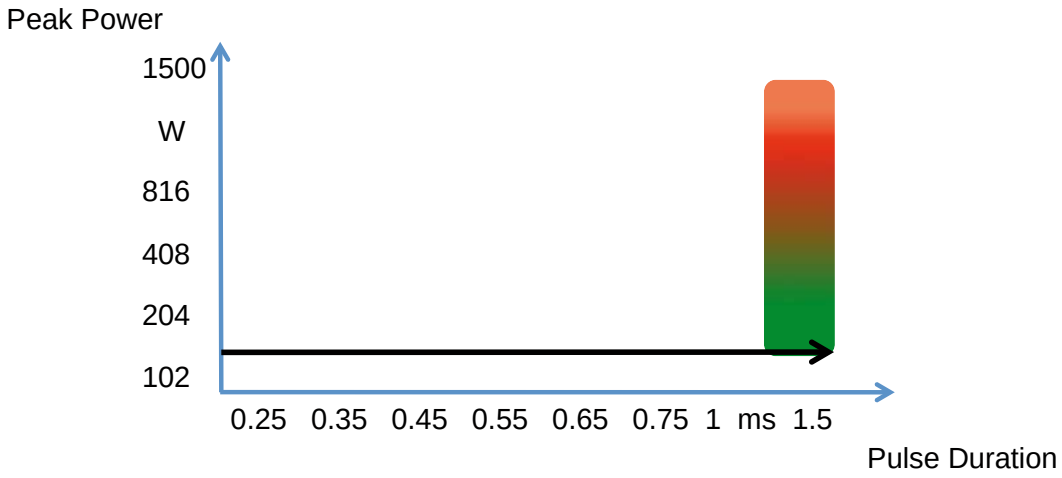

Figure A1.3: Experimental procedure for the time series of a rectangular pulse.

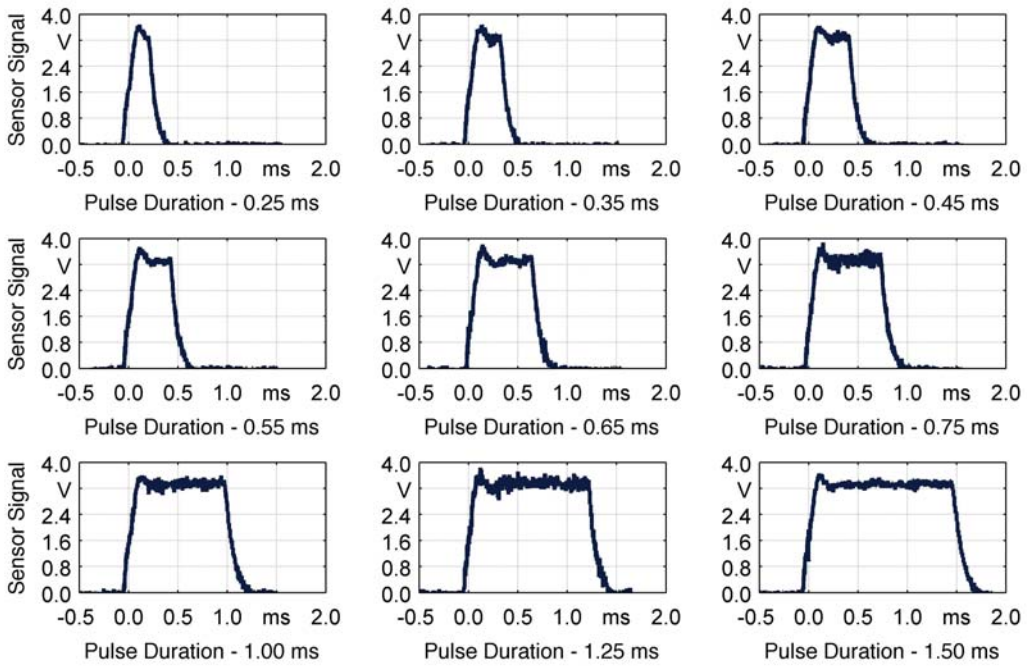

Figure A1.4: Qualitative result of the time-series for a rectangular pulse at 102 W.

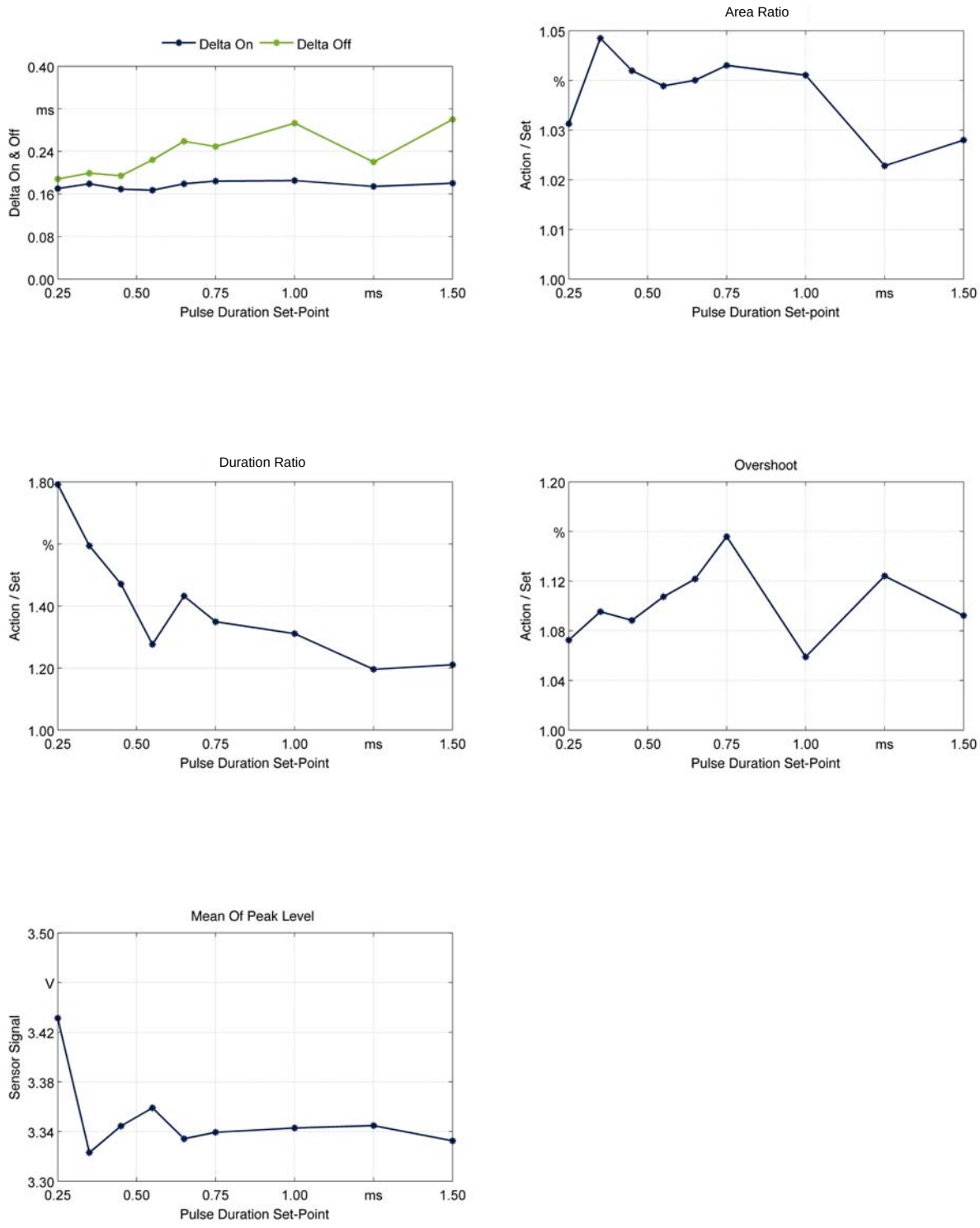

Figure A1.5: Quantitative results of the time-series for a rectangular pulse at 102 W.

Power Series:

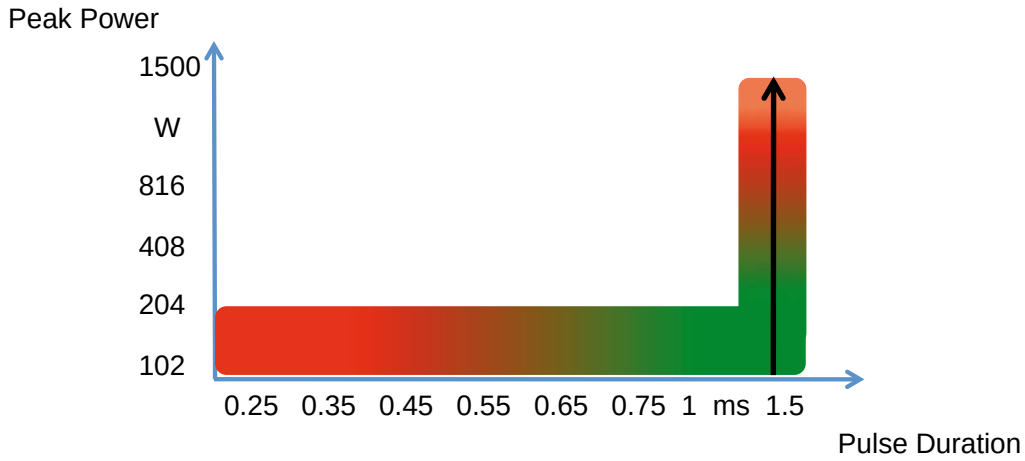

Figure A1.6: Experimental procedure for the power series of a rectangular pulse.

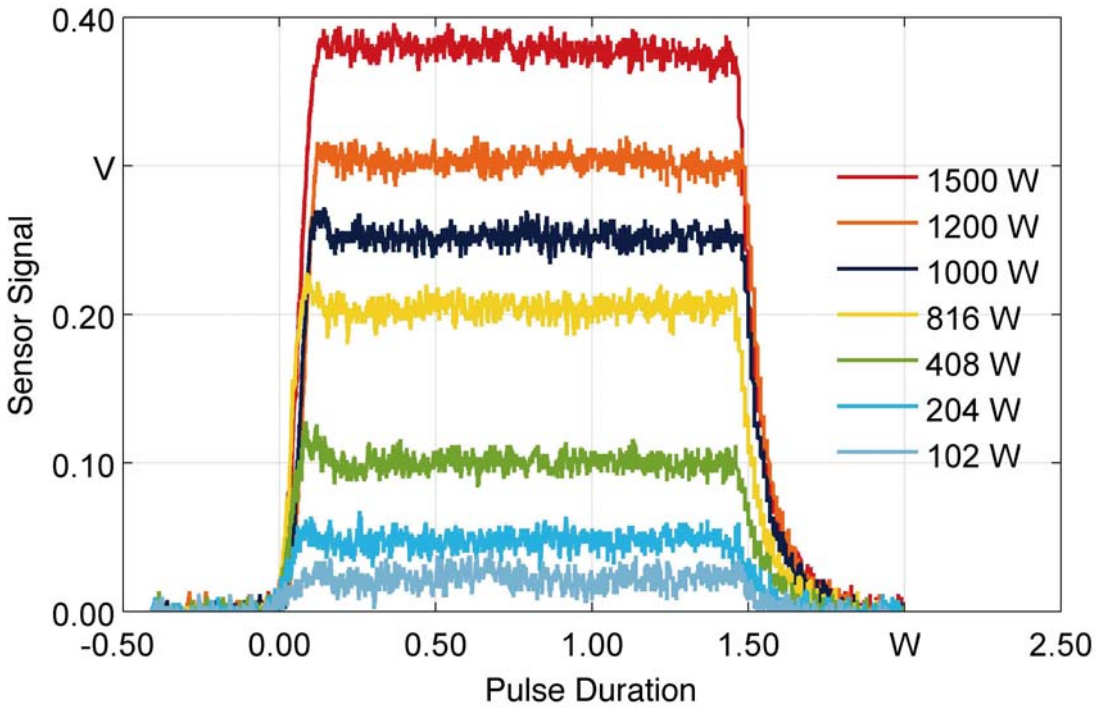

Figure A1.7: Qualitative result of the power series for a rectangular pulse at 1.5 ms.

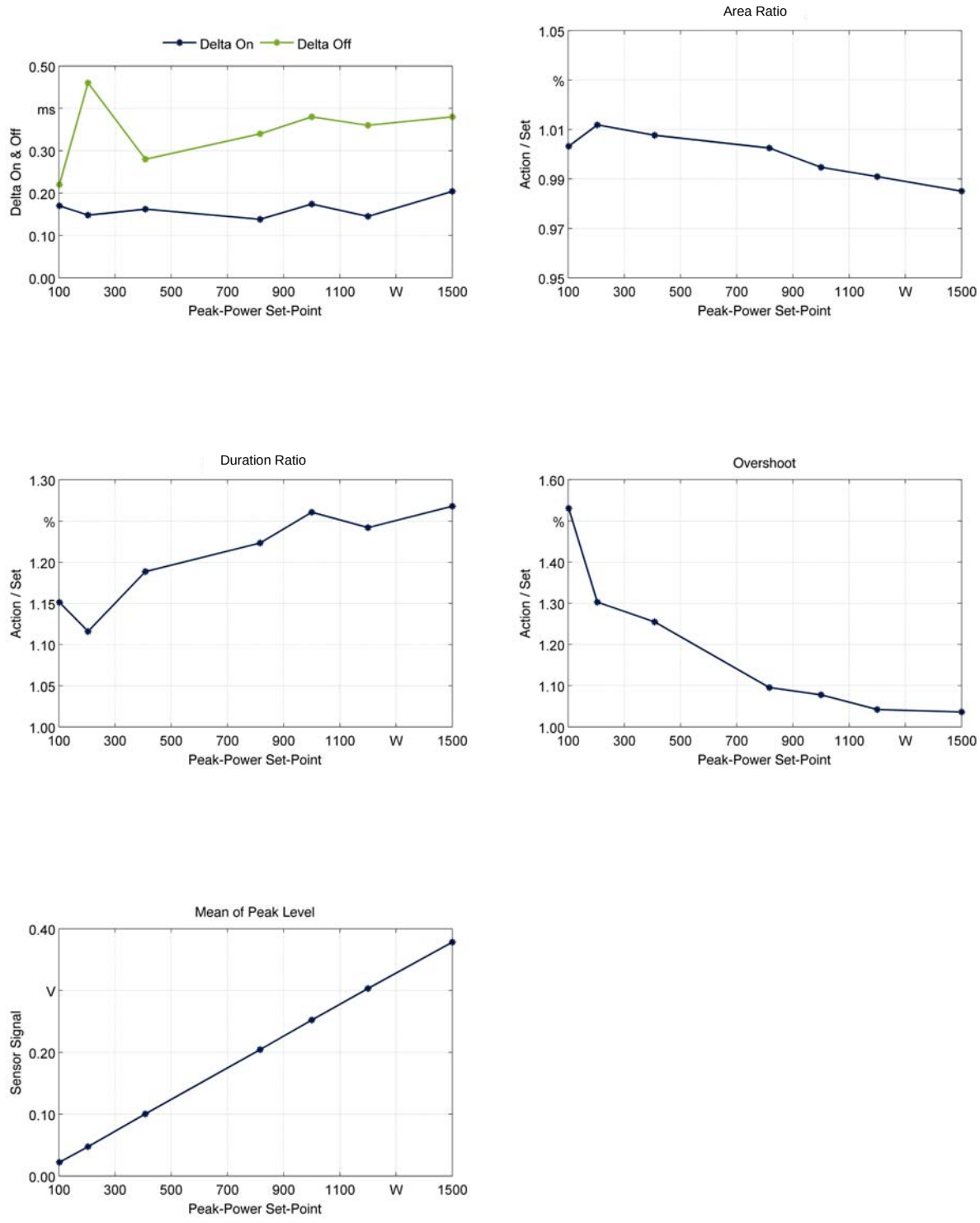

Figure A1.8: Quantitative result of the power series for a rectangular pulse at 1.5 ms.

Double Step Pulse

Time Series:

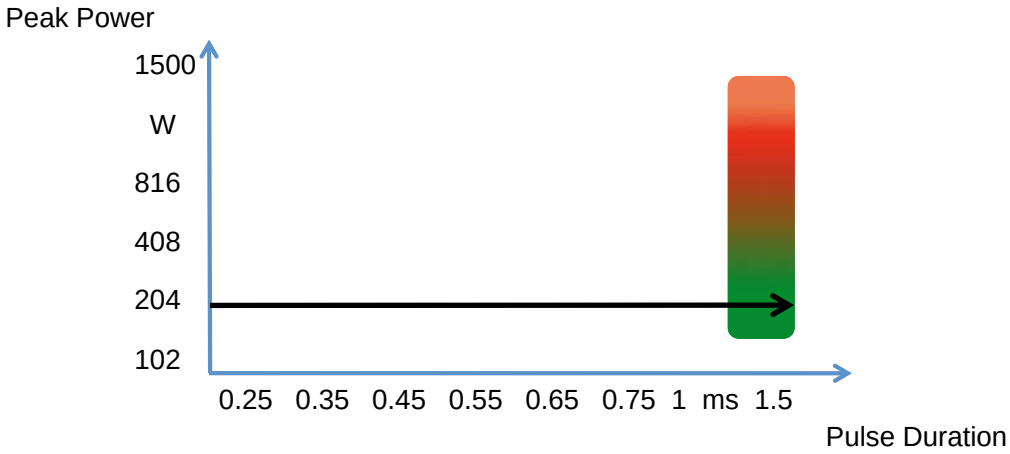

Figure A1.9: Experimental procedure for the time series of a rectangular pulse.

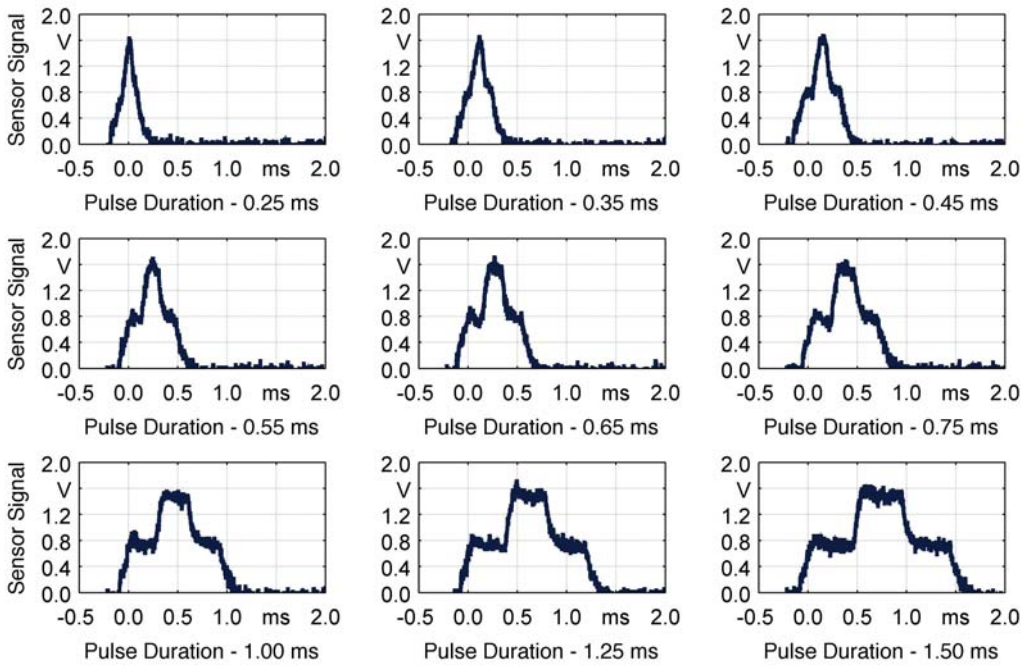

Figure A1.10: Qualitative result of the time series of a double step pulse at 204 W.

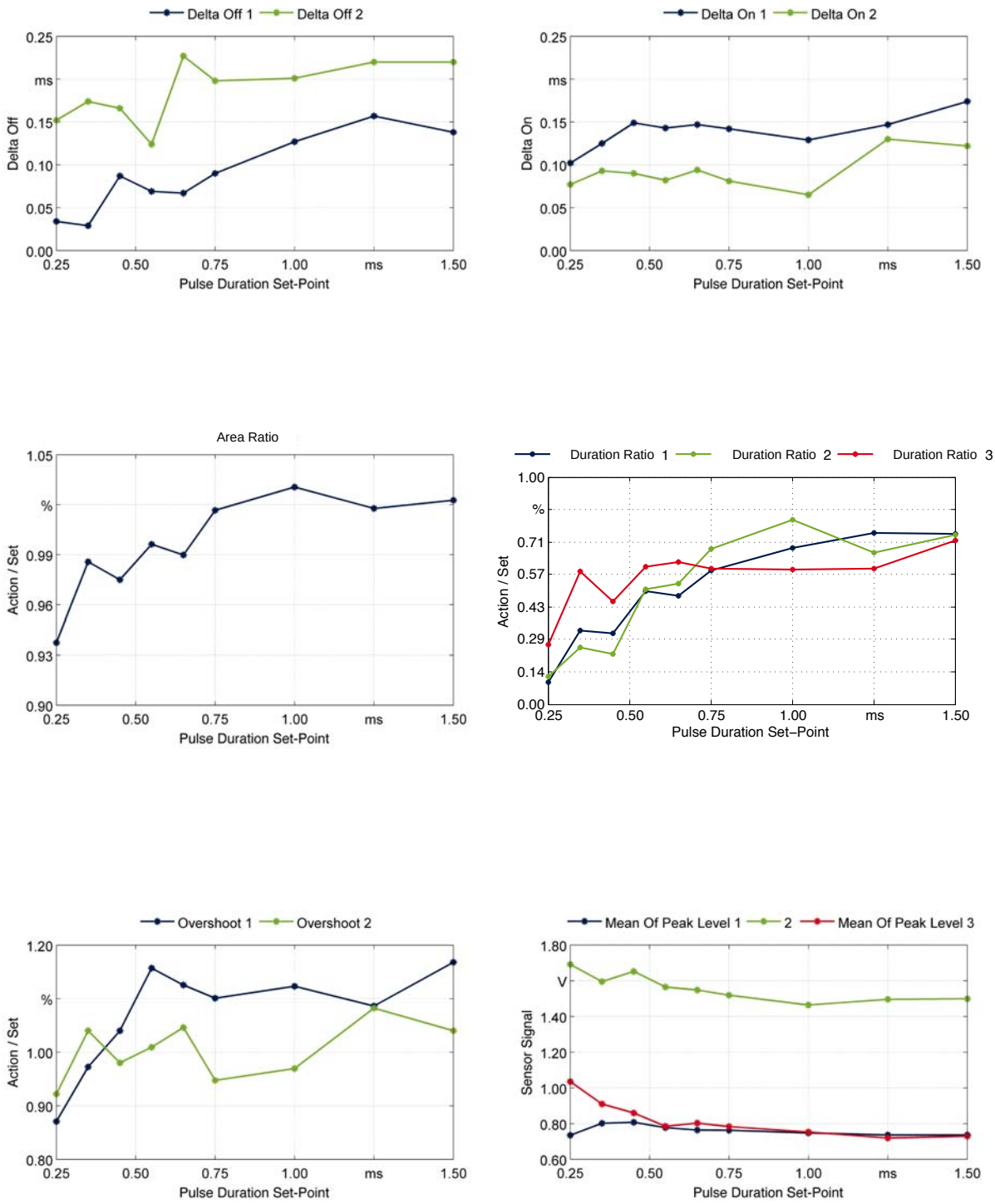

Figure A1.11: Qualitative result of the time series of a double step pulse at 1.5 ms.

Power Series:

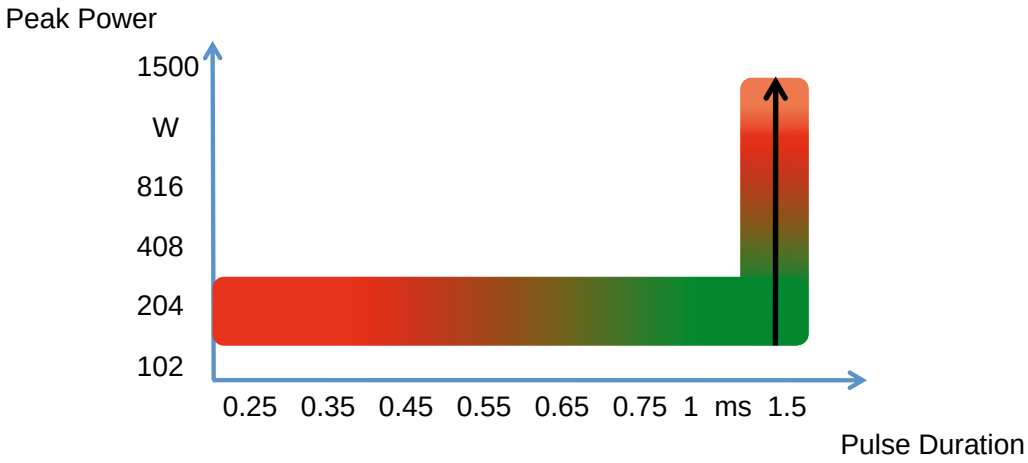

Figure A1.12: Experimental procedure for the power series of a double step pulse.

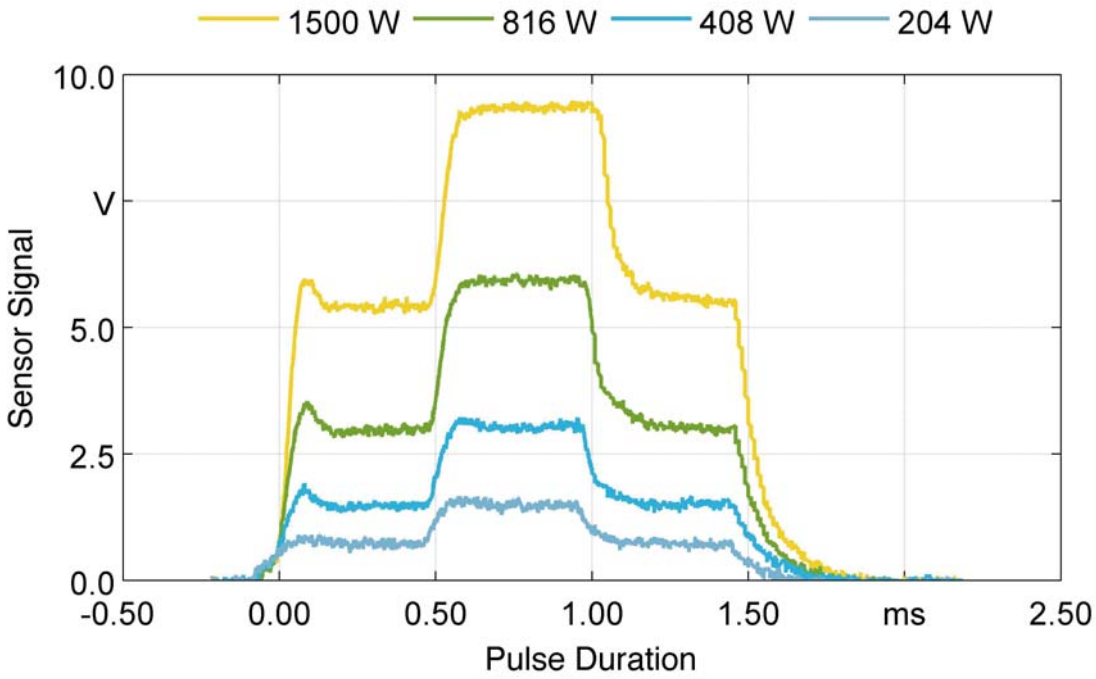

Figure A1.13: Qualitative result of the power series of a double step pulse at 1.5 ms.

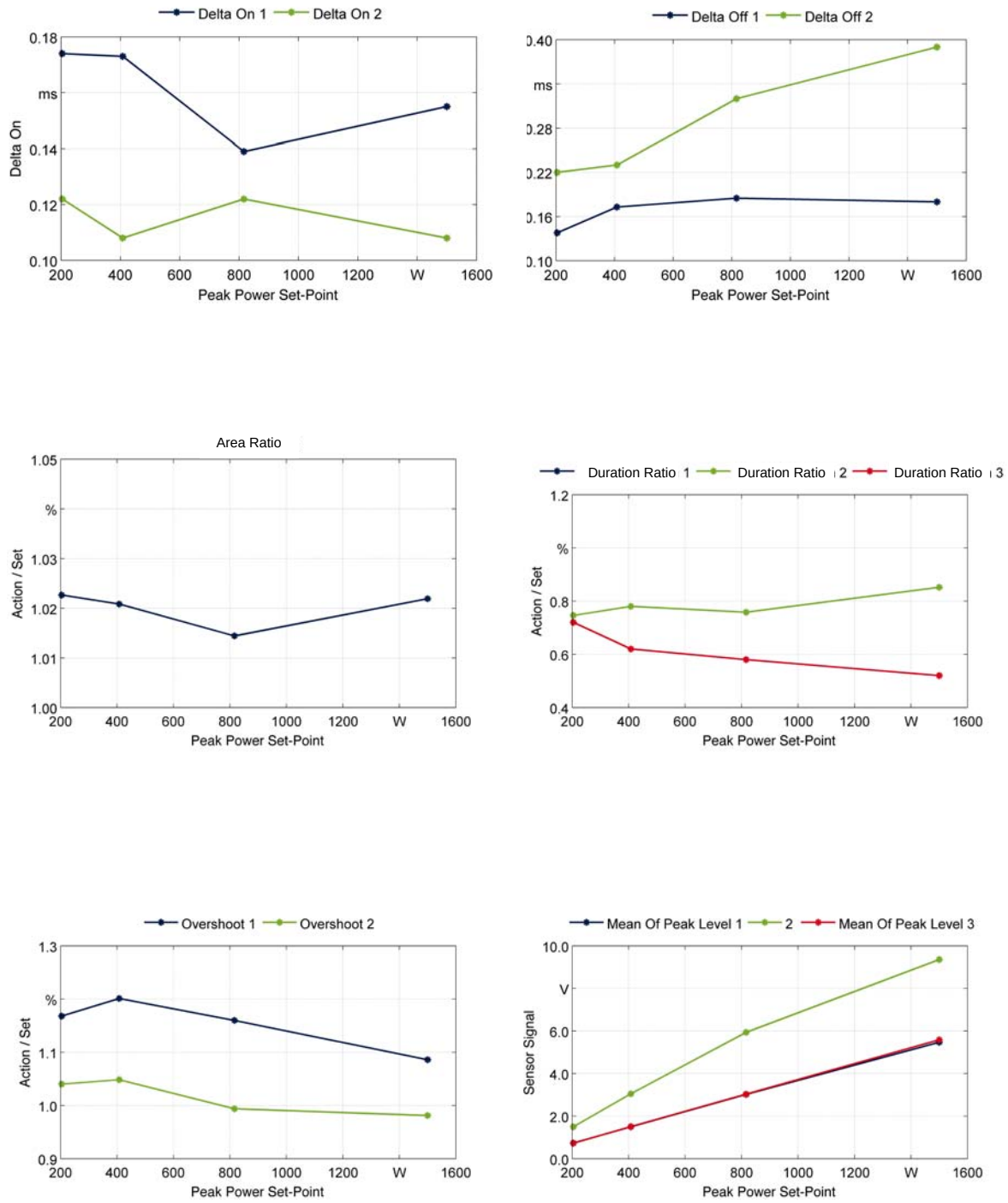

Figure A1.14: Quantitative result of the power series of a double step pulse at 1.5 ms. Note: the duration ratios one and three are equal (only three is visible).

Triangular Pulse

Time Series:

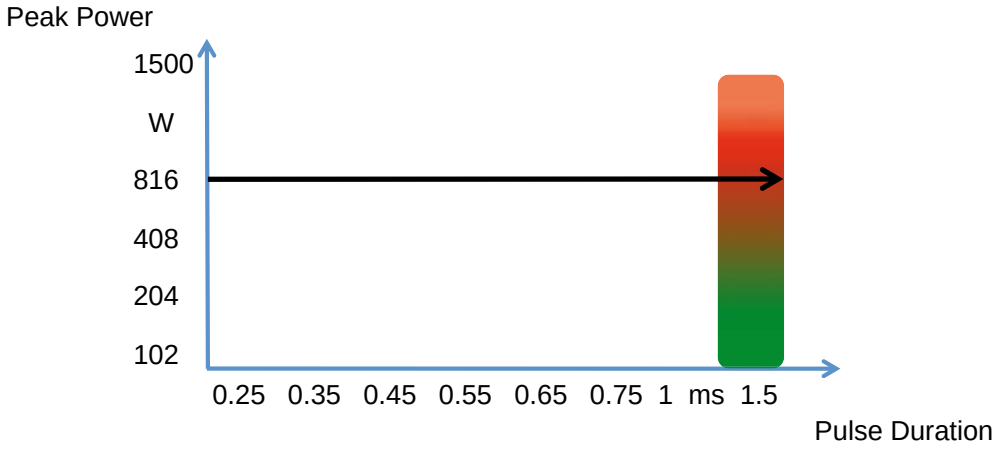

Figure A1.15: Experimental procedure for the time series of a triangular pulse.

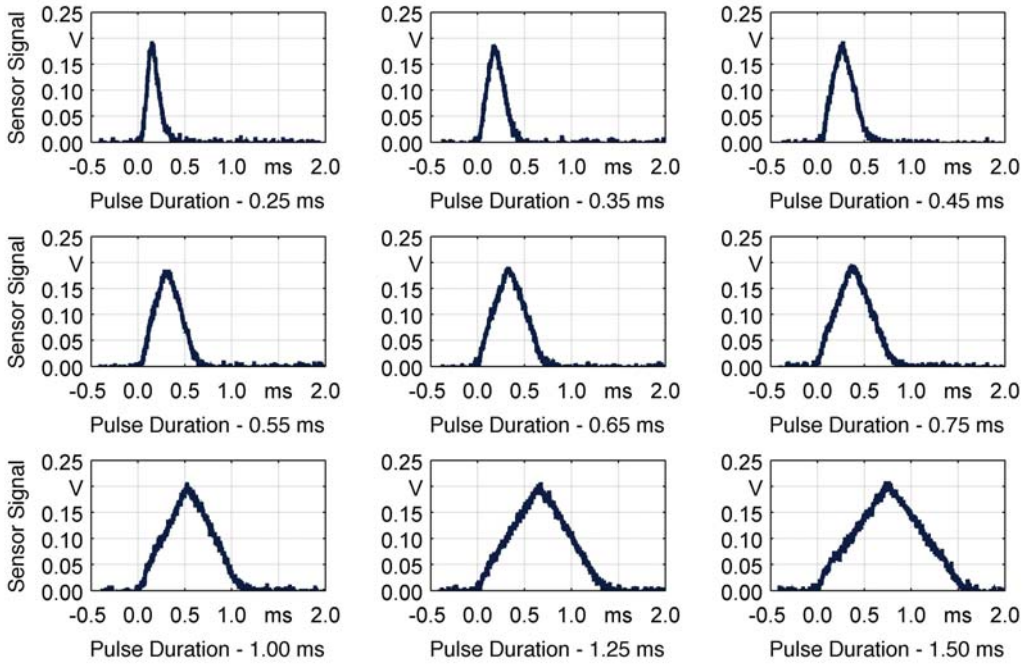

Figure A1.16: Qualitative result of the power series of a triangular pulse at 816 W.

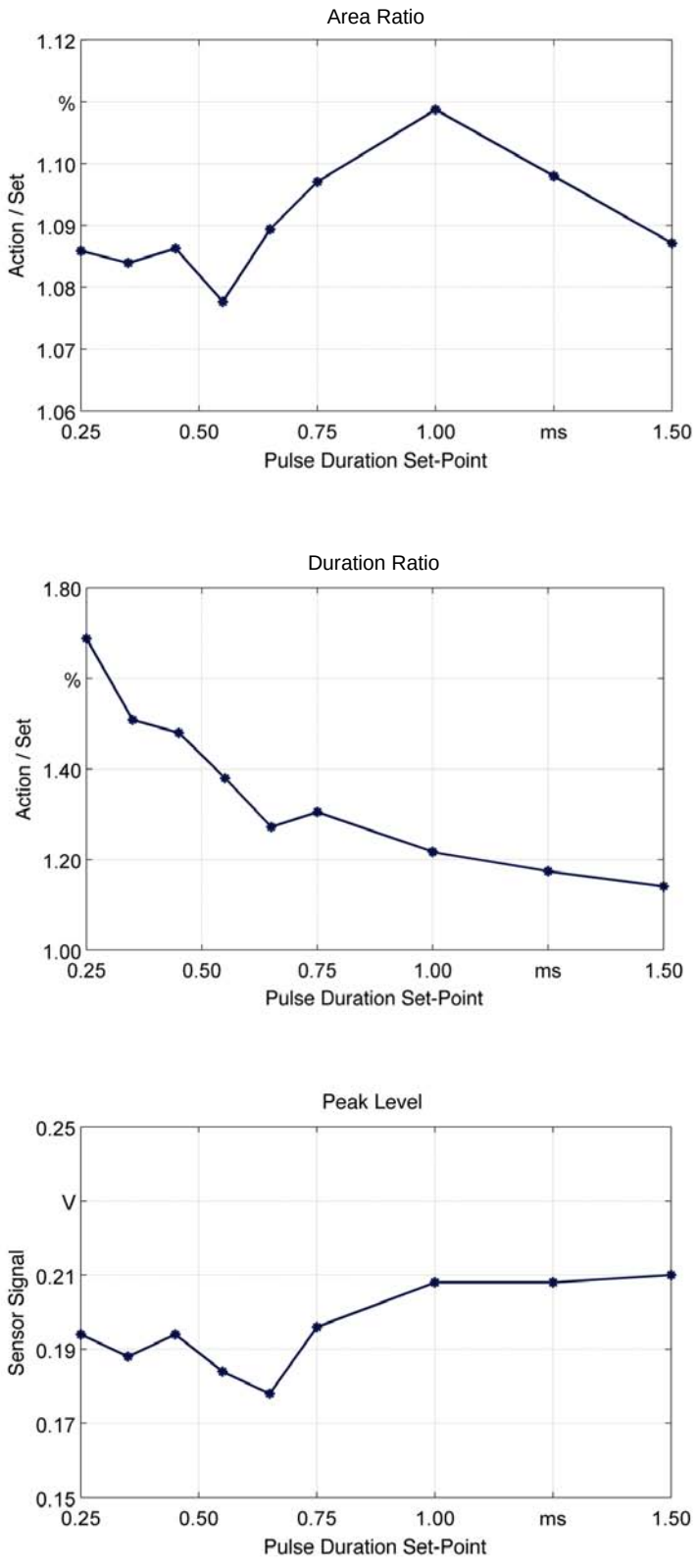

Figure A1.17: Quantitative result of the time series of a triangular pulse at 816 W.

Power Series:

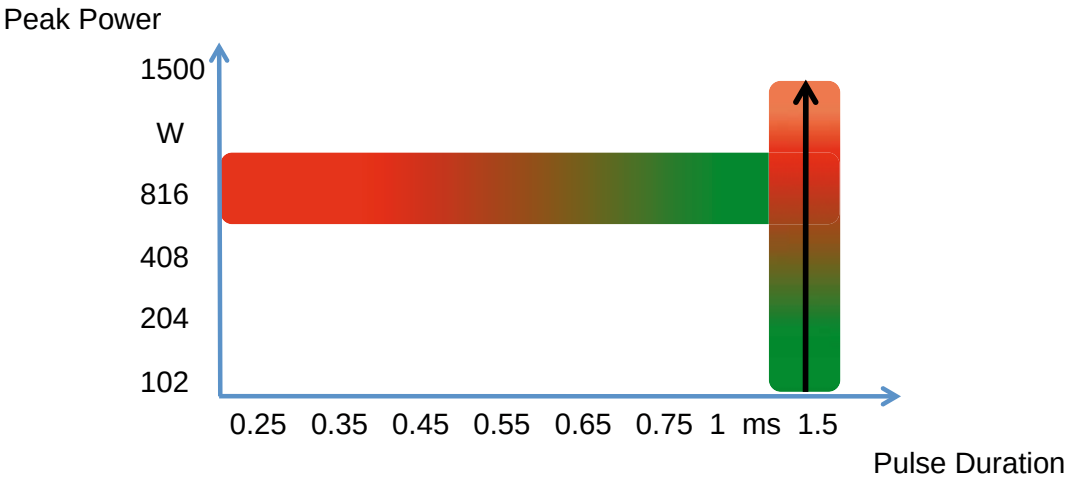

Figure A1.18: Experimental procedure for the power series of a triangular pulse.

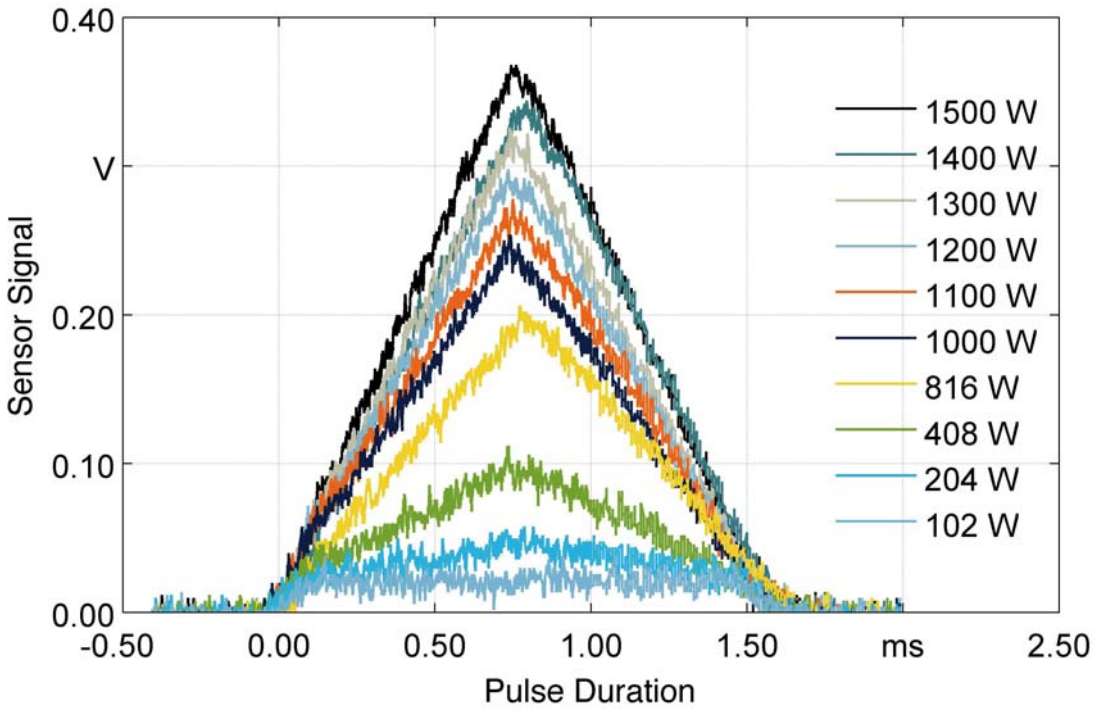

Figure A1.19: Qualitative result of the power series of a triangular pulse at 1.5 ms.

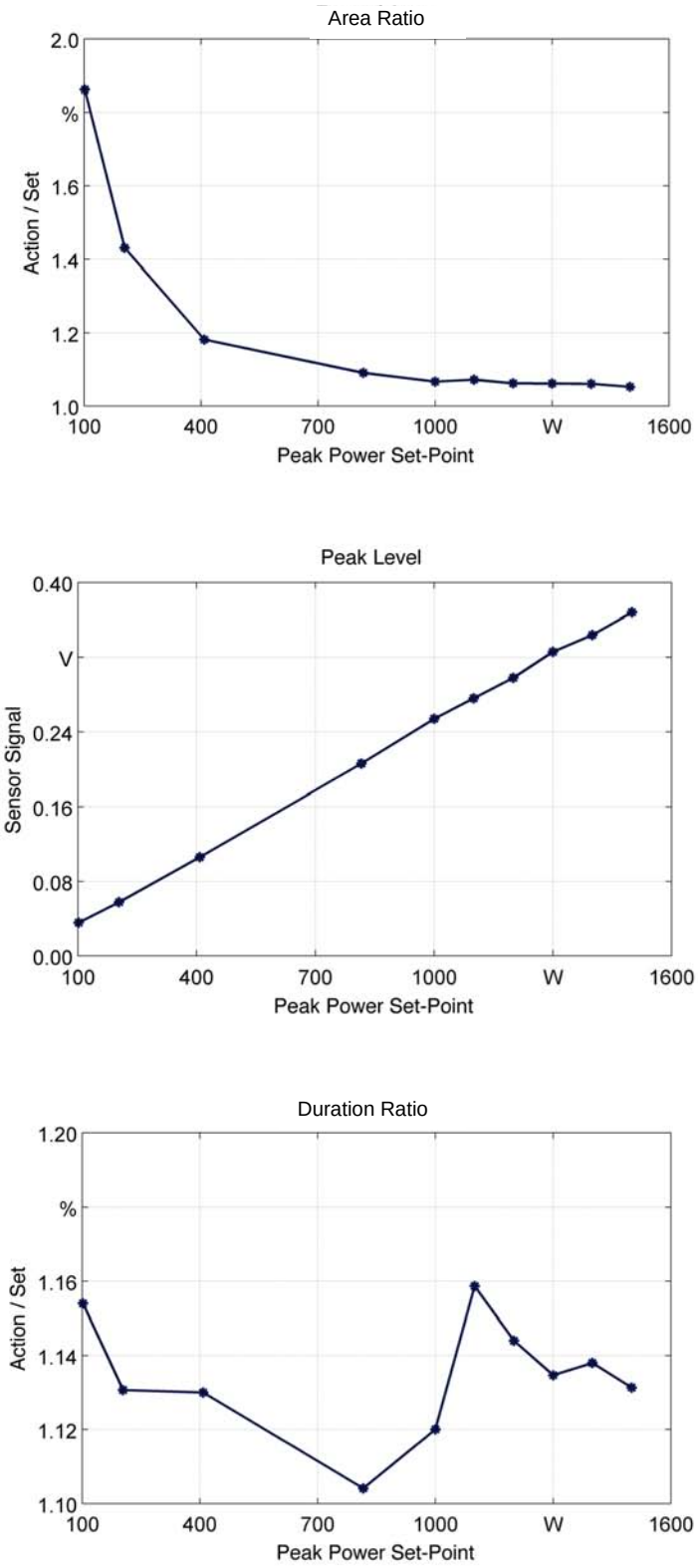

Figure A1.20: Quantitative result of the power series of a triangular pulse at 1.5 ms.

Trapezoid Pulse

Time Series:

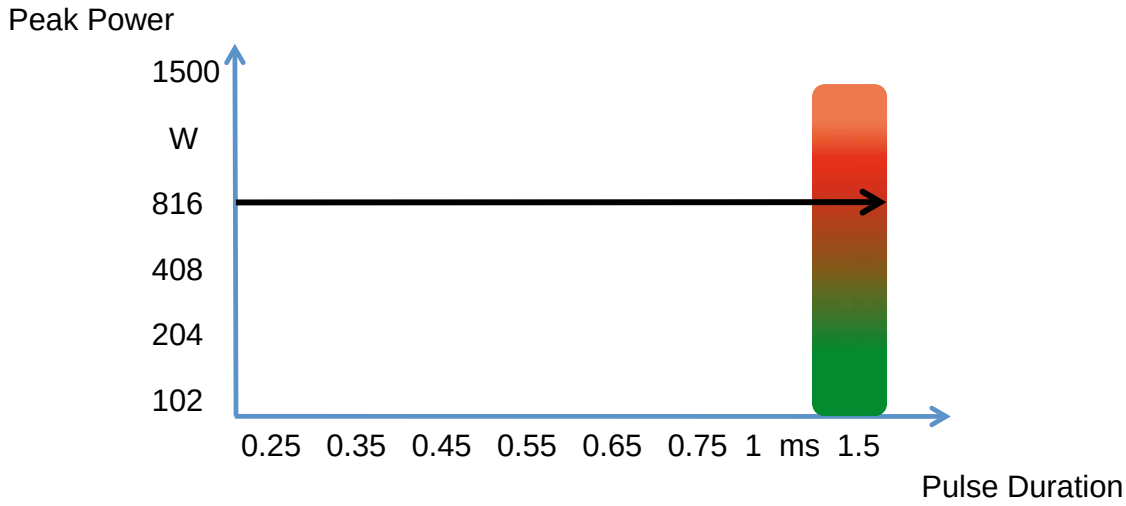

Figure A1.21: Experimental procedure for the time series of a trapezoid pulse.

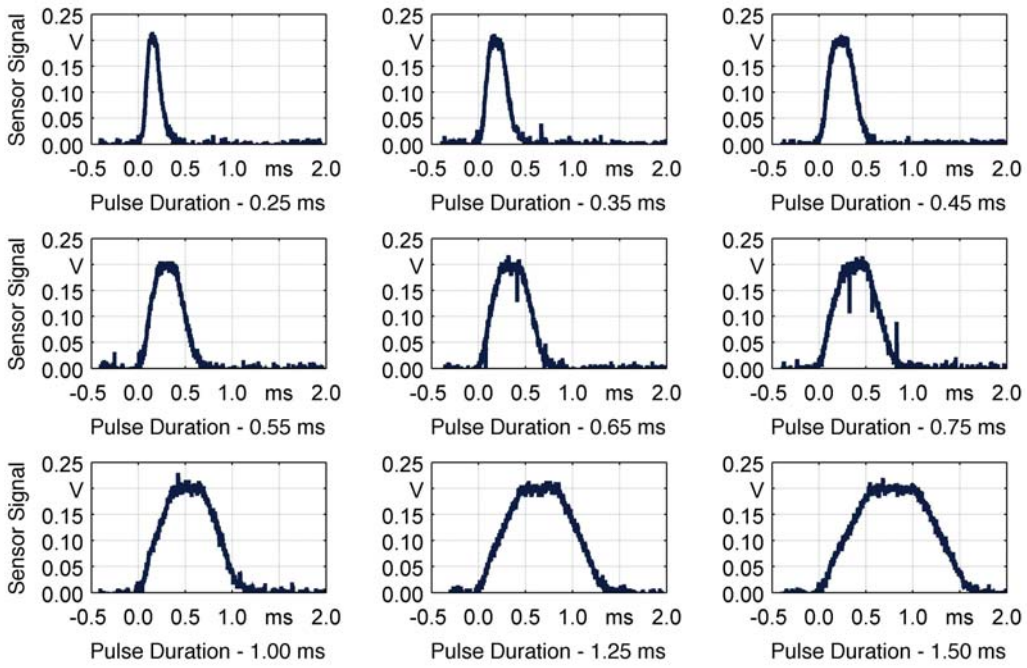

Figure A1.22: Qualitative result of the time series of a trapezoid pulse at 816 W.

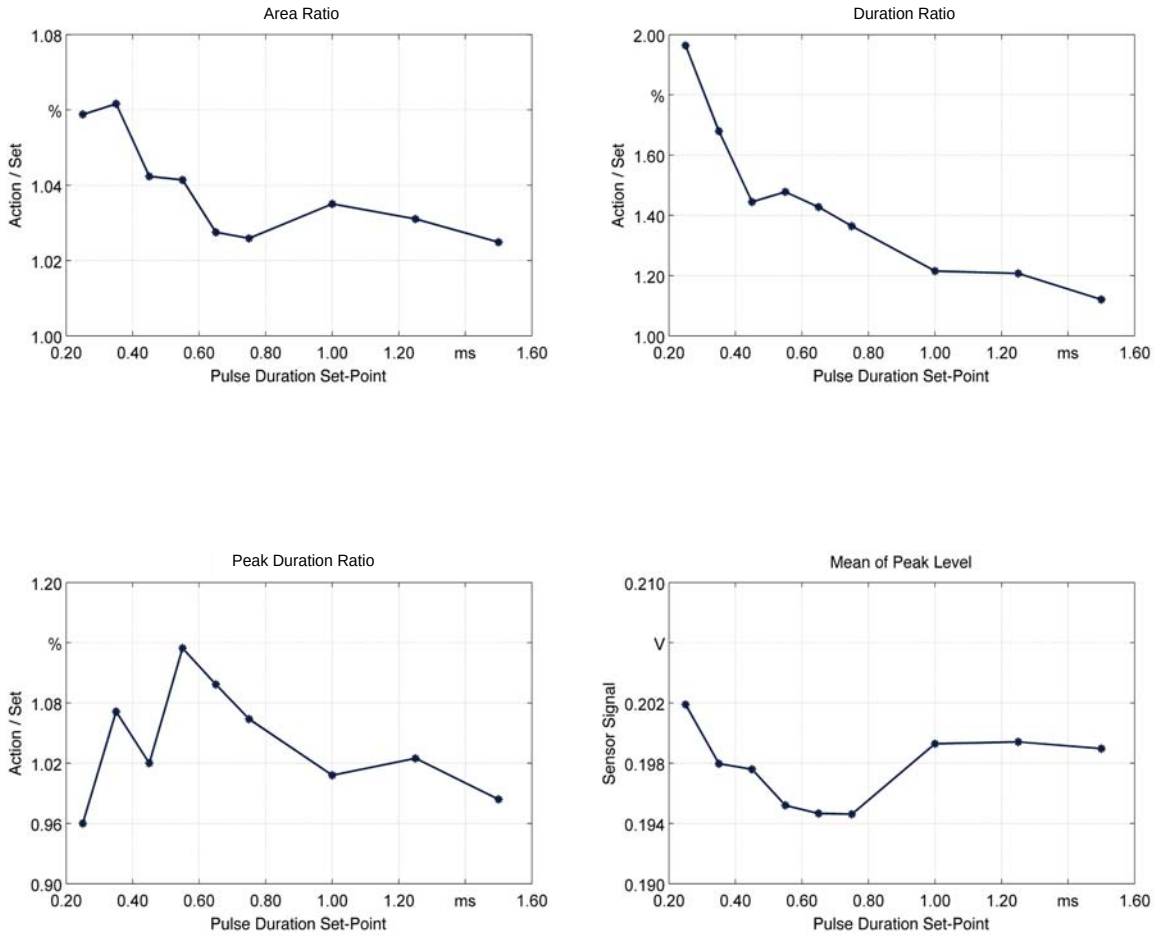

Figure A1.23: Quantitative result of the time series of a trapezoid pulse at 816 W.

Power Series:

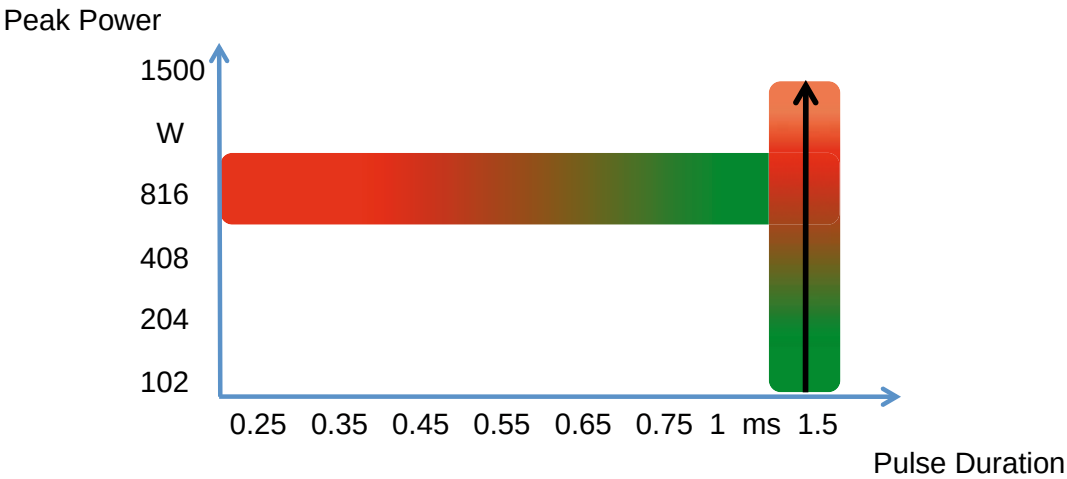

Figure A1.24: Experimental procedure for the power series of a triangular pulse.

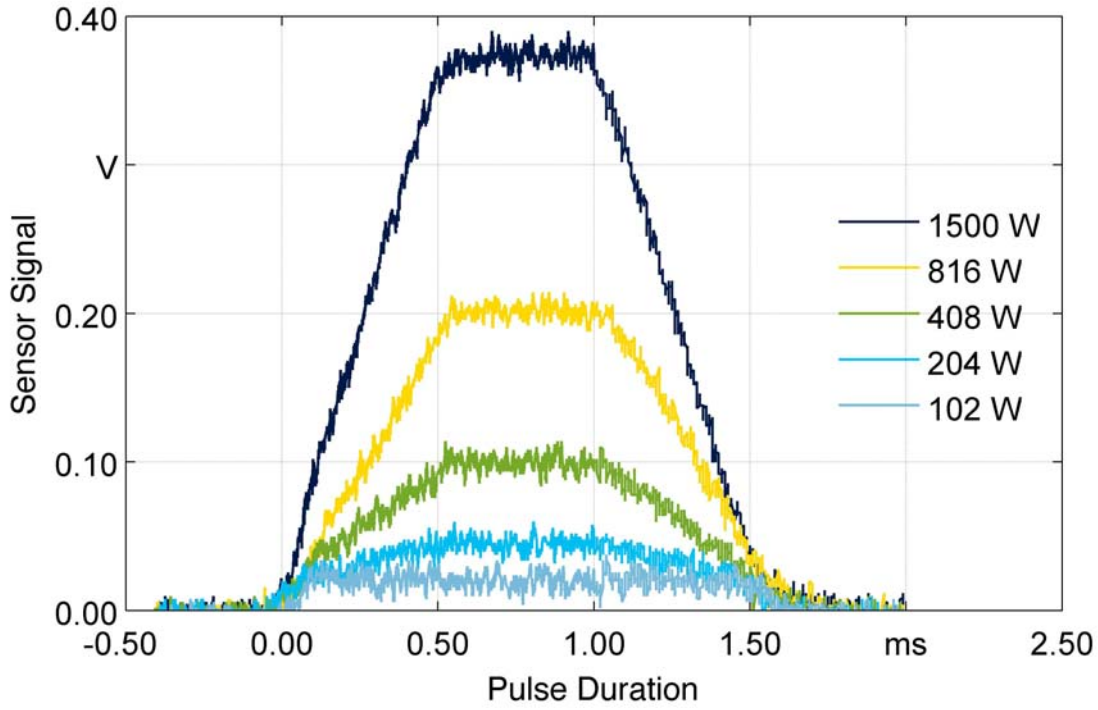

Figure A1.25: Qualitative result of the power series of a trapezoid pulse at 1.5 ms.

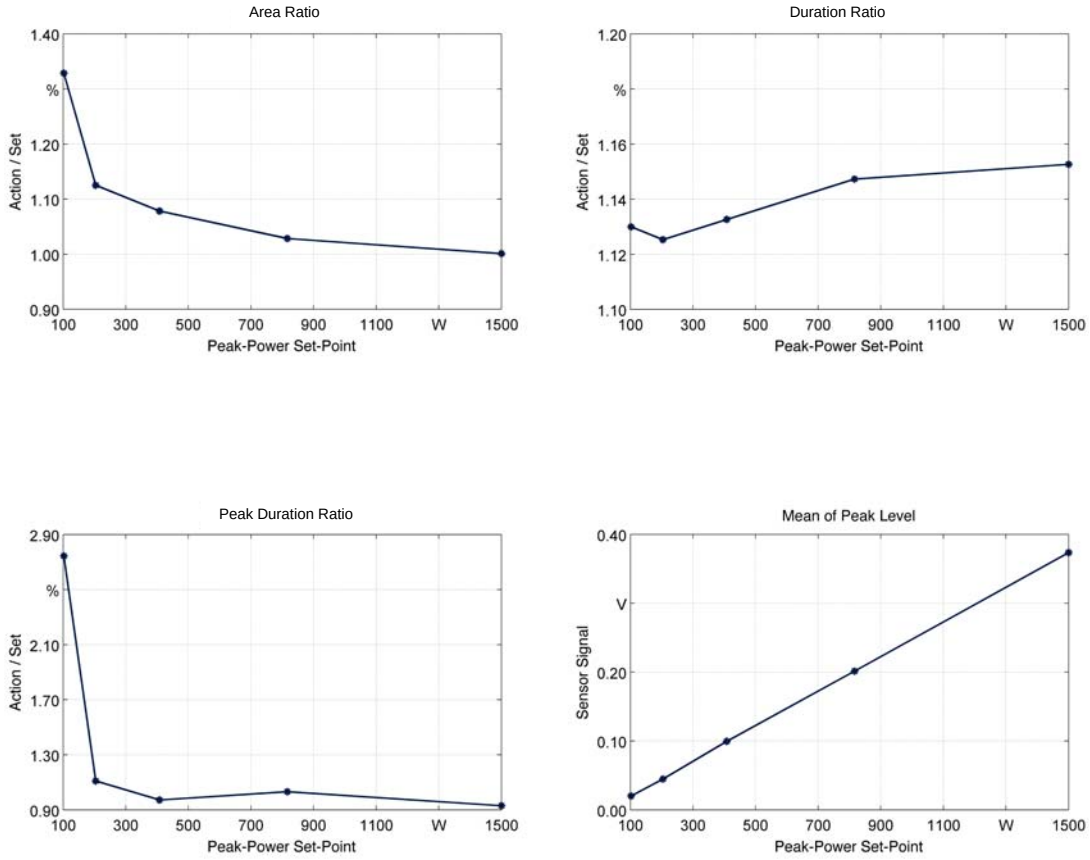

Figure A1.26: Quantitative result of the power series of a trapezoid pulse at 1.5 ms.

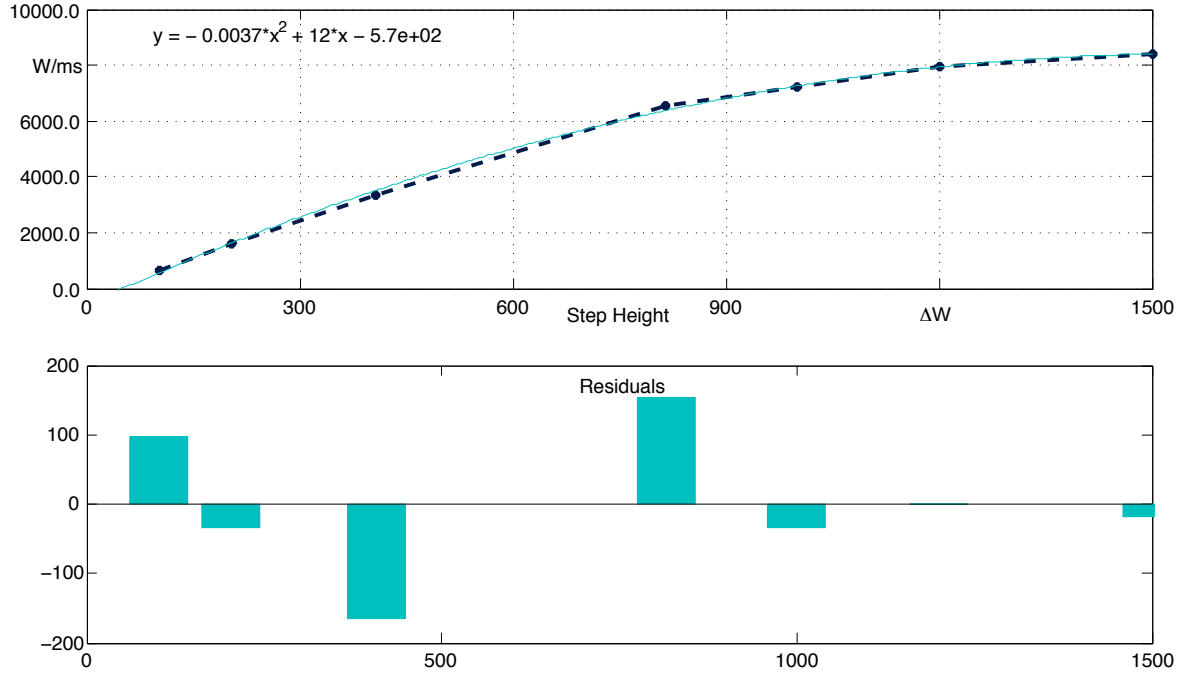

Figure A1.27: Approximated curve of step size versus rise time for steps from 0 W.

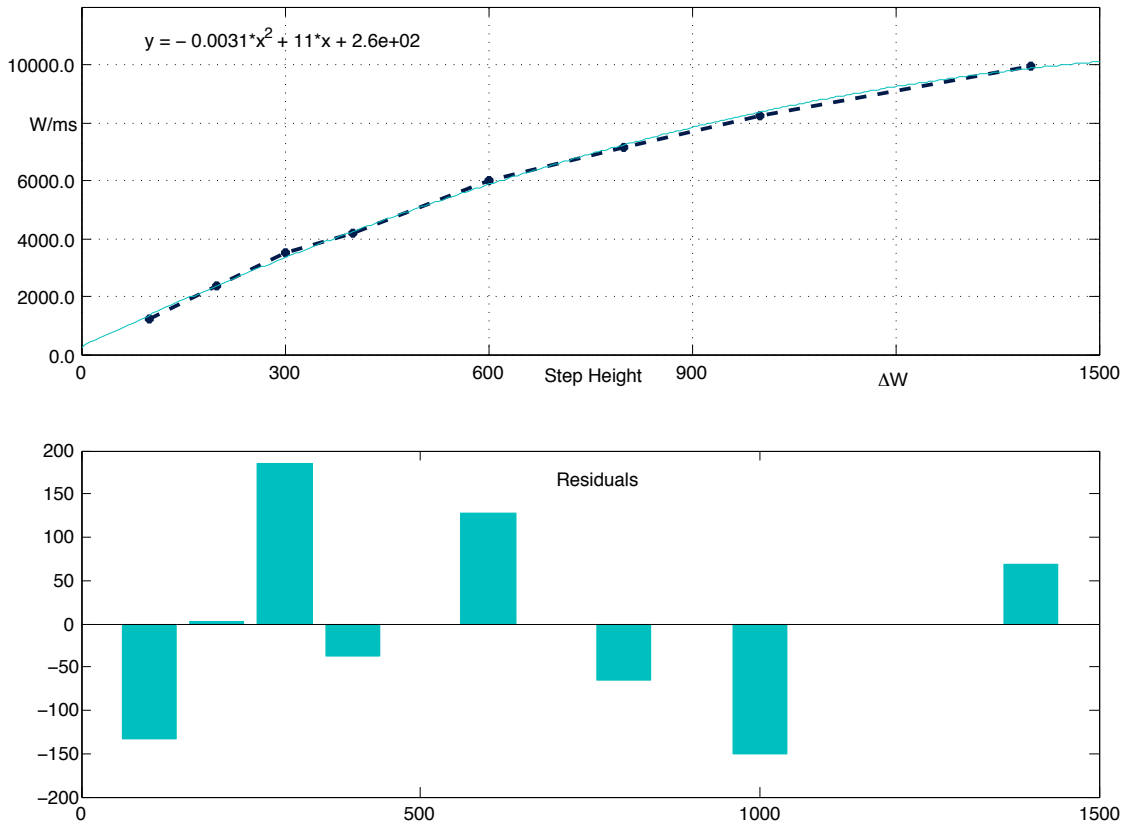

Figure A1.28: Approximated curve of step size versus rise time for steps from 102 W.

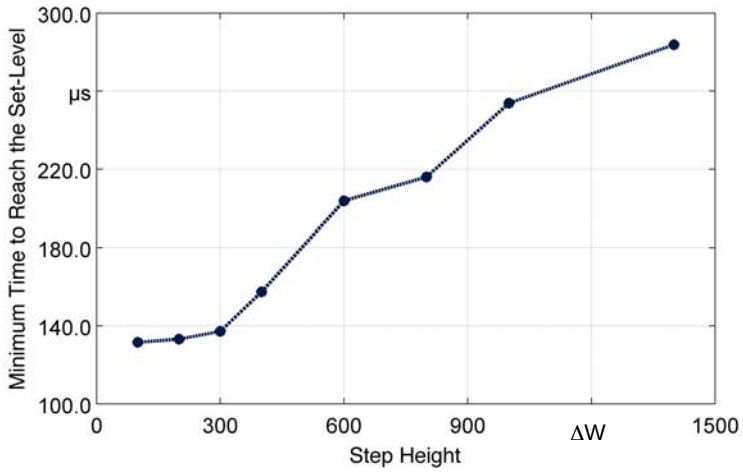

Figure A1.29: Minimum time to fall to the set-point level for rectangular steps (n=5).

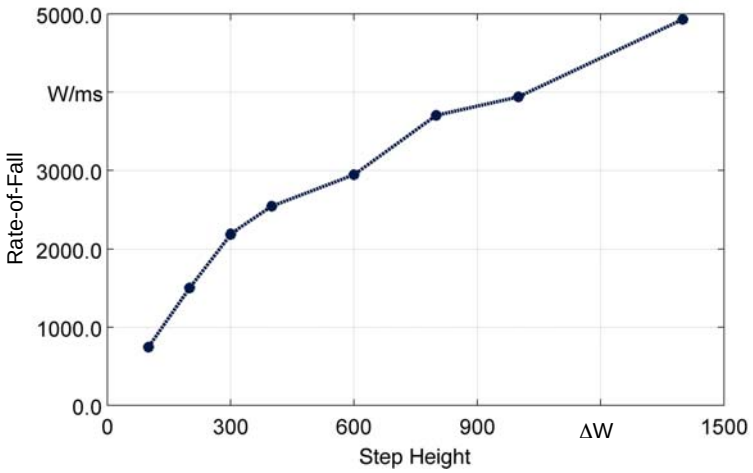

Figure A1.30: Rates-of-Fall for given step heights (n=5).

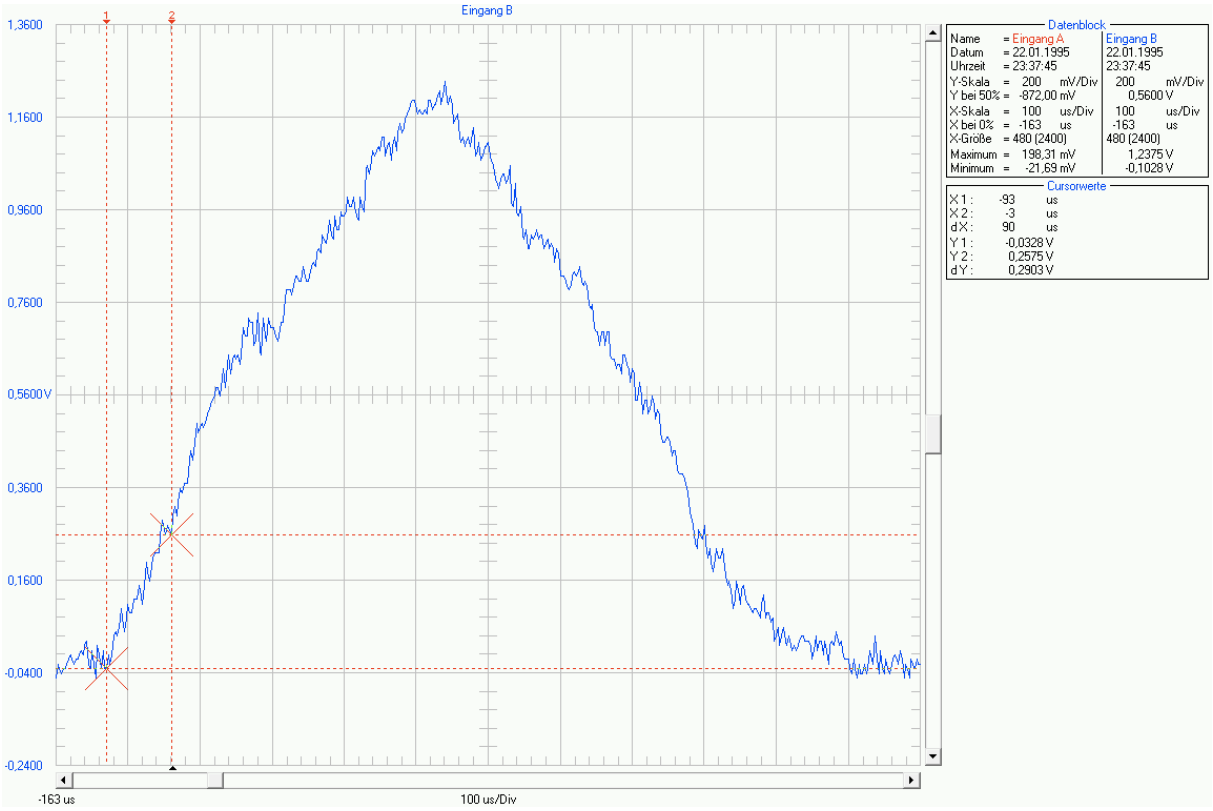

Figure A1.31: Determination of the duration of the on-section for the initial step for triangular pulses. The example shows a pulse at 350 W and 0.75 ms.

A2 Investigation on Welding with Rectangular Pulses

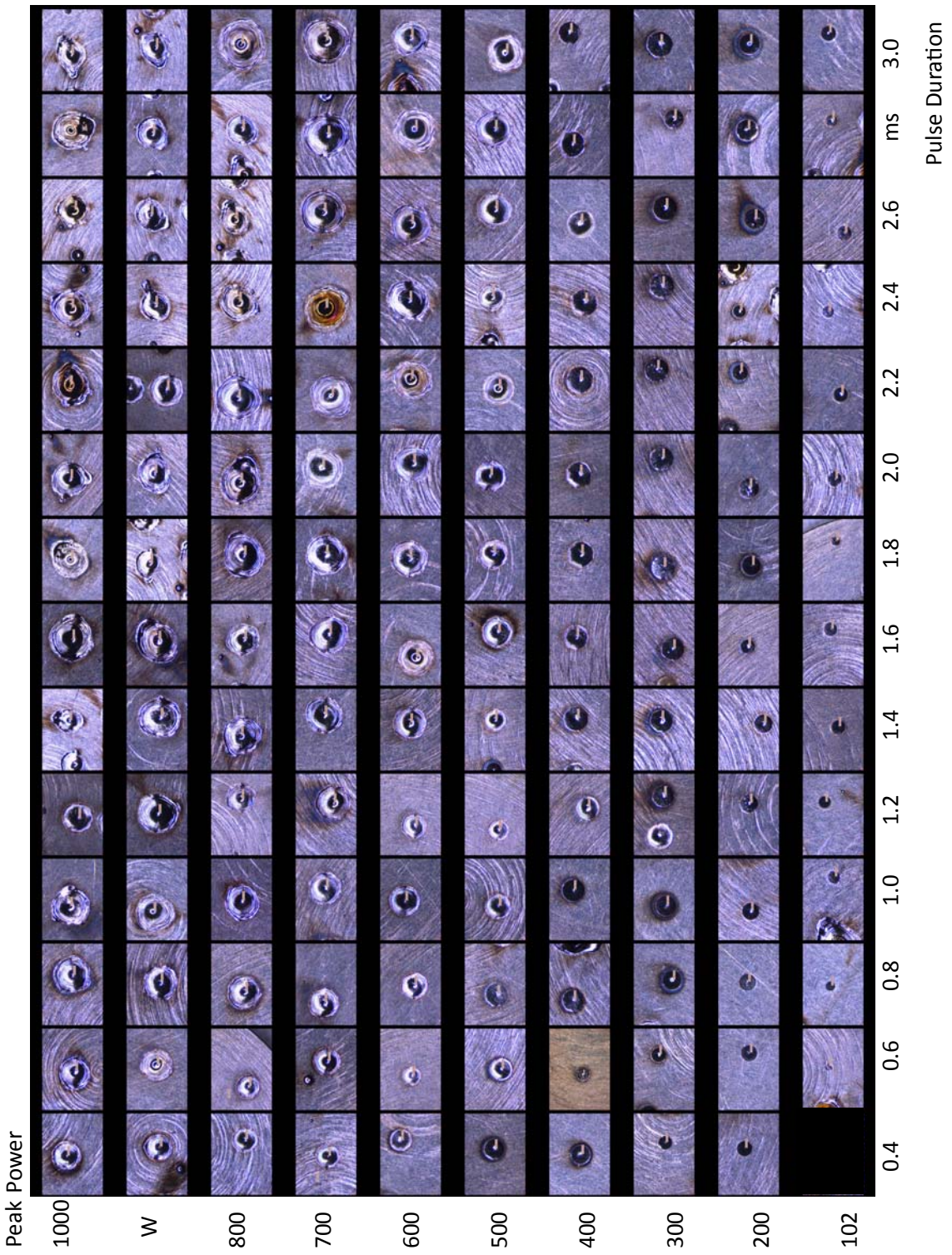

Figure A2.1: Qualitative results of rectangular pulsed welds for Material B. Photos were taken at different magnifications.

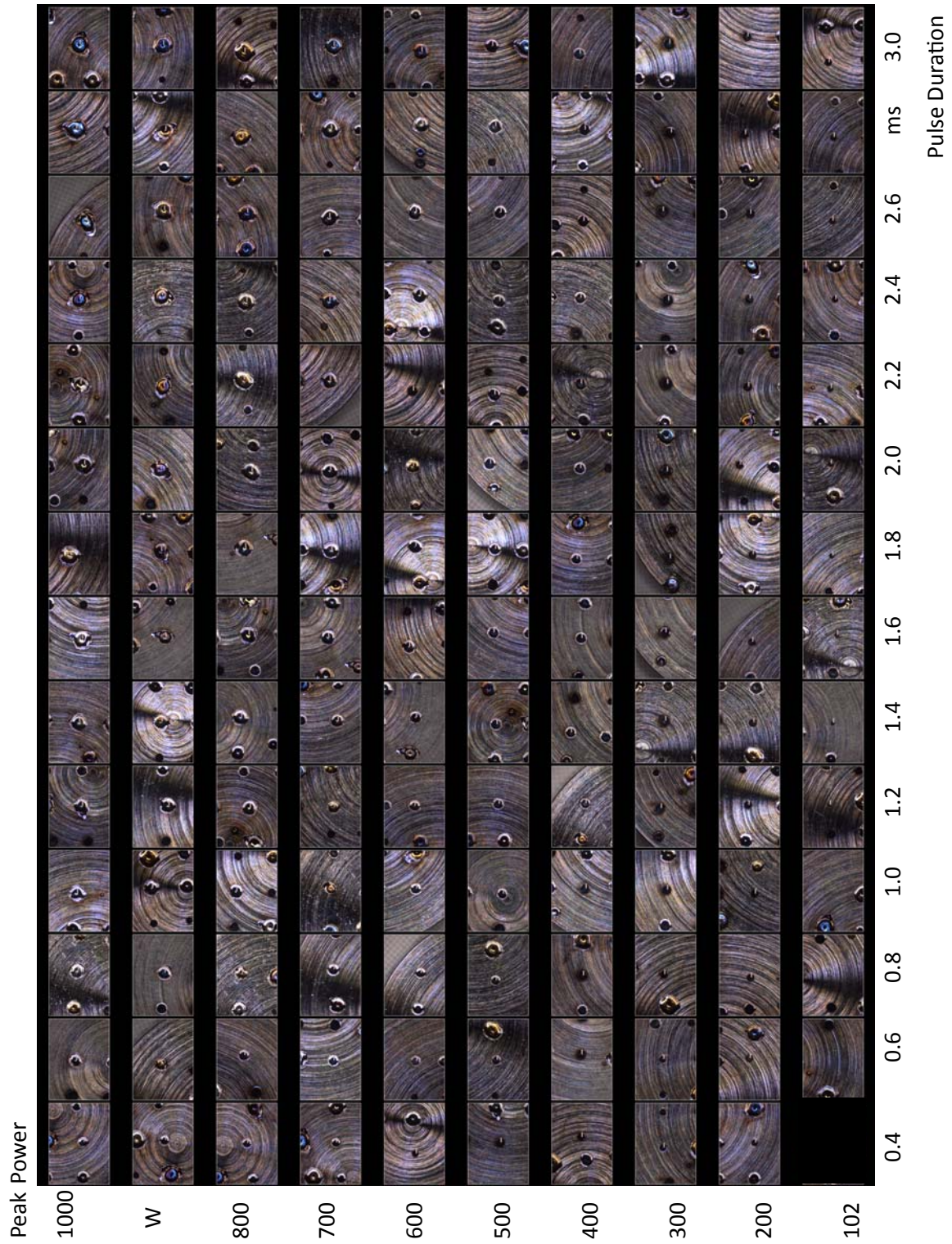

Figure A2.2: Qualitative results of rectangular pulsed welds for Material A. All photos have been taken with the same magnification factor. The central weld is always the current one.

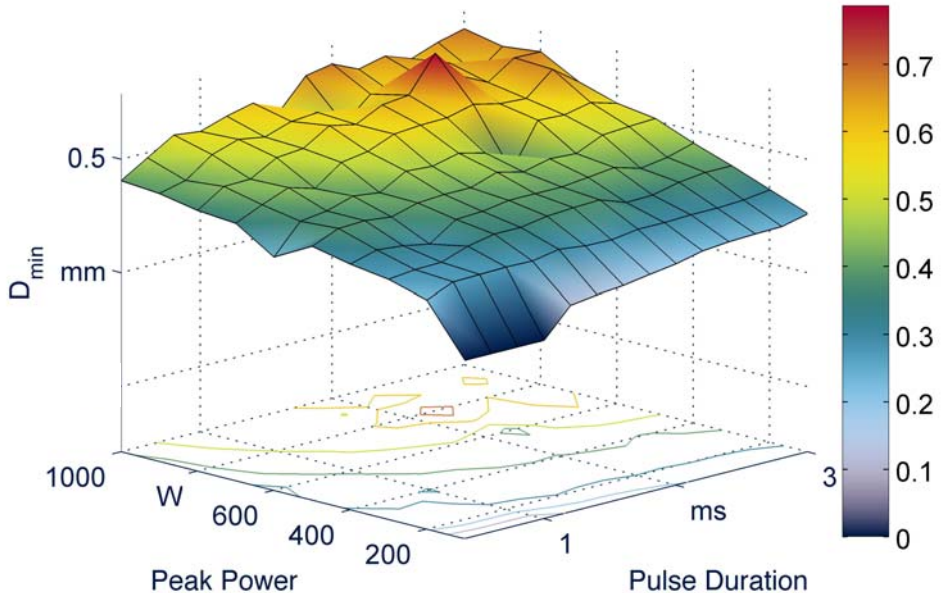

Figure A2.3: D_{min}-measurements from the stereomicroscopic analysis of Material A welds.

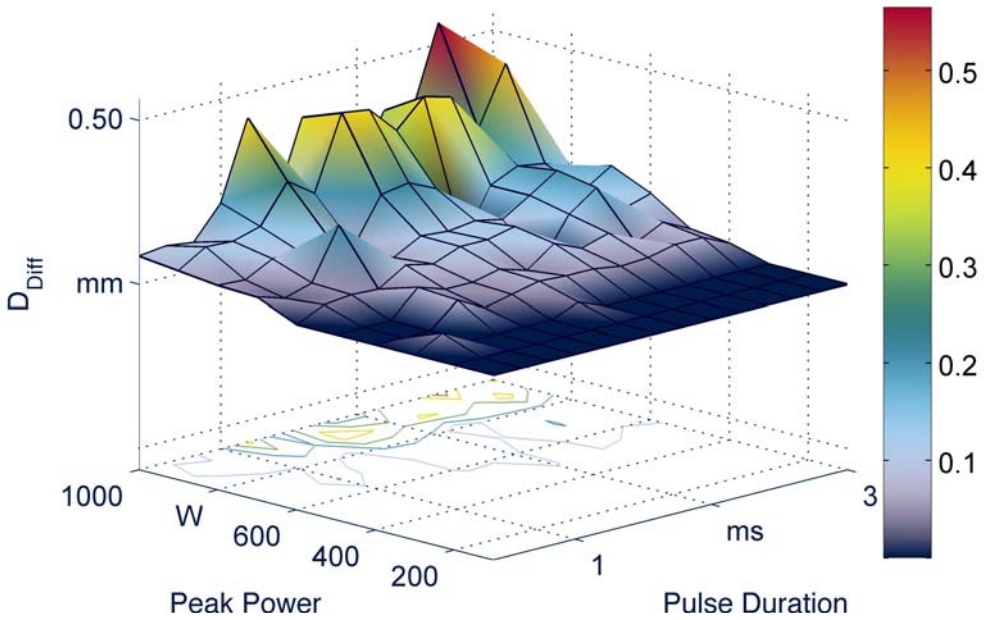

Figure A2.4: D_{Diff}-measurements from the stereomicroscopic analysis of Material A welds.

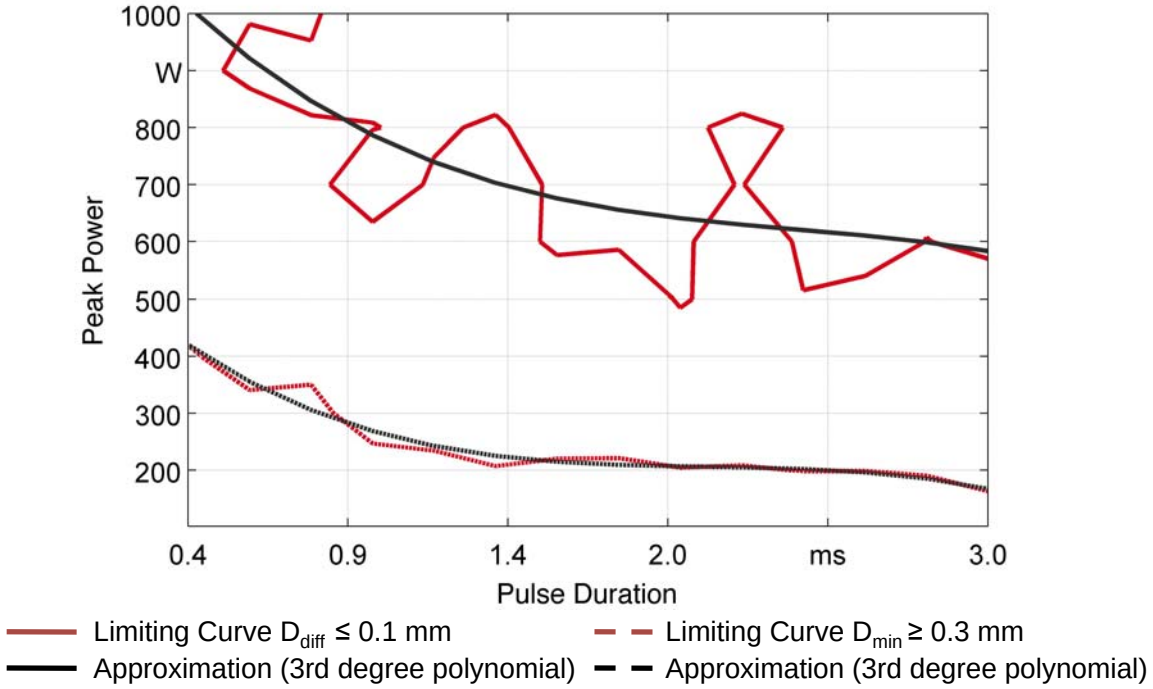

Figure A2.5: Approximation of critical contours to define a process window for Material A.

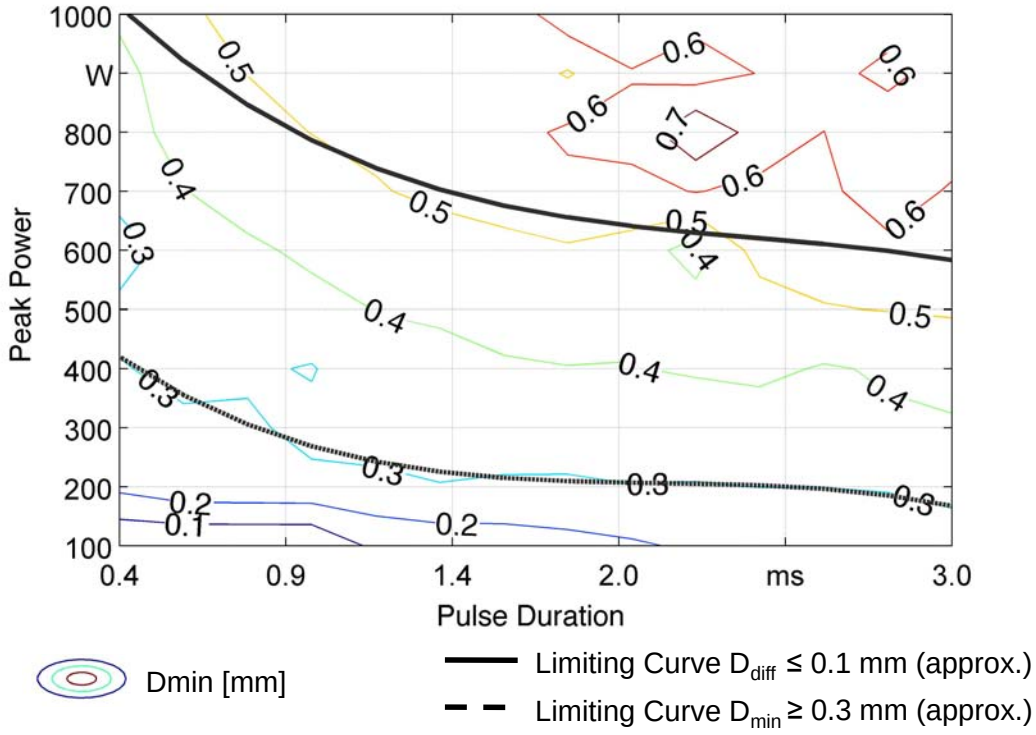

Figure A2.6: Addition of D_{min}-contours to the process window for Material A.

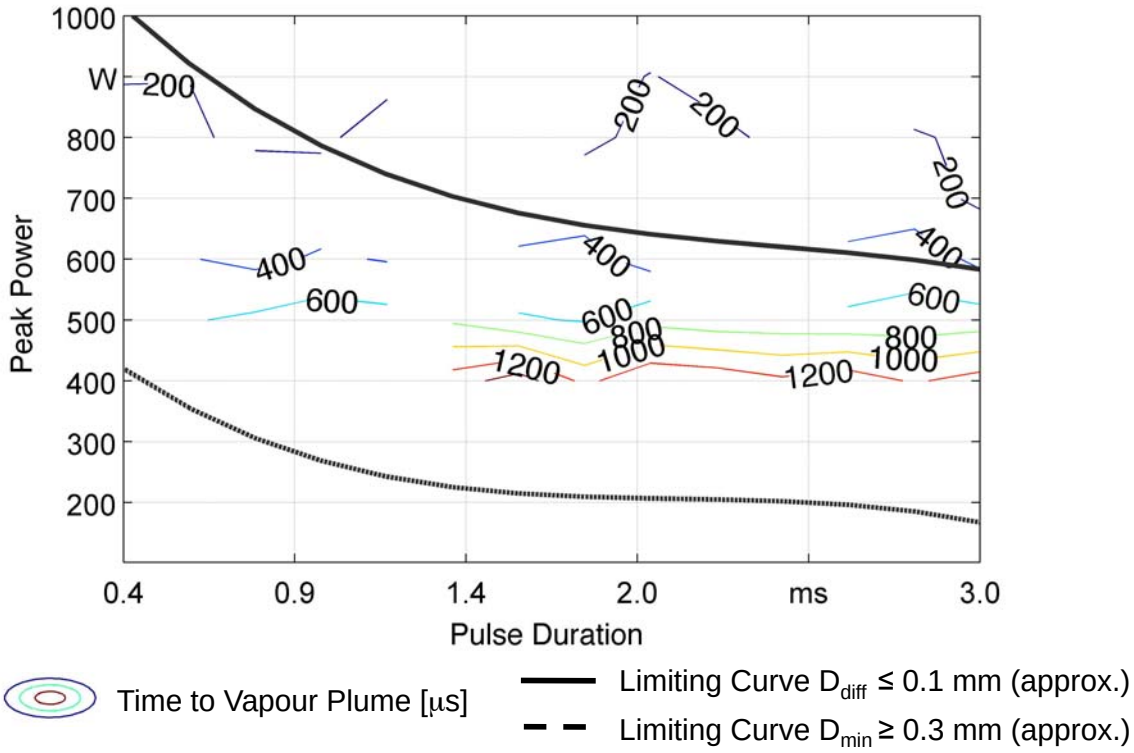

Figure A2.7: Measurements on time to vapour plume occurrence added to the process window for Material A.

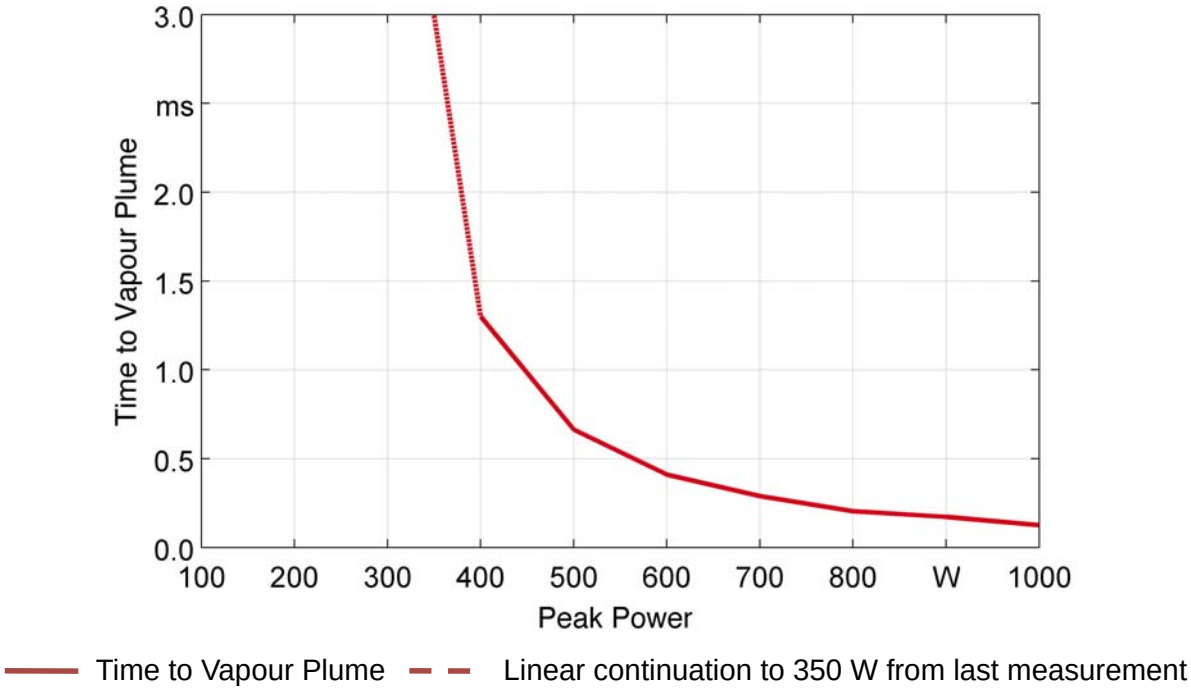

Figure A2.8: Time to vapour plume measurements as a function of applied peak power for Material A.

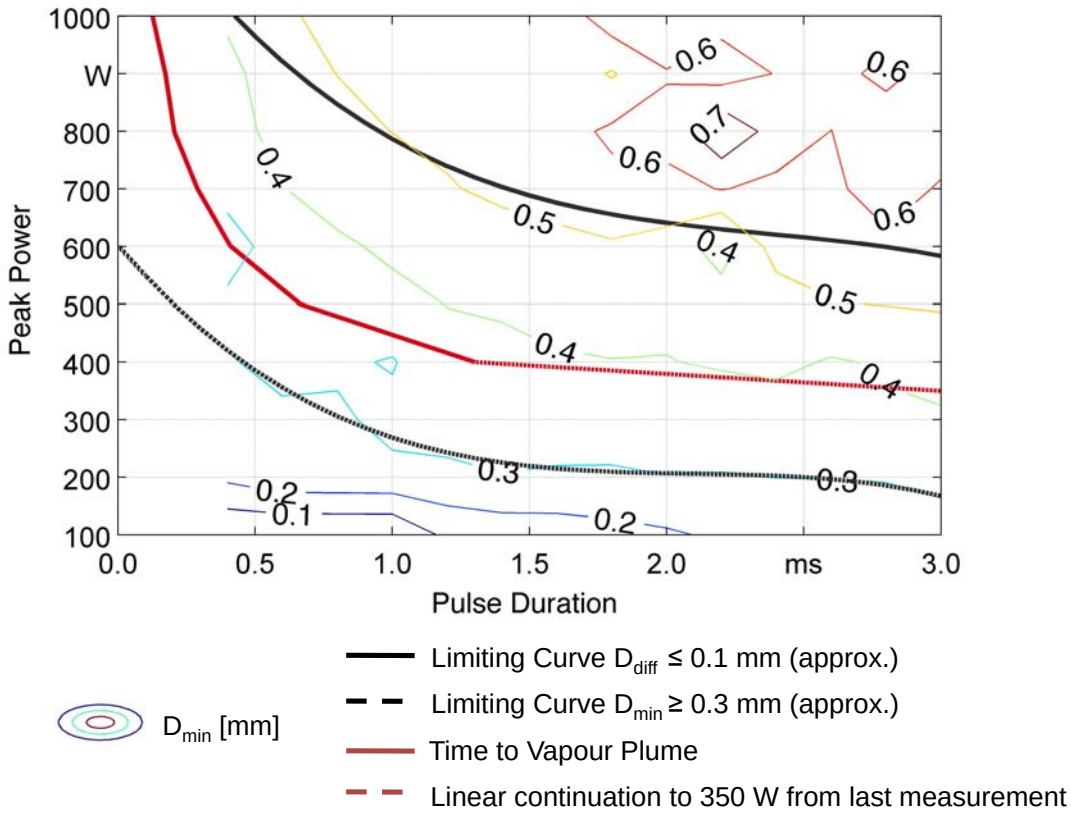

Figure A2.9: Complete process window for Material A welds

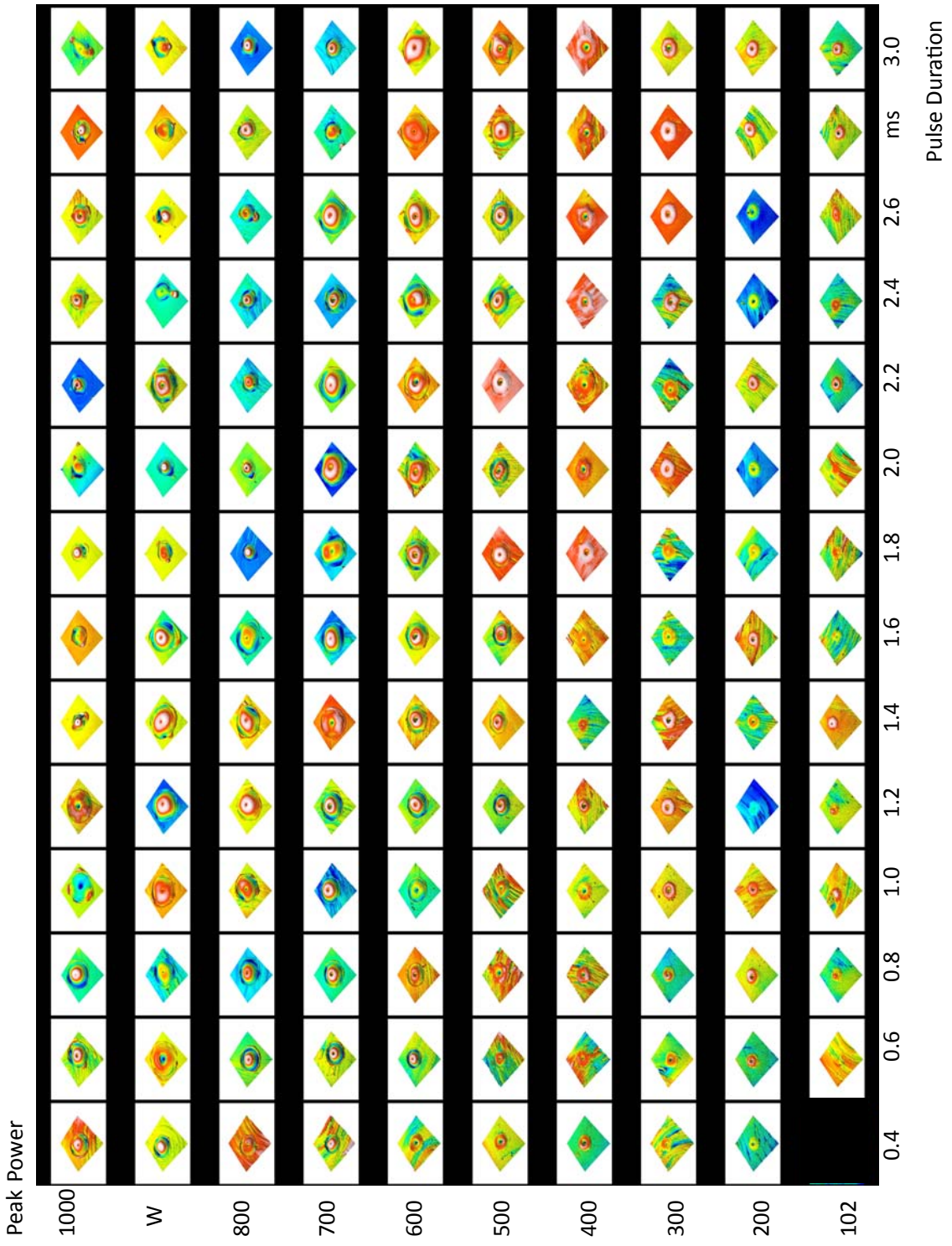

Figure A2.3: Qualitative results of the topography measurements. The scaling of the colour axes as well as the global scale are not uniform.

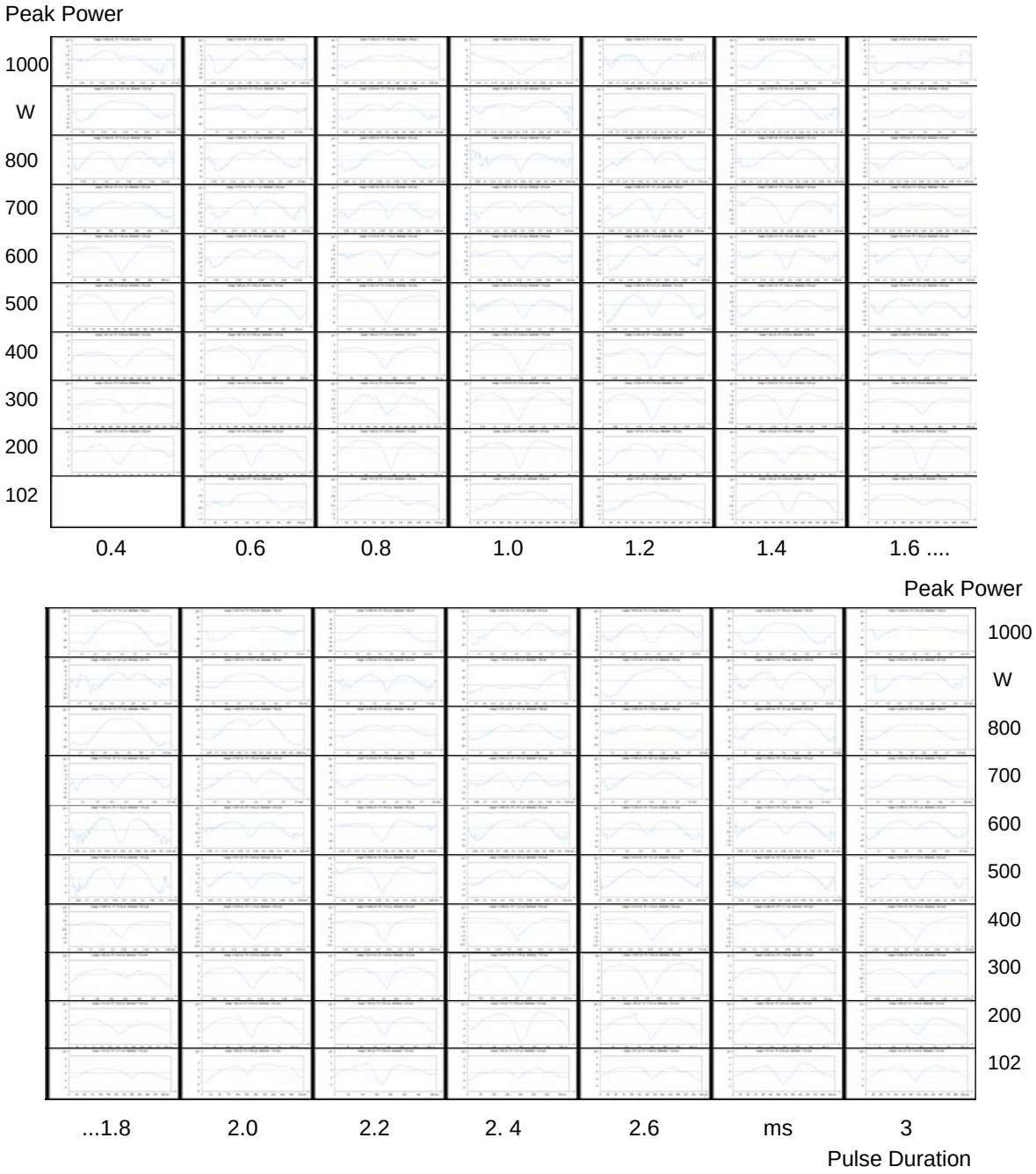

Figure A2.11: Qualitative overview of the evaluated cross sections

.

A3 Main Investigation on Partial Penetration Welding

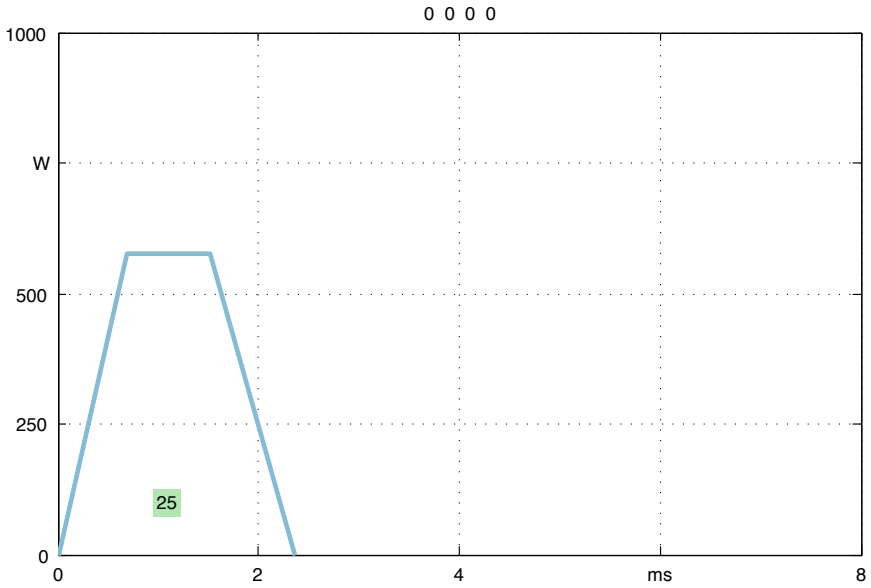

Figure A3.1: Pulse shape at central point settings.

Trial No.	Peak Power [W]	t_1 [%]	t_2 [%]	Energy [J]	Duration [ms]	P. Power Level	t_1 Level	t_2 Level	Energy Level
1	575	0,28	0,72	1,55	3,610	0	0	0	2
2	350	0,18	0,82	1,3	4,352	-1	-1	1	1
3	350	0,38	0,82	1,3	4,737	-1	1	1	1
4	800	0,38	0,82	0,8	1,433	1	1	1	-1
5	575	0,28	0,72	1,05	2,480	0	0	0	0
6	350	0,18	0,62	0,8	2,955	-1	-1	-1	-1
7	575	0,28	0,72	0,3	0,786	0	0	0	-2
8	800	0,18	0,62	1,3	2,260	1	-1	-1	1
9	575	0,08	0,72	1,05	2,241	0	-2	0	0
10	575	0,28	0,92	1,05	2,241	0	0	2	0
11	575	0,28	0,72	1,55	3,610	0	0	0	2
12	800	0,18	0,82	1,3	2,026	1	-1	1	1
13	350	0,38	0,82	0,8	2,955	-1	1	1	-1
14	350	0,18	0,62	1,3	4,737	-1	-1	-1	1
15	575	0,28	0,72	1,05	2,480	0	0	0	0
16	575	0,48	0,72	1,05	2,777	0	2	0	0
17	800	0,18	0,62	0,8	1,433	1	-1	-1	-1
18	575	0,28	0,72	1,55	3,610	0	0	0	2
19	350	0,18	0,62	1,3	4,737	-1	-1	-1	1
20	350	0,18	0,62	1,3	4,737	-1	-1	-1	1
21	800	0,18	0,62	0,8	1,433	1	-1	-1	-1
22	1025	0,28	0,72	1,05	1,481	2	0	0	0
23	350	0,38	0,82	0,8	2,955	-1	1	1	-1
24	125	0,28	0,72	1,05	8,944	-2	0	0	0
25	800	0,18	0,82	0,8	1,285	1	-1	1	-1
26	800	0,38	0,62	0,8	1,620	1	1	-1	-1
27	350	0,18	0,82	1,3	4,352	-1	-1	1	1
28	800	0,38	0,62	0,8	1,620	1	1	-1	-1
29	800	0,18	0,62	1,3	2,260	1	-1	-1	1
30	575	0,28	0,52	1,05	2,777	0	0	-2	0
31	575	0,28	0,72	1,05	2,480	0	0	0	0
32	800	0,38	0,62	0,8	1,620	1	1	-1	-1
33	575	0,28	0,72	1,05	2,480	0	0	0	0
34	350	0,18	0,82	0,8	2,715	-1	-1	1	-1
35	800	0,18	0,62	0,8	1,433	1	-1	-1	-1
36	575	0,28	0,72	0,3	0,786	0	0	0	-2
37	575	0,28	0,92	1,05	2,241	0	0	2	0
38	125	0,28	0,72	1,05	8,944	-2	0	0	0
39	800	0,38	0,82	1,3	2,260	1	1	1	1
40	1025	0,28	0,72	1,05	1,481	2	0	0	0
41	125	0,28	0,72	1,05	8,944	-2	0	0	0
42	575	0,48	0,72	1,05	2,777	0	2	0	0
43	800	0,18	0,82	0,8	1,285	1	-1	1	-1
44	350	0,18	0,62	0,8	2,955	-1	-1	-1	-1
45	800	0,38	0,62	1,3	2,555	1	1	-1	1
46	350	0,18	0,62	0,8	2,955	-1	-1	-1	-1
47	350	0,18	0,82	0,8	2,715	-1	-1	1	-1
48	575	0,28	0,52	1,05	2,777	0	0	-2	0
49	575	0,08	0,72	1,05	2,241	0	-2	0	0
50	800	0,18	0,62	1,3	2,260	1	-1	-1	1
51	800	0,18	0,62	0,8	1,433	1	-1	-1	-1
52	350	0,38	0,82	0,8	2,955	-1	1	1	-1
53	575	0,28	0,72	1,05	2,480	0	0	0	0
54	575	0,28	0,72	1,05	2,480	0	0	0	0
55	350	0,38	0,62	0,8	3,242	-1	1	-1	-1
56	1025	0,28	0,72	1,05	1,481	2	0	0	0
57	575	0,08	0,72	1,05	2,241	0	-2	0	0
58	350	0,38	0,82	0,8	2,955	-1	1	1	-1
59	125	0,28	0,72	1,05	8,944	-2	0	0	0
60	350	0,38	0,62	0,8	3,242	-1	1	-1	-1
61	350	0,18	0,62	0,8	2,955	-1	-1	-1	-1
62	575	0,28	0,72	1,05	2,480	0	0	0	0
63	575	0,28	0,72	0,3	0,786	0	0	0	-2
64	575	0,28	0,92	1,05	2,241	0	0	2	0
65	350	0,38	0,62	1,3	5,196	-1	1	-1	1
66	575	0,28	0,52	1,05	2,777	0	0	-2	0
67	350	0,38	0,82	1,3	4,737	-1	1	1	1
68	800	0,18	0,82	0,8	1,285	1	-1	1	-1
69	800	0,18	0,82	1,3	2,026	1	-1	1	1
70	800	0,18	0,82	0,8	1,285	1	-1	1	-1
71	350	0,18	0,82	1,3	4,352	-1	-1	1	1
72	575	0,08	0,72	1,05	2,241	0	-2	0	0
73	575	0,28	0,92	1,05	2,241	0	0	2	0
74	800	0,38	0,62	0,8	1,620	1	1	-1	-1
75	575	0,28	0,72	1,05	2,480	0	0	0	0
76	800	0,38	0,82	0,8	1,433	1	1	1	-1
77	575	0,48	0,72	1,05	2,777	0	2	0	0
78	575	0,28	0,72	0,3	0,786	0	0	0	-2
79	575	0,28	0,72	1,05	2,480	0	0	0	0
80	350	0,38	0,62	1,3	5,196	-1	1	-1	1
81	350	0,38	0,62	1,3	5,196	-1	1	-1	1
82	350	0,38	0,82	1,3	4,737	-1	1	1	1
83	800	0,38	0,82	0,8	1,433	1	1	1	-1
84	350	0,38	0,62	1,3	5,196	-1	1	-1	1
85	800	0,38	0,82	0,8	1,433	1	1	1	-1
86	350	0,18	0,82	0,8	2,715	-1	-1	1	-1
87	800	0,38	0,62	1,3	2,555	1	1	-1	1
88	800	0,38	0,82	1,3	2,260	1	1	1	1
89	575	0,28	0,72	1,05	2,480	0	0	0	0
90	800	0,18	0,62	1,3	2,260	1	-1	-1	1
91	350	0,18	0,82	1,3	4,352	-1	-1	1	1
92	800	0,38	0,62	1,3	2,555	1	1	-1	1
93	800	0,38	0,82	1,3	2,260	1	1	1	1
94	575	0,48	0,72	1,05	2,777	0	2	0	0
95	350	0,38	0,62	0,8	3,242	-1	1	-1	-1
96	800	0,18	0,82	1,3	2,026	1	-1	1	1
97	350	0,38	0,82	1,3	4,737	-1	1	1	1
98	800	0,18	0,82	1,3	2,026	1	-1	1	1
99	575	0,28	0,72	1,05	2,480	0	0	0	0
100	575	0,28	0,52	1,05	2,777	0	0	-2	0
101	350	0,38	0,62	0,8	3,242	-1	1	-1	-1
102	575	0,28	0,72	1,05	2,480	0	0	0	0
103	800	0,38	0,62	1,3	2,555	1	1	-1	1
104	1025	0,28	0,72	1,05	1,481	2	0	0	0
105	800	0,38	0,82	1,3	2,260	1	1	1	1
106	350	0,18	0,82	0,8	2,715	-1	-1	1	-1
107	575	0,28	0,72	1,55	3,610	0	0	0	2
108	350	0,18	0,62	1,3	4,737	-1	-1	-1	1

Table A3.1: Experimental settings for main welding experiments.

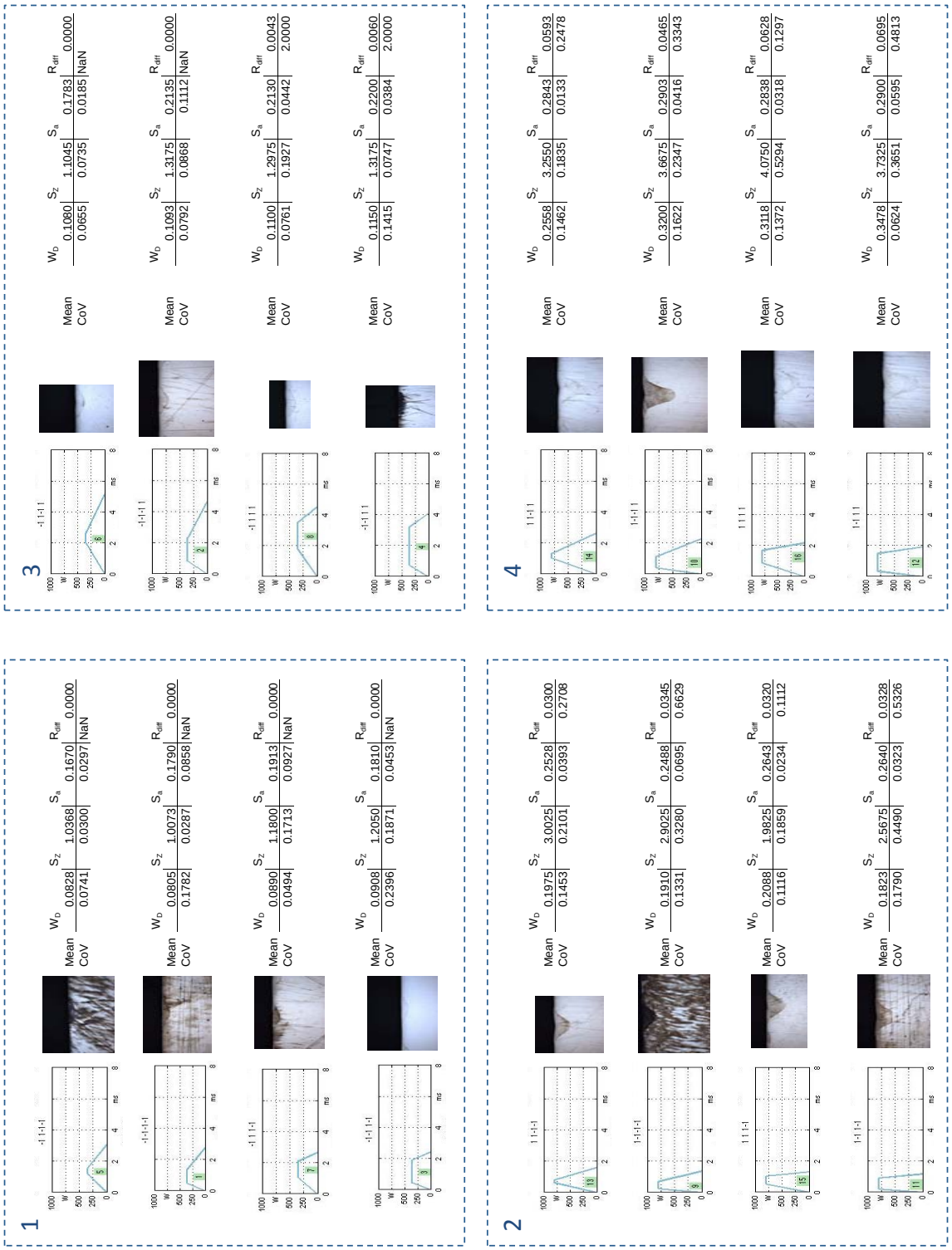

Figure A3.1: Compiled results for the factorial core (NaN is equal to zero).

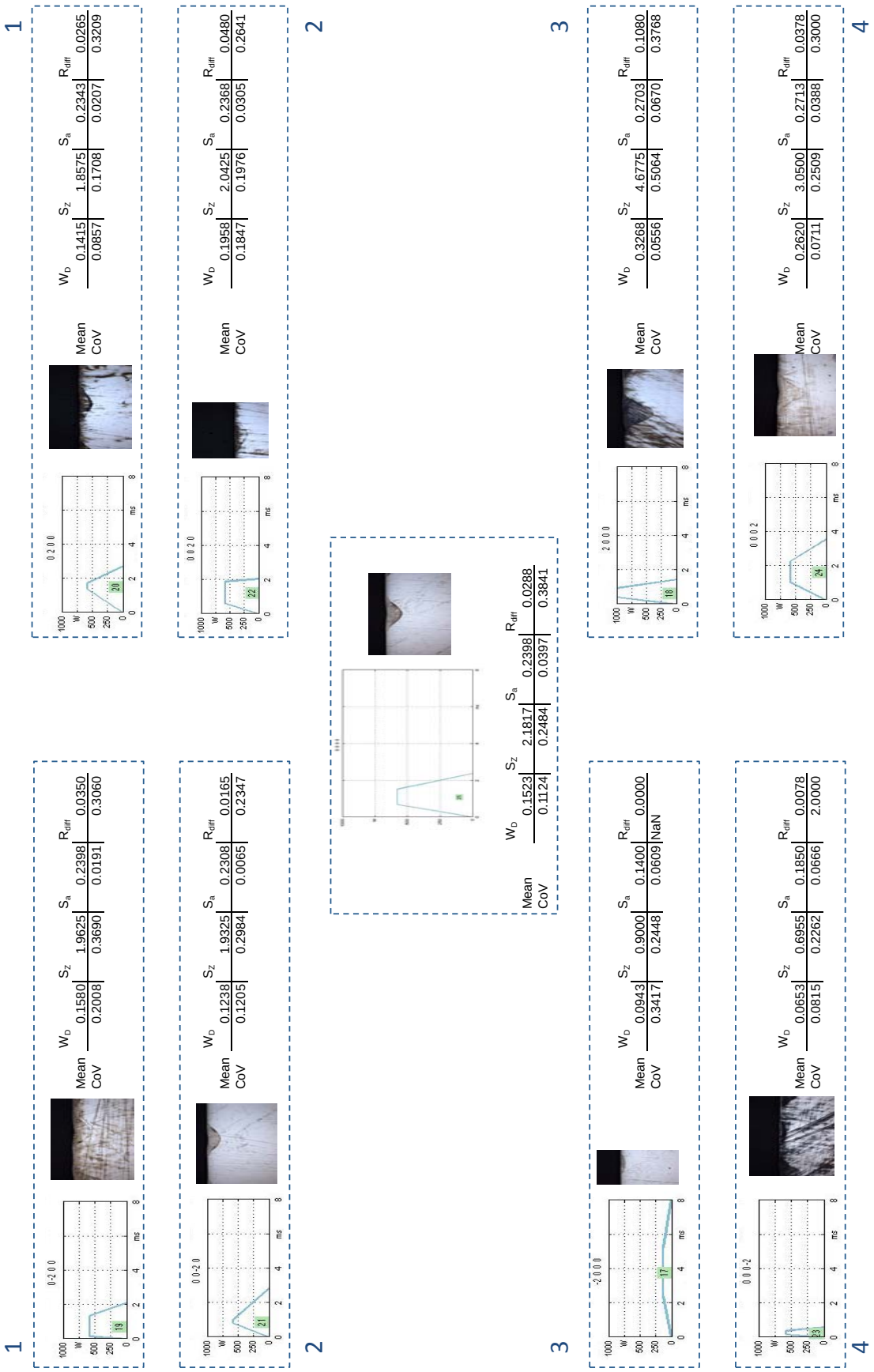

Figure A3.2: Compiled results for star- and centre-points (NaN is equal to zero).